A Fast Hybrid Method For Analysis and Design of Photonic Structures

by

Arash Rohani

A thesis
presented to the University of Waterloo
in fulfillment of the
thesis requirement for the degree of
Doctor of Philosophy
in
Electrical and Computer Engineering

Waterloo, Ontario, Canada, 2006

I hereby declare that I am the sole author of this thesis. This is a true copy of the thesis, including any required final revisions, as accepted by my examiners. I Understand that my thesis may be made electronically available to the public.
Arash Rohani

Abstract

This thesis presents a very efficient hybrid method for analysis and design of optical and passive photonic devices. The main focus is on unbounded wave structures. This class of photonic systems are in general very large in terms of the wavelength of the driving optical sources. The size of the problem space makes the electromagnetic modelling of these structure a very challenging problem. Our approach and main contribution has been to combine or hybridize three methods that together can handle this class of photonic structures as a whole.

The basis of the hybrid method is a novel Gaussian Beam Tracing method GBT. Gaussian Beams (GB) are very suitable elementary functions for tracing and tracking purposes due to their finite extent and the fact that they are good approximations for actual laser beams. The GBT presented in this thesis is based on the principle of phase matching. This method can be used to model the reflection and refraction of Gaussian beams from general curved surfaces as long as the curvature of the surface is relatively small. It can also model wave propagation in free space. The developed GBT is extremely fast as it essentially uses simple algebraic equations to find the parameters of the reflected and refracted beams once the parameters of the incident beam is known. Therefore sections of the systems whose dimensions are large relative to the optical wavelength are simulated by the GBT method.

Fields entering a photonic system may not possess an exact Gaussian profile. For example if an aperture limits the input laser to the system, the field is no longer a GB. In these and other similar cases the field at some aperture plane needs to be expanded into a sum of GBs. Gabor expansion has been used for this purpose. This method allows any form of field distribution on a flat or curved surface to be expanded into a sum of GBs. The resultant GBs are then launched inside the system and tracked by GBT. Calculation of the coefficients of the Gabor series is very fast (1-2 minutes on a typical computer for most applications).

In some cases the dimensions or physical properties of structures do not allow the application of the GBT method. For example if the curvature of a surface is very large (or its radius of curvature is very small) or if the surface contains sharp edges or sub-wavelength dimensions GBT is no longer valid. In these cases we have utilized the Finite Difference Time Domain method (FDTD). FDTD is a rigorous and very accurate full wave electromagnetic solver. The time domain form of Maxwell's equations are discretized and

solved. No matrix inversion is needed for this method. If the size of the structure that needs to be analyzed is large relative to the wavelength FDTD can become increasingly time consuming. Nevertheless once a structure is simulated using FDTD for a given input, the output is expanded using Gabor expansion and the resultant beams can then be efficiently propagated through any desired system using GBT. For example if a diffraction grating is illuminated by some source, once the reflection is found using FDTD, it can be propagated very efficiently through any kind of lens or prism (or other optical structures) using GBT. Therefore the overall computational efficiency of the hybrid method is very high compared to other methods.

Acknowledgments

This thesis would not exist without the encouragement and support provided by many people.

I am thankful and indebted to Prof. Rouzbeh Moini Mazandarani, who introduced me to the fascinating world of Electromagnetics, as my undergraduate supervisor.

I am deeply grateful to my supervisors at the university of Waterloo, Prof. Safieddin Safavi Naeini and Prof. Sujeet K. Chaudhuri for providing support, guidance, and inspiration throughout the course of my graduate studies.

I extend my sincere gratitude to other committee members, Prof. Yahia M.M. Antar , Prof. Peter Forsyth, Prof. Melanie Campbell, and Prof. Rafaat Mansour for accepting to read my thesis and provide me with their feed back.

I am deeply thankful to the staff of the Department of Electrical and Computer Engineering of University of Waterloo for having been so helpful and supportive. Special thanks to Wendy Boles for her tireless patience, kindness and assistance in all matters.

I express my appreciation to the organizations that funded this research. Financial support for this work was provided mainly by the Natural Sciences and Engineering Research Council (NSERC) and Research in Motion (RIM).

Finally I would like to thank Samar Saneinejad for her invaluable help in editing this thesis.

Contents

List of Tables

List of Figures

Table of Abbreviations

GB	Gaussian Beam
GBT	Gaussian Beam Tracing
GAGB	General Astigmatic Gaussian Beam
CSP	Complex Source Point
FDTD	Finite Difference Time Domain
PML	Perfectly Matched Layer
TF/SF	Total Field / Scattered Field

Chapter 1

Introduction

Performance of hybrid and monolithic integrated photonic circuits and components in modern optical systems highly depends on vectorial (polarization) and scalar characteristics of interconnecting components and junctions between various optical and electronic devices. The components that form a typical photonic device can be divided into two major categories:

1. Active devices, such as optical lasers and optical amplifiers.

2. Passive devices, such as waveguides, lenses, prisms and diffraction gratings.

Active devices are not dealt with in this research. The passive components in a photonic system can further be subdivided into two major categories: guided wave structures and unbounded wave structures. The guided wave section, containing structures such as simple waveguides, waveguide junctions, waveguide couplers and power dividers, have been the subject of extensive research for many years. There are analytical formulas describing the characteristics of such guiding structures for a number of simple geometries [1]. For other more complex geometries many approximate but very accurate methods such as Vectorial and Semivectorial Finite Difference Beam Propagation Method [2, 3], have been developed during the past two decades. Rigorous methods such as Finite Difference Time Domain (FDTD) [4, 5, 6] have also been applied successfully to such structures. The analysis and design of such guiding wave structures are not included in this research. Nevertheless the coupling of power to such structures must be considered. In addition to simple waveguide and fiber junctions and guiding structures in general, novel interconnect and transition structures containing complex combinations of micro-lens, micro-prisms, tapered segments, curved structures, semi-open regions (star couplers), polarizing devices, and MEMS devices

have been proposed and implemented in state-of-the-art emerging components. Simulation and design optimization of these structures, which are primarily non-guided wave substructures, are extremely challenging electromagnetic problem. Existing full-wave simulation tools, such as those based on the Finite Element Method (FEM) and FDTD for example, are computationally very expensive if applied on their own and therefore are not appropriate for such components. The main reason being that such structures, as miniaturized as they might have become, are still very large compared to the wavelength of light sources and may have dimensions in the order of hundreds or even thousands of wavelengths. On the other hand geometrical optics and scalar physical optics methods cannot model vector scattering properties of the optical interconnects with sufficient accuracy. In this research a very fast and yet reasonably accurate computational scheme for modelling such photonic interconnects is developed. The approach, which is based on the combination of a newly developed Gaussian Beam Tracing (GBT) technique with Gabor type expansion and its hybridization with the finite difference time domain method, is particularly suitable for design optimization of such open and semi-open transitional structures and interconnects. In this scheme, the entire structure is divided into the active devices, modal guiding parts (coupled waveguides and non-radiating transitions) and radiation in open or semi-open 3-D regions (lenses, prisms, micro-lenses, gratings, etc.). The focus of this research is the last category. For these open and semi-open radiation/scattering regions (containing lenses and MEMS micro-mirror), our vectorial 3-D Gaussian Beam Tracing is utilized in conjunction with a Gabor type beam expansion formulation and these are hybridized with FDTD in regions where the Gaussian Beam Expansion/Tracing fail to produce accurate results.

1.1 Overview of the Hybrid Method

According to what was presented above, the general form of the problem that is targeted is shown in Fig.(1.1).

The input fiber(s), waveguide(s) or laser(s) launch an electromagnetic field inside the system. The input structures are treated as apertures, whose radiation would propagate through the system. Paraxial Gaussian beams (GBs) are very good approximations for output of laser sources. Other sources of electromagnetic fields such as special laser types (producing truncated Gaussian Beams) or output of fibers and/or waveguides can be expanded as a sum of Gaussian Beams. These facts make the paraxial Gaussian Beam a very attractive candidate as an elementary beam entity for modelling of propagation phenomena in open and semi-open structures. The hybrid method developed in this research

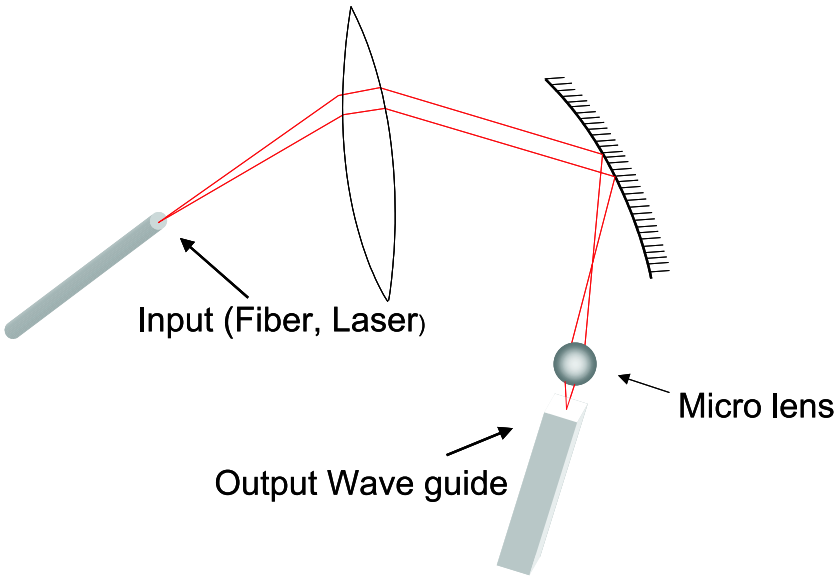

Figure 1.1: Geometry of the general form of the problem

is therefore based on this new Gaussian Beam tracing method. When the input(s) to the system do not possess a purely Gaussian Profile, their aperture field has to be expanded in terms of a set of Gaussian Beam elementary beam functions. In this research Gabor representation of aperture fields has been used for this purpose.

The combination of the Gabor Expansion and the Gaussian Beam Tracing can handle a relatively large class of problems, but nevertheless they fail in certain situations. If the dimensions of the structures become very small in terms of wavelength, this method fails. Furthermore, the combination of GBT and Gabor expansion can not handle periodic structures such as diffraction gratings and the problem of coupling to the output waveguide(s). For these situations hybridization of the FDTD method with the Gaussian Beam Expansion/Tracking method has been used. Although a complete FDTD was developed during the course of this research the actual hybridization is of paramount importance to us. Therefore the "combination" of the different methods that constitute the hybrid method is our major contribution.

1.2 Thesis Organization

This thesis is organized as follows:

In Chapter 3. first the different types of GBs are introduced and their basic properties are explained. This is done by extending the definition of a narrow bundle of rays by

defining complex radii of curvature of the phase front. In sec.(3.3) the reflection and transmission of a general astigmatic GB from an arbitrary surface is considered. Subsequently the fast GB tracing method (GBT) is formulated: given the parameters of an arbitrary GB and the equation of a general curved surface the parameters of the reflected and refracted beams are obtained. 2D GBT is explained in Appendix C. After a short discussion of the Goos-Hanchen shift and the pulsed GB a number a examples are given that demonstrate the speed and versatility of GBT. Finally a verification is presented by comparing the results of GBT with the physical optics method.

In Chapter 4 first the one dimensional aperture representation using Gabor expansion is introduced. It is shown that a one dimensional aperture which gives rise to 2D fields can be represented by a number of shifted and rotated GBs. The representation of a 2D aperture which gives rise to 3D fields is then formulated (based on the works of Felsen et. al.) Subsequently the beam representation in the paraxial regime for the 1D case is given. An attempt is made to extend the beam field representation to the 2D case. Only the case where the beams are narrow in one direction but possess an arbitrary waist in the other direction is considered. After tabulating the well known properties of Gabor expansion, a number of examples that are combinations of Gabor expansion and GBT are given.

In Chapter 5. the main focus is on Hybridization of Gabor expansion and GBT with FDTD. Nevertheless after testing a number of commercial FDTD software it was concluded that an implementation of this method was required. The total field/scattered (TF/SF) field formulation is used to model a GB launched at arbitrary angle inside an FDTD lattice. This combines GBT with FDTD for a single GB. If the input to the FDTD algorithm is not a pure GB, it needs to be expanded using Gabor expansion. Therefore the FDTD used needed to be able to launch multiple GBs (shifted and rotated) simultaneously. After numerous test it is shown that the implemented FDTD can in fact handle multiple GBs very efficiently. A very efficient near field to far field transformation is also utilized in order to rigorously propagate the fields found by FDTD to any other point in space. This concludes the combination of FDTD with Gabor expansion and GBT.

In Chapter 6 the hybrid method is applied to three classes of problems: 1) Scattering type problems 2)Transmission type problems 2)Coupling problems. After obtaining the general grating formula for a dielectric grating a systematic approach is used to ensure the accuracy of the results obtained. First two dielectric grating with different pitches are illuminated by a GB at different angles and the peaks of the scattered field is compared with the general grating formula. The accuracy of the predicted angles shows the applicability of the hybrid method to this rather numerically extensive problem. Convex and concave

gratings are considered next. The interesting results predicted by this method is then compared with a phased array approach. A problem comprising all the components of the hybrid method is considered next. In this problem a phased cosine field illuminates a dielectric grating. The phased cosine field is expanded using Gabor expansion to yield a number of shifted and rotated GBs. The GBs are then launched inside the FDTD lattice and the field is observed close to the TF/SF region. This field is then passed through a thin lens. To the author's knowledge the results obtained for this complicated problem can not be compared with any other method as a whole. Nevertheless as each component has been successfully tested individually it is concluded that the results are accurate.

Chapter 2

Literature Review

2.1 Gaussian Beam Tracing

As was mentioned above the developed GBT is the basis for our hybrid method. GB tracing and tracking have been investigated and reported in the literature. The main methods are reviewed below:

2.1.1 Ray Matrix Method

In this method, an optical structure such as a lens or slab or lens-like structure is modelled by its ray matrix method [7, 8, 9, 10]. The propagation of a simple astigmatic GB[1] is found by transforming its complex curvature. This is the simplest and the most common way for tracking beams. Although there are some modified versions of this method [10], they all have the following strengths and weaknesses:

a) Strengths:

   1. The methods are all very fast.
   2. A Cascade of several optical structures can be easily analyzed by simply multiplying the ray matrices of the individual structures.

b) Weaknesses:

   1. Inaccurate.
   2. Can not handle general surfaces.

[1] See Chapter (3) for the definitions of simple and general astigmatic GBs

3. Can not model general astigmatism.
4. The beams must be paraxial with respect to the optical axis; therefore tilts and offsets can not be accurately modelled.
5. The reflection of light from the surface of lenses is not taken into account.
6. The polarization effects are not taken into account.

2.1.2 Complex Source Point Presentation and Complex Ray Tracing

Deschamps [11] (1971) showed that a stigmatic GB can be represented as a bundle of complex rays, meaning a bundle of rays originating from a point in the complex plane (Complex Source Point method CSP). This representation has been used by many authors in different ways to trace GBs through an optical system. Arnaud [12] used this representation combined with the ray matrix to find more accurate ways for modelling GB propagation through an optical system. Felsen *et.al* [13, 14, 15, 16, 17, 18] who have done the most extensive research on this method, used the CSP representation together with Complex Ray Tracing methods. Felsen *et.al* traced the rays originating from a source point to a typical observation point. The source is then transformed to a point in the complex plane and the propagation of a GB is modelled by rays originating from this complex point. As ray tracing is the basis of this method, the results are valid in the far field of the source. Quite lengthy search algorithms are needed to find the point of incidence for any observation point. These methods' strengths and weaknesses can be summarized as follows:

a) Strengths:

1. They are very accurate in the far field of the source.
2. Polarization of the fields are taken into account.
3. No assumptions are made a priori on the form of the reflected and refracted beams.
4. There are no limitations on the waists of the GBs and/or on the radii of curvature of the surface upon which the GB is incident.

b) Weaknesses:

1. Due to the lengthy search algorithms needed to find the point of incidence, these methods are relatively slow.

2. Only two dimensional problems have been considered.
3. General astigmatism is not explicitly taken into account.
4. Only flat and circular surfaces have been analyzed but, theoretically, the method can be extended to more complex surfaces.

2.1.3 Uniform Asymptotic Solution

Pathak *et.al* [19, 20] used the Green's function formulation (which can be shown to be equivalent to the Kirchhoff's integral representation) together with the physical optics approximation to find the reflection and diffraction of an arbitrary GB from a smooth surface with an edge. Pathak *et.al* explicitly used the physical optics approximation in far field radiation integrals (Green's function formulation). Assuming that the reflected beam from the surface under consideration remains a GB, they found a closed form for this beam using asymptotic methods to calculate the radiation integral. They developed closed form solutions to this problem. Their method is specifically developed for large reflector antennas, and the diffraction from the edges of the antenna is also taken into account. The only problem with this method is that it has been formulated for reflection of GBs from a smooth surface and therefore, the refraction of such beams into dielectric surfaces (lenses and other structure that are used in photonic structures) is not considered. Although, theoretically, it is possible to extend this method to refractive surfaces, such an extension is quite involved and can be the subject of a Ph.D thesis on its own. The strengths and weaknesses of this method is summarized below:

a) Strengths:

1. The method is extremely fast (closed form solution).
2. Polarization of the fields are taken into account.
3. Edge diffraction is taken into account.
4. General Astigmatism is implicitly taken into account.

b) Weaknesses:

1. They are developed only for reflective surfaces.
2. The reflected GB is assumed to remain a GB. This condition holds true only if the radii of curvature of the surface under consideration is at least twice the size of the beam waist at the point of incidence.

2.1.4 Other Methods

There are also other methods found in the literature *e.g* [21, 22, 23]. In [21] the scattering of a GB is found from a homogenous sphere by the combination of the CSP method and the exact analytical solution of the problem involving the scattering of a spherical wave from a sphere [2] The results which are exact in the paraxial regime, are only applicable to a homogenous sphere and can not be extended to other geometries. Nevertheless, they can be used to verify other approximate methods. Siegman [23] used direct phase matching to find the reflected and refracted scalar GBs from an ellipsoid. The axis of the GB in their work was assumed to be aligned with one of the axes of symmetry of the ellipsoid. In addition General Astigmatism and the vectorial nature of the GB were not considered.

2.1.5 GB Tracing method (GBT)

The Gaussian Beam Tracing method that is presented here, uses an extension of phase matching [24] as applied to GBs. It is an extremely fast, fully vectorial three dimensional method. Given an arbitrary Vectorial 3D General Astigmatic incident Gaussian Beam and the analytic equation of a surface (dielectric, conductor or any media that can be modelled by an effective dielectric constant), the parameters (waist, center and direction of propagation and the complex angle of rotation) [3]of the reflected and transmitted GBs are found using phase matching by approximating the surface with a quadratic function. Whenever a simple Astigmatic GB is incident on a non-orthogonal [25] surface, a General Astigmatic GB is produced; therefore, this kind of astigmatism is a very important and essential part of GBT. Fresnel reflection and transmission coefficients are then used to account for the vectorial nature of the beams considered. The method, therefore, takes the polarization of beams into account. Lenses and other similar structures can be analyzed by considering multiple reflections and refractions from the different surfaces of these structures. In this work the method has been verified by comparing the results with Physical Optics method and it has been applied to several practical problems. The accuracy of the method in calculating higher order abberations need to be investigated.

a) Strengths:

   1. The method is extremely fast (a number of algebraic equations).
   2. Polarization of the fields are taken into account.

[2]We had derived the same results without knowing about this work.
[3]Refer to Chapter (3)

3. Tilted and off axis surfaces can be analyzed with no difficulty.
4. General Astigmatism is explicitly taken into account.
5. No caustics are produced, upon any number of reflections and refractions.
6. Both reflective and refractive surfaces can be treated.

b) Weaknesses:

1. The reflected and refracted GBs from the surface are assumed to remain GB. This is valid if the radii of curvature of the surface under consideration is at least twice the waist of the incident GB at the point of incidence.
2. Edge Diffraction is not taken into account.

2.2 Gaussian Beam Expansion

To our knowledge the only well investigated method for discretization of an aperture field into a set of Gaussian elementary functions (which give rise to GBs) are based on Gabor series [26, 27, 28, 29, 30, 31] and the work by Pathak *et.al* [20]. In this research the Gabor representation [27] has been used. The work by Pathak *et.al* [20] is specifically designed for fast analysis of reflector antennas. In this special case the aperture (the feed of the reflector) is much smaller than the reflector; therefore, this method is not general enough to be extendable to arbitrary ratios of aperture to scatterer dimensions. In a hypothetical photonic structure this ratio could become very small (*e.g.* a fiber illuminating a thick lens) close to one (*e.g.* a large aperture laser illuminating a thick lens (Chapter(4))) or very large (*e.g.* a number of GBs with large waist illuminating a small lens.) A more general method is therefore needed. The Gabor series is such a general scheme. The waist of the GBs at the aperture plane in this method can be chosen virtually arbitrarily . The waists of the GBs at the aperture plane will then dictate their waist at the position of the scatterer. In [27] the Gabor series was used in 1D aperture field discretization. Following [27], Felsen *et.al* [28] developed a systematic method for one dimensional aperture discretization for narrow waisted, matched and large waisted 2D GBs. In Dec 2002 they extended their 2D formulation to a 2D aperture (3D GBs). The Gabor series inherently does not impose any restrictions on the size of the waists of the GB elementary functions. The recent work by Felsen *et.al* [29, 30] is based on a narrow waisted formulation. In this special case, the aperture field is sampled at different points. Parallel Stigmatic circular GBs with waists that are much smaller than the aperture dimensions are then launched from the aperture

plane. In this research, a method is proposed that would potentially extend this method to astigmatic GBs with arbitrary waists in one direction and narrow waists in the other direction.

2.3 Hybridizing the GB Expansion/Tracing with the Finite Difference Time Domain Method (FDTD)

The final topic in this research is the hybridization of the GB Expansion/Tracing with FDTD. FDTD has been investigated extensively in the past number of decades since its first 2D and 3D implementations [32, 33]. This method has been used in the Microwave and Photonics group at the University of Waterloo [34, 35, 4, 5, 6, 36, 37]. This work includes: hybridization of FDTD with ray tracing method for modelling of indoor radio wave propagation and the application of FDTD for studying of dielectric waveguide problems and modelling guided-wave junctions. Specific issues, such as truncating boundary conditions for FDTD are still areas of extensive research and can be the subject of several Ph.D theses. Although the implementation of an FDTD method is not a new contribution, nevertheless it became necessary and therefore a very suitable FDTD was written as part of this research. It should be noted that the main goal in this area, is the actual hybridization of the FDTD with GB Expansion/Tracing method. There were many challenges associated with this task and it forms a major contribution of this research.

Chapter 3

Vectorial General Astigmatic Gaussian Beam Tracing

In this chapter a novel Gaussian Beam Tracing method (GBT) is formulated. This method is based on the phase matching procedure introduced by Deschamps [24]. A similar formulation is derived in Appendix A for the sake of completeness. First, the simple astigmatic Gaussian Beam (GB) is defined as an analytic continuation of the geometictrical optics field. A GB is usually defined by a transformation of the z coordinate to the complex plane [11]. The procedure introduced in this chapter is a more general form of this transformation. Next the fundamental properties of a GB are described. The *General* Astigmatic GB is then defined by formally attaching a complex angle to the phase term of a simple GB. The novel GB tracing method, which is based on phase matching, is subsequently introduced. Examples are presented that demonstrate the speed of this method and its strengths and weaknesses. Finally a comparison is made between GB Tracing scheme and Physical Optics integrals which provided a simple verification for the method. This comparison identified the limits of validity of the method.

3.1 General Astigmatic GBs

Here the Vectorial General Astigmatic GB is introduced in a way which is both insightful and useful for the development of the other components of the hybrid method (this fact will be seen in later chapters) . Astigmatic rays and narrow bundles of rays (pencil of rays) are first introduced, Astigmatic GBs are then defined by transforming two of the elements of its curvature matrix. The standard defining formula of the GB can then be easily derived

from this form. It can then be verified that such a beam satisfies the paraxial Helmholtz equation. The Vectorial General Astigmatic GB is then found by formally attaching a complex value to the angular orientation of the coordinate system in which the GB is expressed . Throughout this work an $\exp(jwt)$ time dependence is assumed.

3.1.1 Narrow Bundles of Rays (Pencil of Rays)

It is shown in Appendix(B) that the leading term in the asymptotic representation (Lunberg-Kline) of the electric field yields the geometrical optics field:

$$\mathbf{E}(s) = \mathbf{E}(0)\sqrt{\frac{R_1 R_2}{(R_1+s)(R_2+s)}}e^{-jnks} \tag{3.1}$$

The rays that are very close to an axial ray are called a pencil of rays or a bundle of rays. The rays of a bundle are normal to a family of surfaces (the wavefronts). Normally a single ray passes through each point in space; therefore, the rays of a pencil constitute a so called *congruence*. This congruence is normal to a family of surfaces and is therefore called a normal congruence. It can be shown [38] that a normal congruence remains a normal congruence upon any number of reflections and refractions. Although the form of the field may change due to the change in radii of curvature. The field of an arbitrary paraxial ray in the bundle can be related to the axial ray Fig.(3.1)in the following manner (assuming that the axial ray is in the z direction and $k = nk_0$) :

$$\mathbf{e}(z) = \mathbf{e}(0)\sqrt{\frac{R_1 R_2}{(R_1+z)(R_2+z)}}e^{-jkz}$$

Because the rays in the pencil are very close to each other and they are nearly parallel, the variation of the amplitude with z is ignored; therefore if (x_1, x_2, z) is a point in space near the axial ray the following is obtained:

$$\mathbf{e}(x_1, x_2, z) = \mathbf{e}(0)\sqrt{\frac{R_1 R_2}{(R_1+z)(R_2+z)}}e^{-jk\phi(x_1,x_2,z)}$$

Where again $k = nk_0$ is used instead of k_0. Now from Fig(3.1) it is clear that $l_1 \simeq l_2$; therefore, the phase at point (x_1, x_2) is the phase at point $(0, 0, z)$ plus the normal distance (with a sign) of the phase front at (x_1, x_2, z) from the tangent plane at z or l_1. If the phase front is approximated by a quadratic function then:

$$l_1 = -\frac{1}{2}\mathbf{x}\bar{\mathbf{Q}}\mathbf{x}^T$$

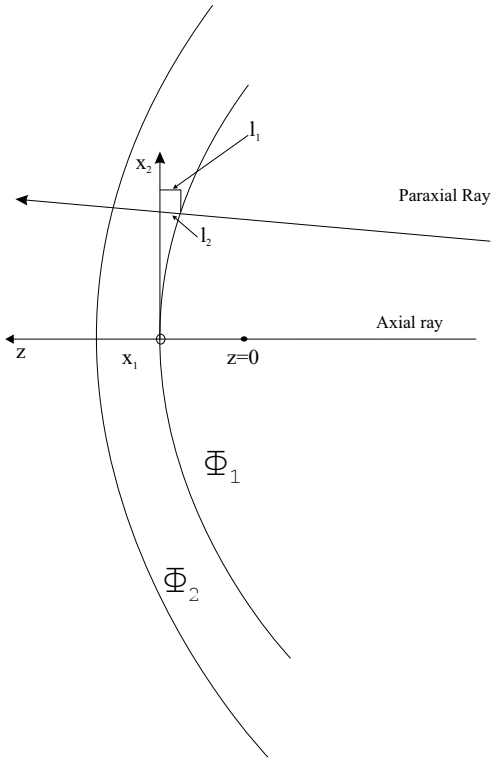

Figure 3.1: Two rays from a pencil of rays.

where $\mathbf{x} = [x_1, x_2]$ and $\bar{\mathbf{Q}}$ is a symmetric matrix called the curvature matrix (a diverging pencil is designated by a positive curvature). If $\hat{x}_1$ and $\hat{x}_2$ are taken in the direction of the lines of curvature [39] of the phase front then $\bar{\mathbf{Q}}$ would become diagonal:

$$\bar{\mathbf{Q}}(z) = \begin{bmatrix} \frac{1}{R_1+z} & 0 \\ 0 & \frac{1}{R_2+z} \end{bmatrix} \tag{3.2}$$

where R_1 and R_2 are the principal radii of curvature of the phase front at z. With any other choice for $\hat{x}_1$ and $\hat{x}_2$ then $\bar{\mathbf{Q}}$ will still be symmetric and it can be shown that the radii of curvature of the phase front are its eigenvalues [24]. Therefore the phase can be represented as:

$$\phi(x_1, x_2, z) = z + \frac{1}{2}\bar{\mathbf{x}}\bar{\mathbf{Q}}\bar{\mathbf{x}}^T$$

The amplitude variation can also be related to $\bar{\mathbf{Q}}$. It is obvious that if R_1 and R_2 are the principal radii of curvature of the phase front at $z = 0$, then the principal radii of curvature at z would be $R_1 + z$ and $R_2 + z$ and also:

$$\det \bar{\mathbf{Q}}(z) = \frac{1}{(R_1 + z)(R_2 + z)}$$

therefore:

$$\mathbf{e}(x_1, x_2, z) = \mathbf{e}(0)\sqrt{\frac{\det \bar{\mathbf{Q}}(z)}{\det \bar{\mathbf{Q}}(0)}}e^{-jk(z+\frac{1}{2}\bar{\mathbf{x}}\bar{\mathbf{Q}}\bar{\mathbf{x}}^T)} \tag{3.3}$$

3.1.2 Simple Astigmatic GB

A simple GB is usually defined by considering the solution to the free space Helmholtz equation (3D Green's function):

$$G = \frac{e^{-jkR}}{R}$$

and transforming the z coordinate to the complex plane $z \rightarrow z + jb$ (where b is a real number). If this function is substituted into Helmholtz equation and the paraxial approximation is utilized a simple GB is obtained [11]. In this work a more general approach is introduced. The real curvature matrix of an astigmatic ray is represented by Eqn.(3.2). As this equation is derived directly from Maxwell's equations and solutions of Maxwell's equations can be analytically continued to the complex plane by direct transformation of one coordinate, it is natural to define a more general curvature matrix in the following form:

$$\bar{\mathbf{Q}}(z) = \begin{bmatrix} \frac{1}{z-z_{0x}+jz_{rx}} & 0 \\ 0 & \frac{1}{z-z_{0y}+jz_{ry}} \end{bmatrix} = \begin{bmatrix} \frac{1}{q_x} & 0 \\ 0 & \frac{1}{q_y} \end{bmatrix} \tag{3.4}$$

z_{rx}, z_{ry}, z_{0x} and z_{0y} being real numbers. Therefore complex radii of curvature, $R_1 = -z_{0x} + jz_{rx}$ and $R_2 = -z_{0y} + jz_{ry}$ are assigned to the bundle of rays. When $z_{rx} = z_{ry} = z_r$ and $z_{0x} = z_{0y} = 0$, Eqn.(3.4) can be interpreted as a transformation of the origin of the coordinate system to the complex point $(0, 0, jz_r)$ [11]. Substituting Eqn.(3.4) into Eqn.(3.3) the following form (x_1 is replaced by y) is obtained:

$$\begin{aligned} \mathbf{E}(\mathbf{x}, \mathbf{y}, \mathbf{z}) &= \mathbf{E}(0)\sqrt{\frac{1}{q_x q_y}}\exp[-jk(z + \frac{1}{2}(\frac{x^2}{q_x} + \frac{y^2}{q_y})] \\ &= \mathbf{E}(0)\psi\exp(-jkz) \end{aligned} \tag{3.5}$$

It can be verified (through simple but rather long algebra) that ψ is a solution of the paraxial Helmholtz equation:

$$\frac{\partial^2\psi}{\partial x^2} + \frac{\partial^2\psi}{\partial y^2} - 2jk\frac{\partial\psi}{\partial z} = 0$$

Therefore, Eqn.(3.5) is valid in the paraxial regime, which was quite obvious as it was obtained from the equation of a bundle of paraxial rays. Following some straightforward algebra, Eqn.(3.5) can be written in the following standard form:

$$\mathbf{E}(x,y,z) = \mathbf{E_0}\frac{\sqrt{w_{0x}w_{0y}}}{\sqrt{w_x(z)w_y(z)}}\exp\{-jk[z+\frac{1}{2}(\frac{x^2}{q_x(z)}+\frac{y^2}{q_y(z)})]+j\eta(z)\} \tag{3.6}$$

where:

$$\begin{aligned}
\frac{1}{q_i(z)} &= \frac{1}{R_i(z)} - j\frac{\lambda}{\pi n w_i^2(z)} \\
w_i(z) &= w_{0i}\sqrt{1+(\frac{z-z_{0i}}{z_{ri}})^2} \\
R_i(z) &= (z-z_{0i})[1+(\frac{z_{ri}}{z-z_{0i}})^2] \\
z_{ri} &= \frac{w_{0i}^2 n\pi}{\lambda} \quad \text{for} \quad i=x,y \\
\eta(z) &= \frac{1}{2}\tan^{-1}(\frac{z-z_{0x}}{z_{rx}}) + \frac{1}{2}\tan^{-1}(\frac{z-z_{0y}}{z_{ry}}) \\
\mathbf{E}_0 &= E_{0x}\hat{x} + E_{0y}\hat{y}
\end{aligned} \tag{3.7}$$

This is called a *Simple* Astigmatic GB. The properties of an Astigmatic GBs can be found in [9]. The spots of such beam are ellipses. The minimum waist in the x and y directions, w_{0x} and w_{0y} as well as their positions z_{0x} and z_{0y} are different. The plot of $R(z)$, $w(z)$ and $\eta(z)$ for a simple GB are given in Fig.(3.2). As it is well known, GBs are very good approximations for the output of laser sources. Furthermore because most of the energy of the GB is confined to the space near its waist, it represents a much better basis function for tracing formalisms than the plane wave, therefore GBT forms the base of the Hybrid method created in this work.

3.2 General Astigmatic Gaussian Beams (GAGB)

When a simple astigmatic GB passes through a non-orthogonal system, such as a sequence of astigmatic lenses placed at oblique angle relative to one another, it has been shown experimentally [25] that a new form of beam is formed, whose elliptical spot rotates as the beam propagates in free space. This is called a *General* astigmatic gaussian beam. Arnaud and Kogelnik [25] showed that a General Astigmatic GB can be formally obtained "by attaching a complex value to the angular orientation" of the coordinate system in which

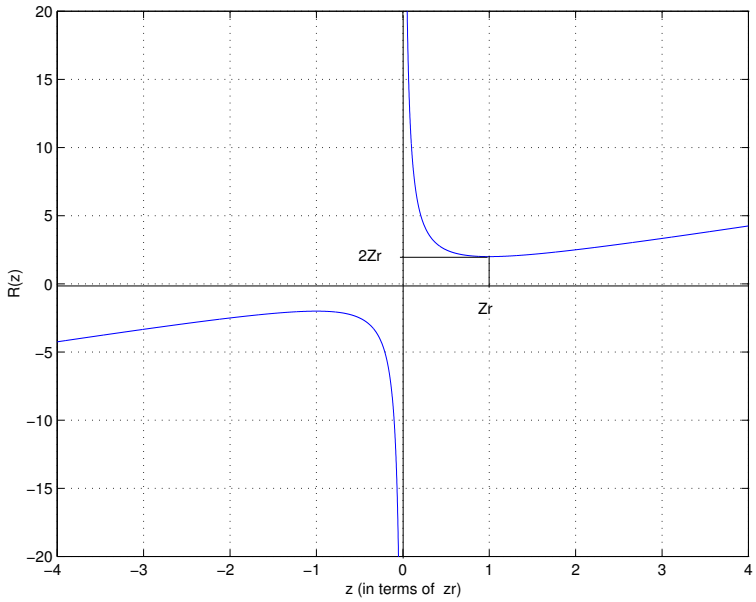

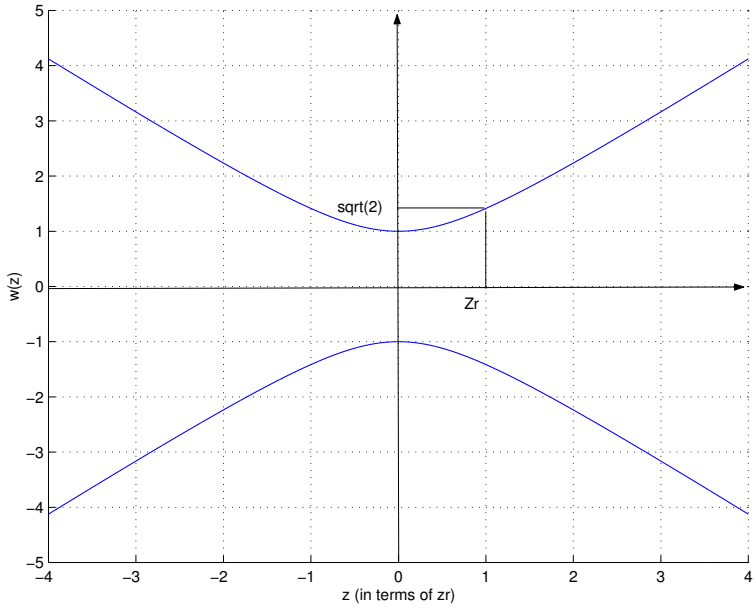

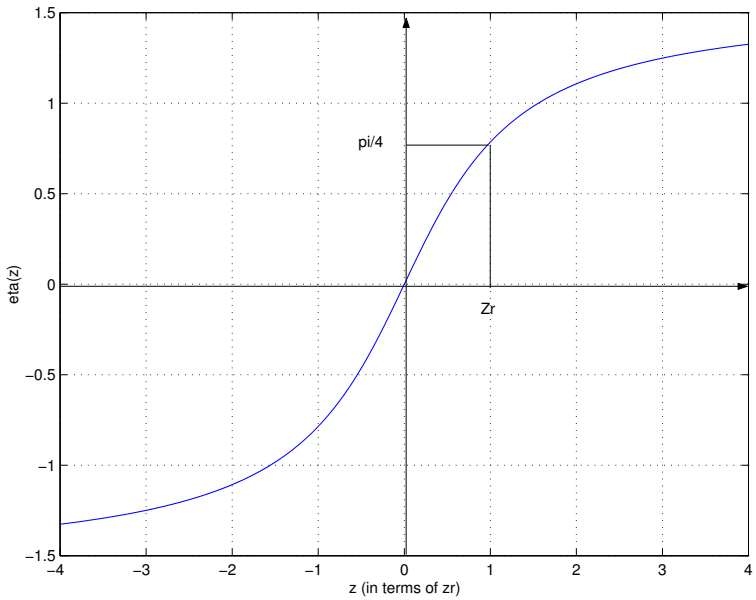

Figure 3.2: $R(z)$, $w(z)$ and $\eta(z)$ of a simple GB

the GB is expressed , and a typical ray fixed coordinate system. Under such complex rotation angle ϕ of the coordinate system, the GB curvature matrix becomes:

$$\bar{\mathbf{Q}}_{\phi} = \bar{\mathbf{J}}_{\phi}\bar{\mathbf{Q}}\bar{\mathbf{J}}_{-\phi} \tag{3.8}$$

$$\bar{\mathbf{J}}_{\phi} = \begin{bmatrix} \cos\phi & \sin\phi \\ -\sin\phi & \cos\phi \end{bmatrix} \tag{3.9}$$

where $\phi = a + jb$ is complex. For such a beam a principal coordinate system can not be defined as it is not possible to eliminate the cross term in both phase and amplitude functions in any coordinate system. In other words the principal coordinate system changes as the beam propagates through free space. It has been shown that for such a General Astigmatic GB the ellipses of irradiance and also the ellipse of phase rotate as the beam propagates in free space, while they maintain a fixed angle relative to one another. It has also been shown that the axes of these quadratic forms can never be aligned. Although a principal coordinate system is not defined for such a beam, it is completely specified by its curvature matrix $\bar{\mathbf{Q}}$ and the complex angle ϕ in a specified ray fixed coordinate system. The GBT method presented in this thesis can handle GAGB very efficiently. This is due to the fact that here the main parameter of interest is the curvature matrix of a GB. For a GAGB this matrix is complex but nevertheless symmetric. Therefore at any point it can be diagonalized and the parameters of the GAGB can then be extracted. This is explained in detail at the end of the next section.

3.3 Reflection and Transmission from a General Curved Surface

Consider a Vectorial GAGB that is incident upon a general curved surface, Fig(3.3). It is assumed that at the point of incidence the waist of the incident beam is smaller than the radii of curvature of the surface. It can be shown that in this case the reflected and transmitted beams are very close to GBs. It has been verified (Sec.3.9)that if the radii of curvature of the surface is twice the beam waist at the point of incidence, the GBT method yields very good results. The goal is to find the reflected and transmitted beams from the interface once the incident beam is known. For this problem two different coordinate systems are considered:

1. Main Coordinate system (x, y, z) is a fixed coordinate system in which the equation of the interface is known.

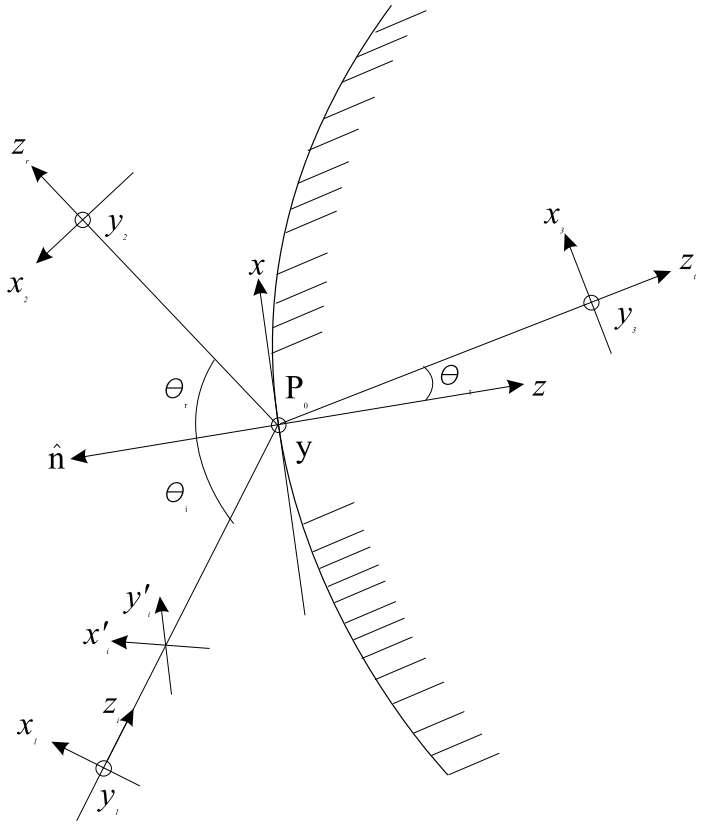

Figure 3.3: The geometry of GB reflection and transmission

2. (x_l, y_l, z_l) refers to the ray fixed coordinate system [40] for $l = 1, 2, 3$ for incident, reflected and transmitted respectively. $[x_1, y_1]$ is denoted by $\mathbf{x}_1$.
The point of incidence with the surface $z = f(x, y)$ is P_0. The normal vector to the surface at the point of incidence is given by

$$\hat{n} = \vec{\nabla}(f(x, y) - z)$$

The reflection and transmission directions are determined from Snell's laws:

$$\hat{z_i}.\hat{n} = \hat{z_r}.\hat{n} \quad \text{or} \quad \theta_i = \theta_r \quad \text{(Law of reflection)} \tag{3.10}$$

$$n_1(\hat{s_i} \times \hat{n}) = n_2(\hat{s_t} \times \hat{n}) \quad \text{or} \quad n_1 sin\theta_i = n_2 sin\theta_t \quad \text{(Law of refraction)} \tag{3.11}$$

where n_1 and n_2 are the refractive indices of the two media shown in Fig(3.3). The case of reflection from a perfect conductor can also be easily handled. The angle of incidence, reflection and transmission are denoted by θ_i, θ_r and θ_t. Once these directions are known the ray fixed coordinate system of the incident, reflected and transmitted beams can be found from (see for example [41]):

$$\begin{aligned}
\hat{x_1} &= \frac{\hat{z_i} \times (\hat{n} \times \hat{z_i})}{|\hat{z_i} \times (\hat{n} \times \hat{z_i})|} \\
\hat{x_2} &= -\frac{\hat{z_r} \times (\hat{n} \times \hat{z_r})}{|\hat{z_r} \times (\hat{n} \times \hat{z_r})|} \\
\hat{x_3} &= \frac{\hat{z_t} \times (\hat{n} \times \hat{z_t})}{|\hat{z_t} \times (\hat{n} \times \hat{z_t})|} \\
\hat{y_l} &= \hat{z_l} \times \hat{x_l} \quad \text{for} l = i, r, t
\end{aligned} \tag{3.12}$$

Being a slowly varying function of z, $\eta(z)$ is dropped [9] as it does not contribute to the changes of phase on the surface which are of primary importance, and has only a bulk effect (for example produces a phase shift of $\frac{\pi}{4}$ at the Raleigh range z_r). The effect of η is taken into account at the last stage of the method Eqn.(3.24). The phases of the incident, reflected and refracted GBs can then be expressed as:

$$\begin{aligned}
&k_1(z_i + \frac{1}{2}\mathbf{x}_1\bar{\mathbf{Q}}_i\mathbf{x}_1^T) \\
&k_1(z_r + \frac{1}{2}\mathbf{x}_2\bar{\mathbf{Q}}_r\mathbf{x}_2^T) \\
&k_2(z_t + \frac{1}{2}\mathbf{x}_3\bar{\mathbf{Q}}_t\mathbf{x}_3^T)
\end{aligned} \tag{3.13}$$

respectively. The phases of the incident, reflected and transmitted beams are matched at points near P_0 in a manner described in [24] and [40]. The only difference here is that

the components of the curvature matrix are complex numbers, but this does not alter the results in any way. The curvature matrix of the reflected and transmitted beams are found from:

$$\bar{\mathbf{Q}}_r = (\bar{\mathbf{K}}_r)^{-1}[\bar{\mathbf{K}}_i^T\bar{\mathbf{Q}}_\mathbf{i}\bar{\mathbf{K}}_i + \bar{\mathbf{C}}(\cos\theta_i + \cos\theta_r)](\bar{\mathbf{K}}_r)^{-1} \tag{3.14}$$

$$\bar{\mathbf{Q}}_t = \frac{n_1}{n_2}(\bar{\mathbf{K}}_t)^{-1}[\bar{\mathbf{K}}_i^T\bar{\mathbf{Q}}_\mathbf{i}\bar{\mathbf{K}}_i + \bar{\mathbf{C}}(\cos\theta_i - \frac{n_2}{n_2}\cos\theta_t)](\bar{\mathbf{K}}_t)^{-1} \tag{3.15}$$

with:

$$\bar{\mathbf{K}}_r = \begin{bmatrix} -\cos\theta_r & 0 \\ 0 & 1 \end{bmatrix}$$

$$\bar{\mathbf{K}}_t = \begin{bmatrix} \cos\theta_r & 0 \\ 0 & 1 \end{bmatrix}$$

$\bar{\mathbf{C}}$ is the curvature matrix of the surface defining the interface relative to the main coordinate system. The fact that the off diagonal elements of $\bar{\mathbf{Q}}_r$ are given by [42]:

$$2C^{11}\cos\theta_i + Q_i^{12}$$

and the off diagonal elements of $\bar{\mathbf{Q}}_t$ are given by:

$$\frac{\sec\theta_t}{k_2}(k_1\cos\theta_i Q_i^{12} - (k_1\cos\theta_i - k_2\cos\theta_t)C^{12})$$

(Q^{ij} and C^{ij} represent the elements of $\bar{\mathbf{C}}$ and $\bar{\mathbf{Q}}$) shows that for any arbitrary choice of $\bar{\mathbf{Q}}_i$ and $\bar{\mathbf{C}}$ (real or imaginary) the curvature matrix of the reflected and transmitted beams are symmetric and can therefore be diagonalized. Once these matrices are diagonalized the eigenvalues or the diagonal elements of the resultant matrix yield the reciprocal of q_x and q_y's of these beams. The real part is the reciprocal of the $R(z)$ and the imaginary part can be used to find the spot size $w(z)$. See Eqn.(3.7). The waist and the position of the waist of the beams can then be found from: (All the subscripts are dropped for convenience)

$$g = \frac{\lambda(z - z_0)}{\pi w_0^2 n}$$

then:

$$g = -\frac{Re[\frac{1}{q}]}{Im[\frac{1}{q}]}$$

and :

$$w_0 = \sqrt{\frac{w(z)}{(1+g^2)}} \tag{3.16}$$

$$z_0 = -\frac{R(z)g^2}{(1+g^2)} \tag{3.17}$$

Now if it is assumed that,

$$\bar{\mathbf{V}} = \begin{bmatrix} v_{11} & v_{12} \\ v_{21} & v_{22} \end{bmatrix}$$

is a matrix whose columns are eigenvectors of $\bar{\mathbf{Q}}_r$ or $\bar{\mathbf{Q}}_t$. This matrix is normalized by dividing each element by $\sqrt{v_{11}v_{11} + v_{21}v_{21}}$ (not by the norm of the eigenvector)[42]. The complex rotation matrix of each beam relative to its ray fixed coordinate system is obtained by finding the inverse cosine (on the appropriate branch) of the first element of the normalized matrix. Note that the origin of the reflected and refracted beams are taken to be the point of incidence. The only remaining unknowns are the amplitudes of the reflected and refracted beams.

3.4 Determination of the Amplitude of the Reflected and Transmitted Beams

The amplitudes of the reflected and transmitted beams are found from Fresnel coefficients:

$$\begin{bmatrix} E_y^r(P_0) \\ E_x^r(P_0) \end{bmatrix} = \bar{\mathbf{R}}(P_0) \begin{bmatrix} E_y^i(P_0) \\ E_x^i(P_0) \end{bmatrix} \tag{3.18}$$

$$\begin{bmatrix} E_y^t(P_0) \\ E_x^t(P_0) \end{bmatrix} = \bar{\mathbf{T}}(P_0) \begin{bmatrix} E_y^i(P_0) \\ E_x^i(P_0) \end{bmatrix} \tag{3.19}$$

where the matrices $\bar{\mathbf{R}}(P_0)$ and $\bar{\mathbf{T}}(P_0)$ are defined as:

$$\bar{\mathbf{R}}(P_0) = \begin{bmatrix} R_{TE} & 0 \\ 0 & R_{TM} \end{bmatrix} \tag{3.20}$$

$$\bar{\mathbf{T}}(P_0) = \begin{bmatrix} T_{TE} & 0 \\ 0 & T_{TM} \end{bmatrix} \tag{3.21}$$

$$\begin{aligned} R_{TE} &= \frac{\sin(\theta_t - \theta_i)}{\sin(\theta_t + \theta_i)} \\ R_{TM} &= \frac{\tan(\theta_t - \theta_i)}{\tan(\theta_t + \theta_i)} \\ T_{TE} &= \frac{2\cos\theta_i \sin\theta_t}{\sin(\theta_t + \theta_i)} \\ T_{TM} &= \frac{2\cos\theta_i \sin\theta_t}{\sin(\theta_i + \theta_t)\cos(\theta_i - \theta_t)} \end{aligned} \tag{3.22}$$

(3.23)

Assuming l is the distance between the origin of the incident beam and P_0, and that the electric vector of this beam is given in its ray fixed coordinate system, the following definition are made:

$$E_{0i}(P_0) = \frac{\sqrt{w_{0ix}w_{0iy}}}{\sqrt{w_{ix}(l)w_{iy}(l)}}\exp(-jk_1 l + j\eta_i(l)) \tag{3.24}$$

$$A_r = \frac{\sqrt{w_{0rx}w_{0ry}}}{\sqrt{w_{rx}(0)w_{ry}(0)}}\exp(j\eta_r(0))$$

$$A_t = \frac{\sqrt{w_{0tx}w_{0ty}}}{\sqrt{w_{tx}(0)w_{ty}(0)}}\exp(j\eta_t(0))$$

Taking the effect of the ignored $\eta(z)$ term into account the following is obtained:

$$\vec{E}_r = \vec{E}_r(0)\frac{\sqrt{w_{0rx}w_{0ry}}}{\sqrt{w_{rx}(z_r)w_{ry}(z_r)}} \qquad \exp\{-jk_1[z_r + \frac{1}{2}(\frac{x_2^2}{q_{rx}(z_r)} + \frac{{y_2}^2}{q_{ry}(z_r)})] + j\eta_r(z_r)\}$$

$$\vec{E}_t = \vec{E}_t(0)\frac{\sqrt{w_{0tx}w_{0ty}}}{\sqrt{w_{tx}(z_t)w_{ty}(z_t)}} \qquad \exp\{-jk_2[z_t + \frac{1}{2}(\frac{x_3^2}{q_{tx}(z_t)} + \frac{{y_3}^2}{q_{ty}(z_t)})] + j\eta_t(z_t)\}$$

where:

$$\vec{E}_r(0) = (E_x^i(0)R_{TM}\hat{x}_2 + E_y^i(0)R_{TE}\hat{y}_2)\frac{E_{0i}(P_0)}{A_r}$$

$$\vec{E}_t(0) = (E_x^i(0)T_{TM}\hat{x}_3 + E_y^i(0)T_{TE}\hat{y}_3)\frac{E_{0i}(P_0)}{A_t}$$

$$\vec{E}_i(0) = E_x^i(0)\hat{x}_1 + E_y^i(0)\hat{y}_1$$

3.5 2D GBT

The FDTD used in this work is a 2D FDTD, therefore a 2D GBT is needed. The formulation of the two dimensional Gaussian beam tracing can not be directly derived from the 3D case and is therefore given in Appendix C.

3.6 The Pulsed GB

It must be noted that through out this work only time harmonic GBs are considered. The temporal form a GB can obviously be other than $\exp(jwt)$. An aperture field whose both temporal and spatial dependency are Gaussian is an example that creates such a field in free space. The properties of Pulsed GBs and their applications have been investigated in the literature mainly by Felsen et. al. [43]- [51] and other groups [52]-[56]). In this work

when a GB is needed in its time domain form it is obtained by multiplying its phasor by $\exp(jwt)$ and taking the imaginary part and dividing by j. A sine function is used because it is more suitable for future combination with the FDTD method. Therefore for a 2D GB (Appendix C) the following time domain form is obtained:

$$E = \Im\{\exp(j\omega t)\sqrt{\frac{jb}{z+jb}}\exp(-jkz - \frac{jk}{2}\frac{x^2}{z+jb})\}/j \tag{3.25}$$

. If the initial driving function has a Gaussian temporal dependency, it will also have a Gaussian spectrum. Therefore the electric field can be obtained from:

$$E(x,z,t) = \int_{-\infty}^{\infty} \tilde{F}(w)\sqrt{\frac{jb}{z+jb}}\exp(-jkz - \frac{jk}{2}\frac{x^2}{z+jb})dw \tag{3.26}$$

Where $\tilde{F}(w)$ is the Fourier transform of the driving temporal pulse. If this integral is evaluated it can be shown [55, 56] there is a coupling between the GB parameters in space and time. The spatial variables become present in the time shape of the pulse and the pulse width effects the phase of the spatial form. Therefore the GB does not retain its Gaussian shape as the beam propagates in free space. If a similar GBT can be formulated for a pulsed GB then the hybrid method can be used for spectral analysis of a photonic system. The derivation of a pulsed GBT is part our future work.

3.7 Goos-Hanchen Shift

It is well known fact [57] that a GB incident on a dielectric interface from a denser medium on a less dense medium, with an angle larger than the critical angle, undergoes a spatial shift. This is due to the fact that the reflection coefficient at an incidence angle greater than the critical angle has unit amplitude but a finite phase. A plane wave is not spatially affected by this phase shift as the spatial extent of a plane wave is infinite. On the other hand a spatial shift (actual shift in the position of the reflected beam) is produced by this shift for a GB. This shift has been calculated in the literature [58]-[64] The classical derivations are given in [58] and [60] but under the assumption that the beam waist is much smaller than the wavelength. The calculation of the Goos-Hanchen shift is greatly simplified in this case and closed form solutions can be obtained. In [57] it is assumed that the phase front of the GB is flat therefore again greatly simplifying the calculation

of the shift. A closed form expression for the shift for a simple GB (not to mention a GAGB) with arbitrary waist does not exist. A closed form Fourier transform of a simple GB does not exist, therefore in order to rigorously calculate the Goos-Hanchen shift the Fourier transform has to be calculated numerically. This was performed for a number of different launch angles and beam waists. The Fourier transform of a GB travelling at an angle θ was calculated. If this transform is denoted by $\tilde{F}(w - w_0)$ where $w_0 = k \sin\theta$ it was observed that in retrieving the original GB through inverse Fourier transform, the main contribution is from the neighborhood of $w = k \sin\theta$. Therefore it was concluded that the results obtained in [57] are approximately correct. This shift has to be taken into account in dielectric guiding structures where the field is trapped between two dielectric surfaces due to total internal reflection. As guiding structures are not part of this research we have not included this shift in this work, although it has been taken into account elsewhere [65]. In Fig.(3.4) the Goos-Hanchen shift between two dielectric surfaces has been qualitatively depicted.

3.8 Numerical Examples

3.8.1 Example I

As a first example the reflected and transmitted beams from a rotated cylindrical surface have been determined. The incident beam is an elliptical GB with waists of $5\mu m$ and $20\mu m$. This beam hits a cylindrical lens, which is rotated about the z axis at an angle of 45 degrees. Because of this rotation, the expression of the cylindrical surface would have a cross product term (xy) in the ray fixed coordinate system and thus is an nonorthogonal system. The beam is therefore transformed into a general astigmatic GB. The geometry of the problem is shown in Fig.(3.5). The parameters of the incident, transmitted and reflected beams are shown in Tables (3.1 and 3.2).

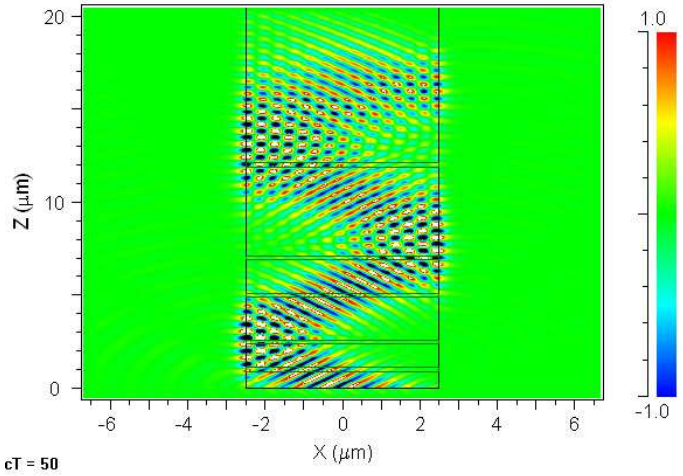

(a)

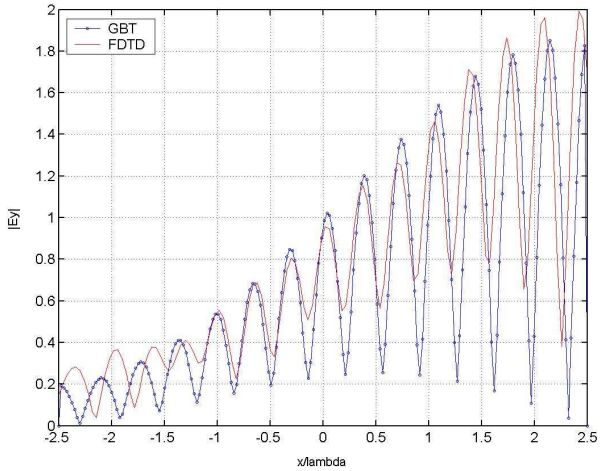

(b)

Figure 3.4: Comparison of GBT with FDTD for a slab waveguide at z=7μm

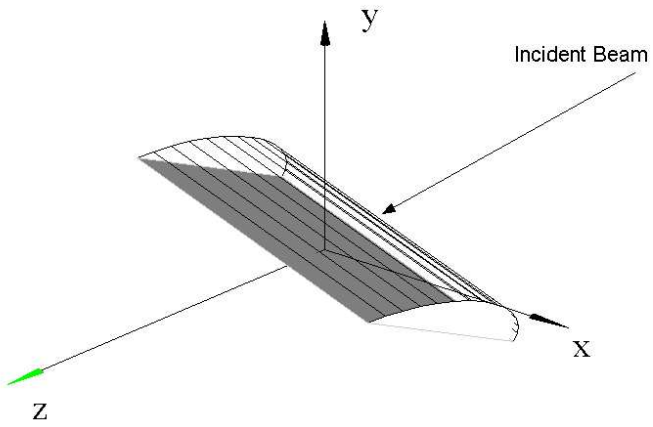

Figure 3.5: The geometry of the problem

Surface	$z = -\sqrt{(50e-6)^2 - \frac{x^2}{2} - \frac{y^2}{2} - \sqrt{(2)xy}}$
w_{0x}	$5\mu m$
w_{0y}	$20\mu m$
z_{0xi}	-100μm
z_{0yi}	-100 μm
E_{0xi}	1
E_{0yi}	1
λ	1.31e-6
n_1	1
n_2	2.5
$\phi = \alpha + j\beta$	0+0j

Table 3.1: Parameters of the incident GB.

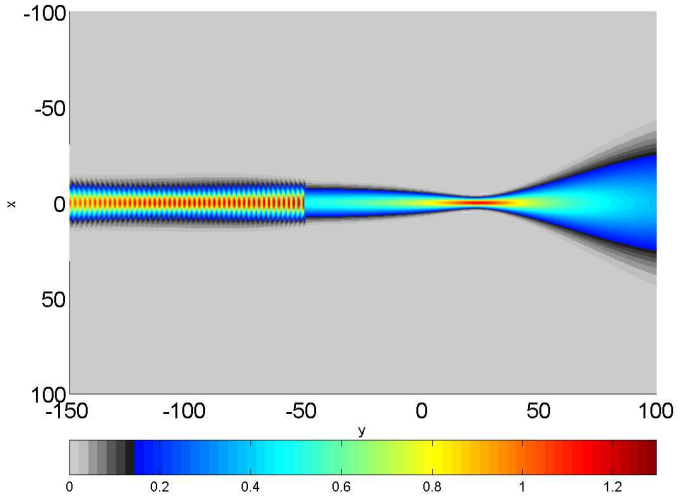

(a)

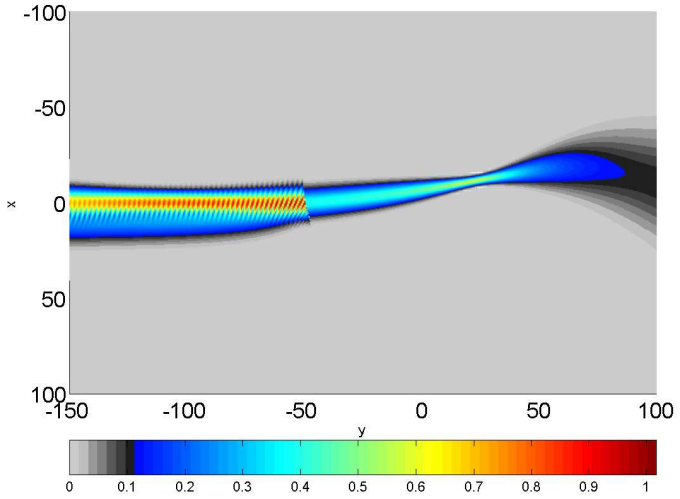

(b)

Figure 3.6: Top XZ view of the field at (a) y=0 and (b) $10\mu m$ respectively, the units are in microns

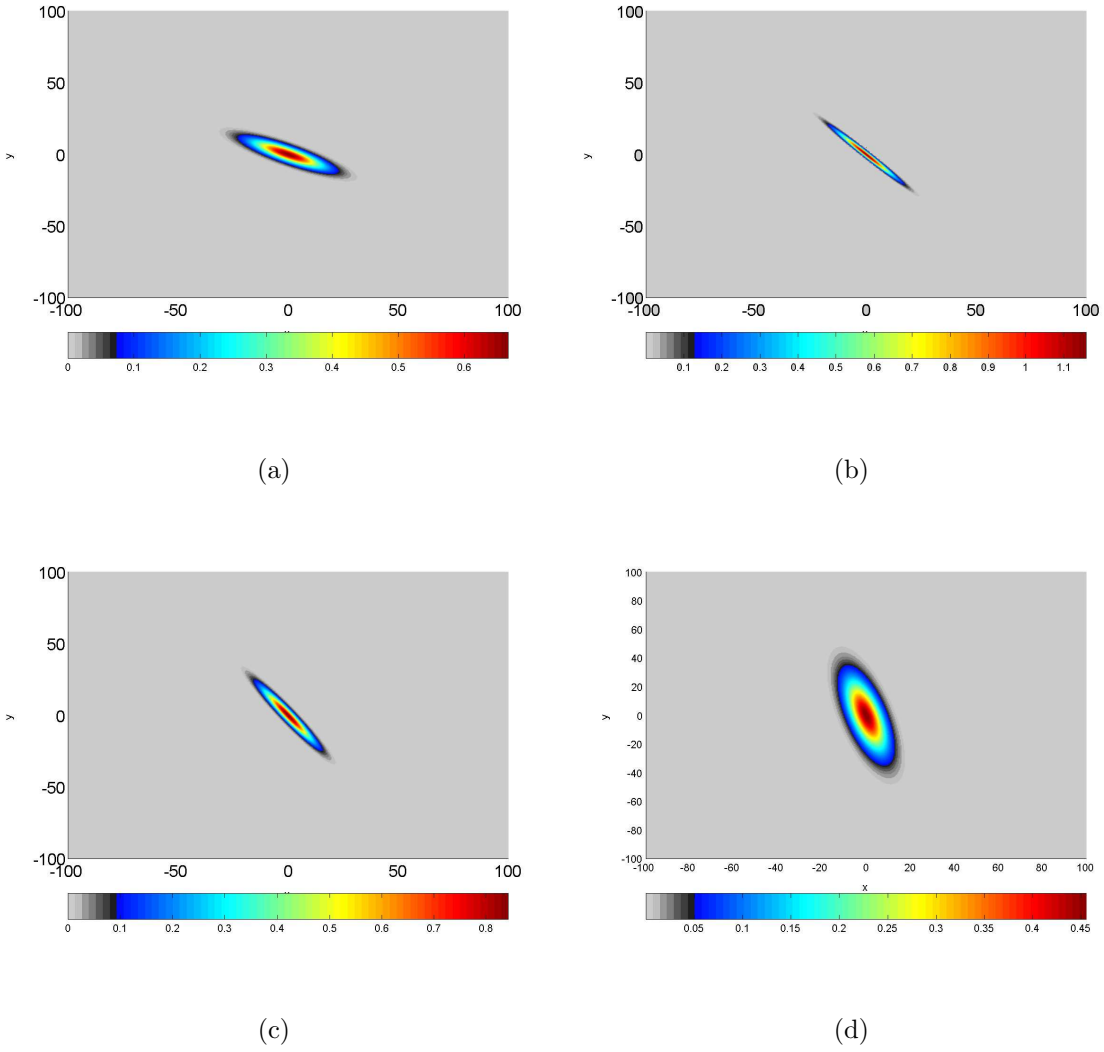

(a) (b)

(c) (d)

Figure 3.7: (a),(b),(c),(d) Top XY view of the field at z=-10, 25, 40 and 80μm the units are in microns

w_{0xt}	$.931\mu m$	w_{0xr}	$4.04\mu m$
w_{0yt}	$6.457\mu m$	w_{0yr}	$1.31\mu m$
z_{0xt}	$-18.41\mu m$	z_{0xr}	$-171.9\mu m$
z_{0yt}	$103.5\mu m$	z_{0yr}	$74.3\mu m$
E_{0xt}	$0.96 - j0.93$	E_{0xr}	$1.84 - j0.47$
E_{0yt}	$-0.96 + j0.93$	E_{0yr}	0
$\phi = \alpha + j\beta$	$0.71 + j0.074$	$\phi = \alpha + j\beta$	$0.69 + j0.097$

Table 3.2: Transmitted and Reflected Beams' Parameters

3.8.2 Example II

As a second example GBT was used to find the collimating effect of a hyperbolic surface of revolution. As it can be seen in Fig.(3.9) the method correctly predicts a nearly constant phase which is an indication of the flatness of the wavefront. The incident GB was placed at the focal plane of the hyperbola and due to the fact that its waist was chosen to be small, it behaves similar to a spherical wave. The equation of the hyperbola is given by

$$z = \frac{n_2 F}{n_2 + 1} + r_c \sqrt{(}1 + \frac{n_2 + 1}{n_2 - 1} \frac{(x^2 + y^2)}{F^2})$$

where n_2 is the refractive index of the lens and is assumed to be 1.435, F is the focal length of the lens and is equal to $100mm$, $r_c = F/(n_2 + 1)$ and the wavelength is $2.667mm$. The waist of the beam is $4.14mm$ and it is placed at a distance of $95.8mm$ from the surface to achieve the desired $100mm$ curvature at incidence.

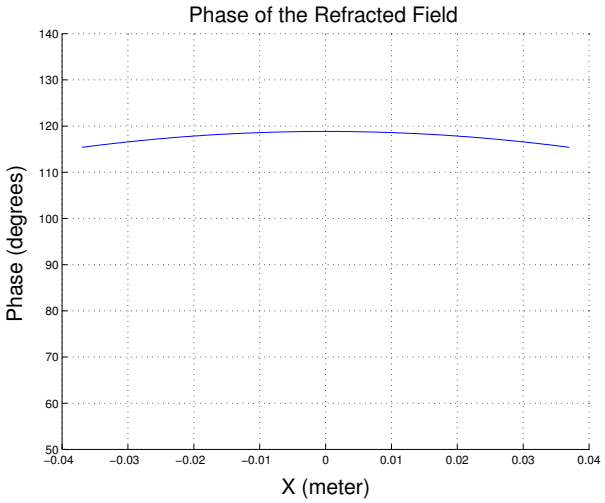

Figure 3.8: Phase of the field after passing through the surface.

3.8.3 Example III

As a third example, the effect of a ball lens placed in front of a GB was determined. Ball lenses are small (usually glass) spheres used in photonic structures to collimate GBs. GBT was used repeatedly (multiple reflections)to find the output field. The first beam creates a reflected and transmitted beam. The transmitted beam then creates a reflected and transmitted beam and so on. Six internal reflections were considered in this example. More reflections are not needed due to the fact that the reflection coefficient is always less than one and therefore the beam amplitude becomes smaller and smaller after each reflection. The standing wave inside the ball lens due to multiple reflections as well as the imperfect collimation of the ball lens should be noted. As mentioned before, this method is extremely fast (it takes less than a second to analyze this structure on a P4 3 GHz). Therefore, it can be used to optimize, for example, the position of the ball lens for optimum collimation (see Figs.(3.10,3.11)).(The distances are given in terms of wavelength.)

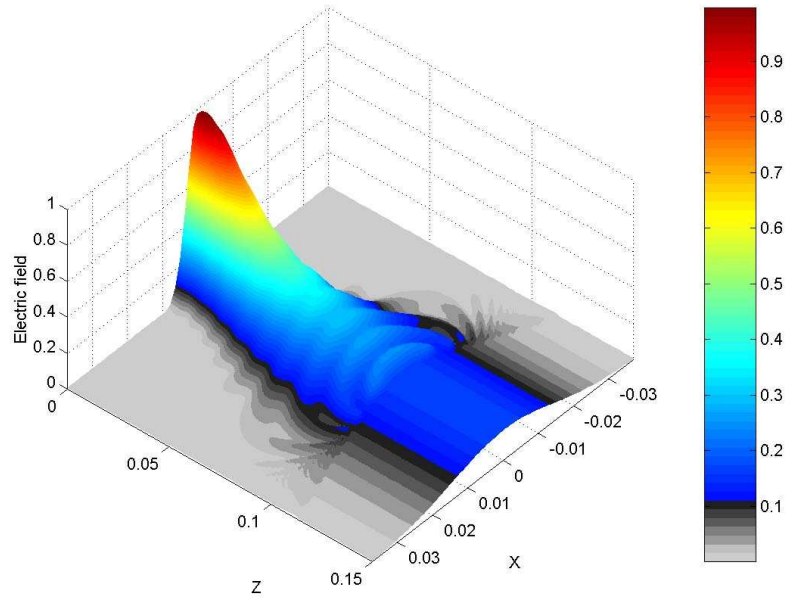

(a)

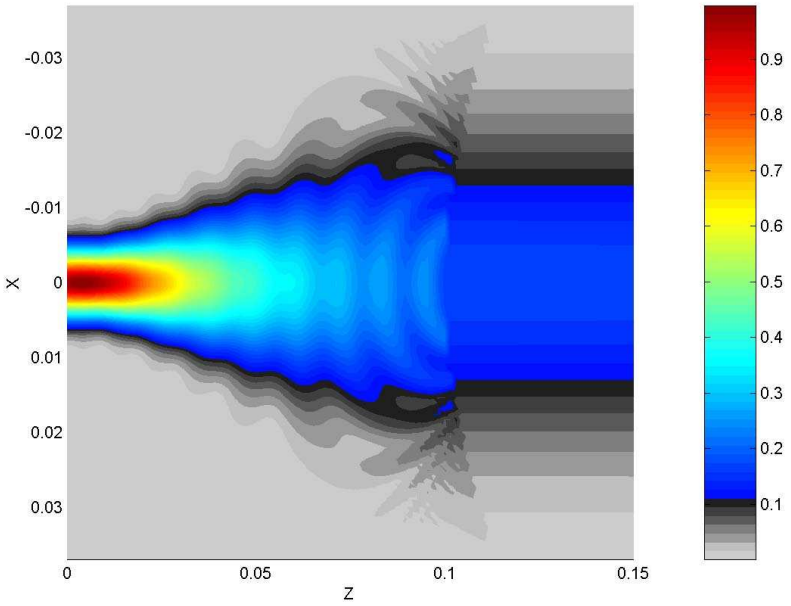

(b)

Figure 3.9: 3D XZ and top XZ view of the field

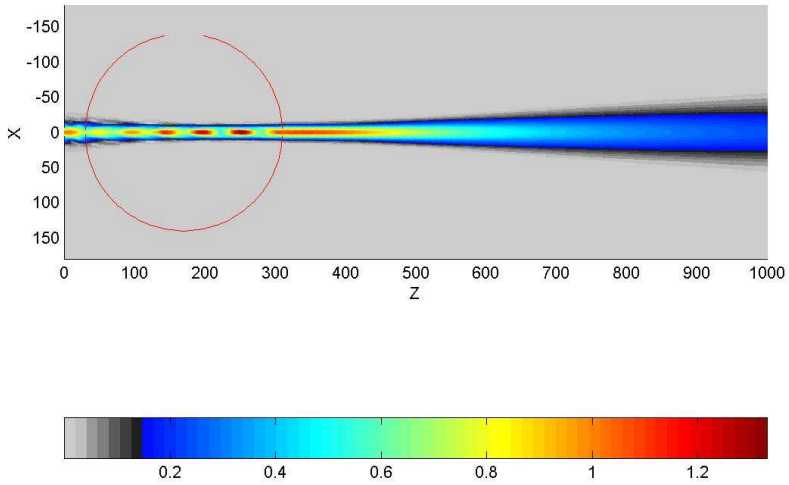

Figure 3.10: GB passing through a ball lens

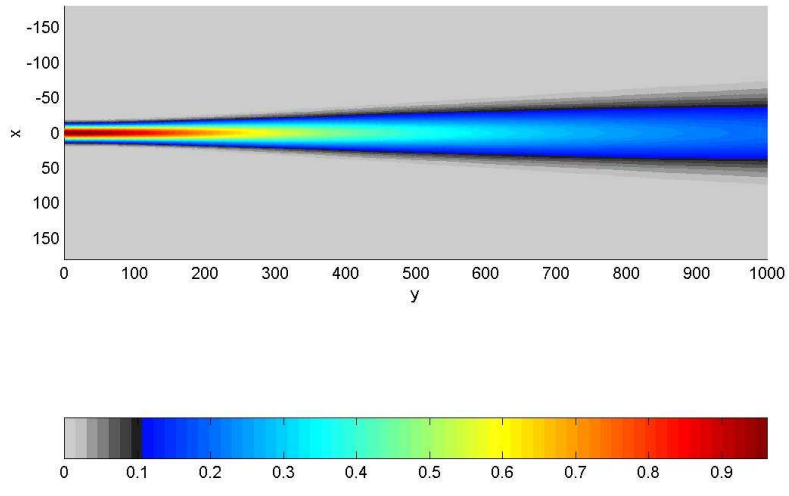

Figure 3.11: GB propagating in free space

3.9 Verification

In this section the results of GBT are compared with the physical optics (PO) method in a manner similar to [66]. To apply PO to this problem (reflection and refraction of a GB from a curved surface) the equivalent electric and magnetic sources on the surface must be found.

$$\vec{J}_{eq} = \hat{n} \times \vec{H}$$

$$\vec{M}_{eq} = -\hat{n} \times \vec{E}$$

where $\vec{E}$ and $\vec{H}$ are the total fields on the surface and $\hat{n}$ is the outward normal (towards the region including the incident beam). Determining these rigorously is not an easy task. Following the method of [66] these total fields are approximated by the physical optics fields over the surface:

$$\vec{J}_{eq} = \vec{J}_{PO} = \hat{n} \times (\vec{H}_i + \vec{H}_r)$$

$$\vec{M}_{eq} = \vec{M}_{PO} = -\hat{n} \times (\vec{E}_i + \vec{E}_r)$$

and $\vec{E}_r$ and $\vec{H}_r$ are found under the assumption that the fields act locally as plane waves and Fresnel coefficients are applicable. The fields inside S are found from the equivalent sources:

$$\vec{J}_{eq} = -\vec{J}_{PO}$$

$$\vec{M}_{eq} = -\vec{M}_{PO}$$

Radiation integrals are then used to find the fields inside and outside of S [67]. Two of these integrals are given below and the rest of the components can be found in [67]:

$$E_{Ax} = \frac{-j\eta}{4\pi\beta} \iint_s \{G_1 J_x + (x-x')G_2[(x-x')J_x + (y-y')Jy + (z-z')Jz]\} e^{-j\beta R} ds'$$

$$E_{Fx} = \frac{-1}{4\pi} \iint_s [(z-z')M_y - (y-y')M_z] G_0 e^{-j\beta R} ds'$$

where:

$$G_0 = \frac{1 + j\beta R}{R^3}$$

$$G_1 = \frac{-1 - j\beta R + \beta^2 R^2}{R^3}$$

$$G_2 = \frac{3 + j3\beta R - \beta^2 R^2}{R^5}$$

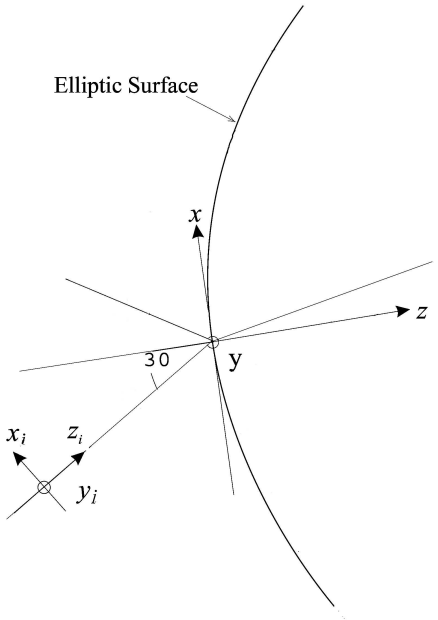

Figure 3.12: The Geometry of the problem used for verification

where ds' is the element of area of the surface over which these integrals must be evaluated. If this surface is given in terms of $(x', y', f(x', y'))$ then this element of area is given by:

$$ds' = \sqrt{1 + (\frac{\partial f}{\partial x})^2 + (\frac{\partial f}{\partial y})^2} dx' dy'$$

and therefore the integrals become normal double integrals in terms of x' and y'. It must be noted that z' in the above formulas has to be expressed in terms of x', y'. As a specific example, the oblique incidence at 30 degrees of a GB with $w_{0x} = 10\mu m$ and $w_{0y} = 5\mu m$ on an elliptic surface was considered. The distance of the waist to the surface is $100\mu m$ and the equation of the surface is $z = \frac{1}{200\lambda}(\frac{x^2}{1} + \frac{y^2}{2})$. The geometry is shown in Fig.(3.12). Three plots showing GBT solution to the reflection and refraction of a GB from the elliptical surface together with PO solution (Fig.(3.13)) show that the two methods yield very close results.

3.10 Conclusion and Summary

An extremely fast GB tracing method which can handle General Astigmatic GBs was developed in this chapter. This asymptotic method forms the basis of our proposed hybrid

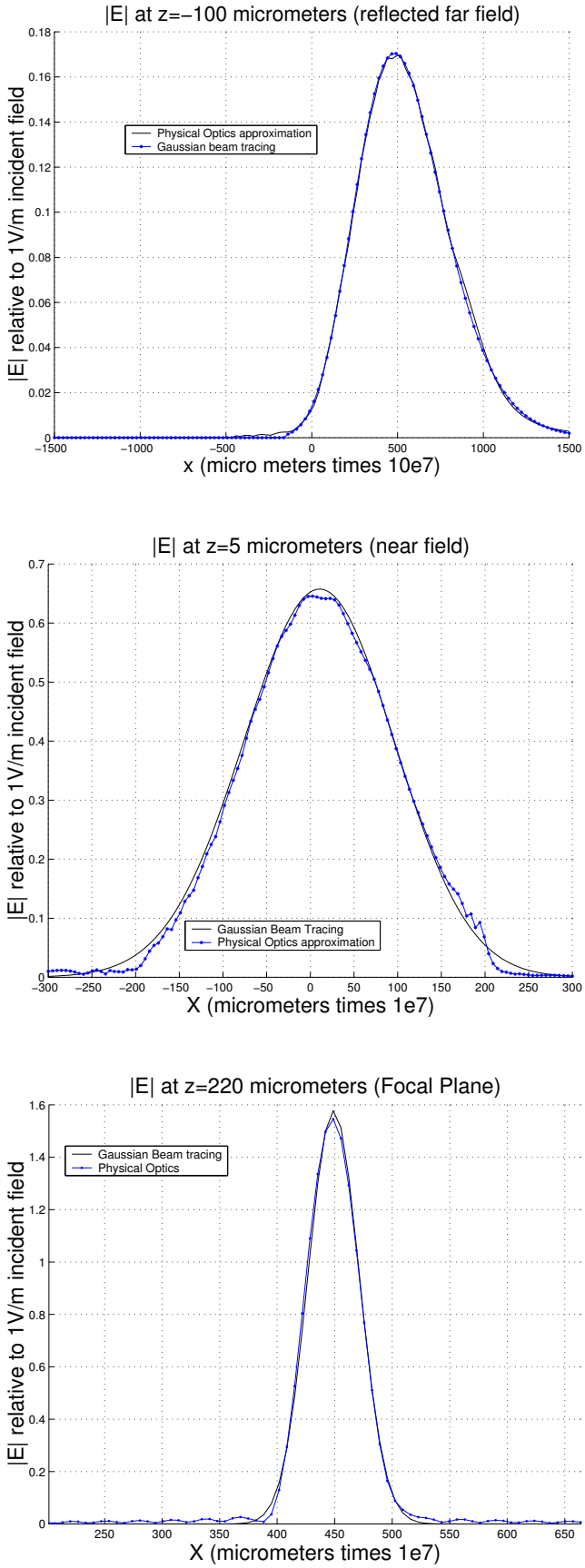

Figure 3.13: Comparison of the GB tracing method with PO

method. It can be used to model GB propagation in free space and its reflection and refraction from general curved surfaces. The medium has to be isotropic but can include losses which can be taken into account through a complex permittivity. Conducting surfaces are also easily analyzed using this method. No edge diffraction has been taken into account. The method cannot be used to model periodic structures such as gratings. The spot size of the GB at point of incidence must be at most half the radii of curvature of the surface at that point.

Chapter 4

Gabor Expansion of the input field

4.1 Introduction

The field distribution at the input of the photonic system may not be a pure Gaussian profile. Therefore in order to use the GB tracing method, the input fields needs to be expanded into a number of GBs. GB expansion has been investigated and reported in the literature, [20, 27, 28, 29, 30, 31]. Apart from the work by Pathak et. al. [20] which is mostly applicable to reflector antennas where the the aperture field is much smaller than the reflector, all the remaining work mentioned above based on Gabor representation [26]. Theoretically, this method can be used to expand an arbitrary aperture field into a sum of shifted and rotated GBs emanating from a 4 dimensional lattice (for a 2D aperture). One of the main advantages of this method is the arbitrariness of the waist of the elementary beams that cover the aperture. This suggests that beams having an appropriate and compatible waist with our GB tracing method can be created from any aperture field. Therefore, by knowing the curvature of the surface upon which the field would eventually impinge, the waists of the beams required at the aperture plane are estimated by working backwards from the surface towards the aperture. The theory of arbitrary beam waist in one direction (either x or y) at the aperture plane is developed in this chapter.

4.2 One Dimensional Aperture Representation Using Gabor Expansion

In [27] the Gabor representation [26] is used in the aperture discretization context for the first time (1986). The field over a one dimensional aperture $f(x)$(giving rise to a 2D field) is

expanded as a double sum of spatially and spectrally shifted elementary functions (window functions):

$$f(x) = \sum_m \sum_n A_{mn} w(x - mL_x) \exp(jn\beta_x x), \quad \beta_x L_x = 2\pi \tag{4.1}$$

and in Fourier domain,

$$\tilde{f}(k_x) = \sum_m \sum_n A_{mn} \tilde{w}(k_x - n\beta_x) \exp(-jmL_x k_x) \tag{4.2}$$

From this point onwards, the functions with a tilde will represent the Fourier transformed function. Although, theoretically, the window can be any finite energy function, here only the Gaussian window is considered:

$$\begin{aligned} w(x) &= (\frac{\sqrt{2}}{L_x}) \exp[-\pi(x/L_x)^2], \quad \int_{-\infty}^{\infty} |w(x)|^2 dx = 1 \\ \tilde{w}(k_x) &= (\sqrt{2}L_x)^{1/2} \exp[-\pi(k_x/\beta_x)^2] \end{aligned} \tag{4.3}$$

This type of non-orthogonal transform was introduced by Gabor in 1946; however, it has had limited use due to the difficulty of calculation of the coefficients and the uncertainty regarding completeness issues. In 1980-1981 Bastian and Jansen showed the completeness of the representation and offered relatively easy ways for calculating the coefficients [68, 69, 70, 71]. It can be shown that the coefficients of these series can be calculated from:

$$\begin{aligned} A_{mn} &= \int_{-\infty}^{\infty} f(x)\gamma^*(x - mL_x) \exp[-jn\beta_x x] dx \\ &= \frac{1}{2\pi} \int_{-\infty}^{\infty} \tilde{f}(k_x)\tilde{\gamma}(k_x - n\beta_x) \exp(imL_x k_x) dk_x \end{aligned}$$

The asterix represents complex conjugate and γ is the so called biorthogonal function given by the condition:

$$\int_{-\infty}^{\infty} w(x)\gamma^*(x - mL_x) \exp[-jn\beta_x x] dx = \delta_m \delta_n, \quad \delta_m = 1 \quad \text{for only} \quad m = 0$$

It can be shown [71] that for a Gaussian function, γ can be found from:

$$\begin{aligned} \gamma(x) &= \gamma_0(x) \sum_{l \geq l_0} (-1)^l \exp[-\pi(l + \frac{1}{2})^2] \\ \gamma_0(x) &= \frac{1}{\sqrt{\sqrt{2}L_x}} (\frac{K_0}{\pi})^{-3/2} \exp \pi[(\frac{x}{L_x})^2] \\ l_0 &= (x/L_x) - 1/2, K_0 = 1.85407 \end{aligned}$$

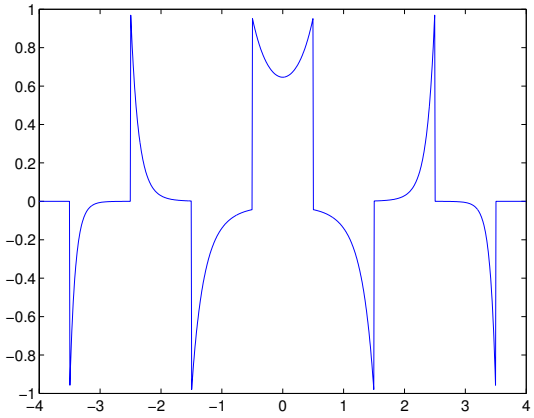

Figure 4.1: Normalized $\gamma(x/L_x)$

A plot of the normalized gamma function is given in Fig.(4.1). Assuming that at $z = 0$ an aperture whose electric field is given by $\mathbf{E}(x, 0) = \hat{y}f(x)$, Eqn.(4.1) is substituted in the plane wave spectrum (Kirchhoff) integral:

$$\mathbf{E}(x,z) = \frac{1}{2\pi}\int_{-\infty}^{\infty} \tilde{f}(k_x)\exp[j(k_x x + k_z z)]dk_x, \quad k_z = \sqrt{k_0^2 - k_x^2}, \quad \Re[k_z] > 0, \Im[k_z] < 0 \tag{4.4}$$

$$\tilde{f}(k_x) = \int_{-\infty}^{\infty} f(x)\exp(-jk_x x)dx$$

It can be shown that by making the transformation:

$$\begin{bmatrix} x - mL_x & z \end{bmatrix} = \begin{bmatrix} \cos\phi_n & \sin\phi_n \\ -\sin\phi_n & \cos\phi_n \end{bmatrix} \begin{bmatrix} x_t \\ z_t \end{bmatrix} \tag{4.5}$$

where $\sin\phi_n = n\beta_x/k = n\lambda/L$ and evaluating this integral using asymptotic techniques in the paraxial regime the following is obtained (the asymptotic technique is elaborated in Section(4.4):

$$\mathbf{E}(x,z) = \sum_m \sum_n A_{mn} B_{mn}(x,z) \tag{4.6}$$

$$B_{mn} = (2^{1/2}/L)^{1/2}\sqrt{ja_n/(z_t + ja_n)}\exp[-jk(z_t + x_t^2/2(z_t + ja_n)] \tag{4.7}$$

Therefore it is observed that the field of aperture has been discretized as a sum of shifted and rotated beams emanating from a 2D lattice. The subscripts “n” represent the rotated beams and subscript “m” represent the shift.

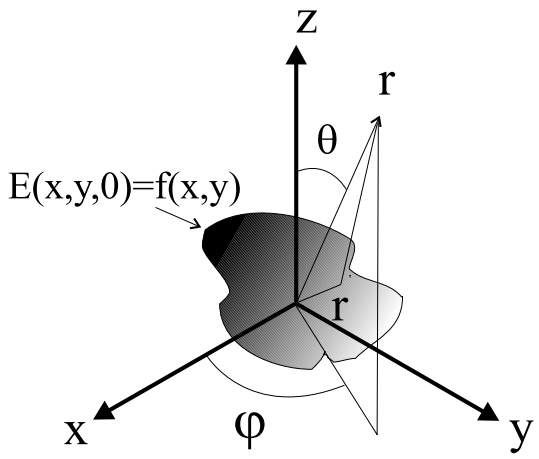

Figure 4.2: The 2D Aperture distribution

4.3 Gabor Representation for the 3D Case

Maciel and Felsen [29, 30] extended this method to the 2D apertures for the special case that the beam waists are much smaller than the dimensions of the aperture. In this method, which is an extension of what was said above, the input 2D field is represented by a four dimensional sum of narrow waisted Gaussian functions [28]. Given the the 2D aperture field shown in Fig.(4.2) the two conventional methods for finding the radiated field are: 1)using spectral domain or expanding the aperture field as an integral over plane waves, 2) using Green's function method or considering the aperture as a sum of point sources each giving rise to the shifted free space Green's function. It is clear that in terms of spatial and spectral distribution these two approaches are the two extreme cases; one having infinite spatial distribution and the other having impulse spatial distribution. These two formulations are given in Eqns.(4.8,4.9). The spectral domain formulation is given by [29]:

$$\mathbf{F}(x,y,z) = \frac{j}{(2\pi)^2}\iint_{-\infty}^{\infty}\frac{1}{k_z}\hat{\mathbf{z}}\times\tilde{\mathbf{f}}(k_x,k_y)\times\exp(j\mathbf{k}.\mathbf{r})dk_xdk_y \tag{4.8}$$

$$\tilde{\mathbf{f}}(k_x,k_y) = \iint_{-\infty}^{\infty}\mathbf{f}(x,y)\times\exp[-j(k_xx+k_yy)]dxdy$$

$$k_z(k_x,k_y) = \sqrt{k^2-k_x^2-k_y^2},\quad \Re[k_z]\leq 0, \Im[k_z]\geq 0$$

$$\mathbf{k} = k_x\hat{\mathbf{x}}+k_y\hat{\mathbf{y}}+k_z\hat{\mathbf{z}},\quad \mathbf{r} = x\hat{\mathbf{x}}+y\hat{\mathbf{y}}+z\hat{\mathbf{z}}$$

where $\mathbf{F}(x, y, z)$ is the electric vector potential defined by $\vec{\nabla} \times \mathbf{F} = \mathbf{E}$. Green's function approach obtains:

$$\mathbf{F}(x, y, z) = 2 \iint_{-\infty}^{\infty} \hat{\mathbf{z}} \times \mathbf{f}(x', y') \times G(|\mathbf{r} - \mathbf{r}'|) dx' dy' \tag{4.9}$$
$$G(|\mathbf{r} - \mathbf{r}'|) = \exp(-jkR)/4\pi R, \quad R = |\mathbf{r} - \mathbf{r}'|$$

Where $G(|r - r'|)$ is the free space Green's function. As was mentioned in the previous section Gabor representation uses an intermediate formulation. Instead of the two double integrals in the previous two formulations this formulation involves quadruple discrete sum of spatial shifted and rotated elementary functions [27, 29]:

$$\mathbf{f}(x, y) = \sum_m \sum_n \sum_p \sum_q \mathbf{A}_{mnpq} w(x - mL_x, y - pL_y) \times \exp[j(n\beta_x x + q\beta_y y)]$$

$$\tilde{\mathbf{f}}(x, y) = \sum_m \sum_n \sum_p \sum_q \mathbf{A}_{mnpq} \tilde{w}(k_x - n\beta_x, k_y - q\beta_y) \times \exp[j(mL_x k_x + pL_y k_y)]$$

With the self consistency equations:

$$\beta_x L_x = \beta_y L_y = 2\pi$$

Maciel and Felsen showed that for a Gaussian window function:

$$w(x, y) = (\frac{2}{L_x L_y})^{\frac{1}{2}} \exp\{-\pi[(\frac{x}{L_x})^2 + (\frac{y}{L_y})^2]\}$$

the coefficients can be found from:

$$\mathbf{A}_{mnpq} = \iint_{-\infty}^{\infty} \mathbf{f}(x,y)\gamma^*(x - mL_x, y - pL_y)\times \exp[-j(n\beta_x x + q\beta_y y)]dxdy$$

$$\gamma(x,y) = \gamma_0(x,y)\sum_{l\geq l_0}(-1)^l \exp[-\pi(l+\frac{1}{2})^2]\times \sum_{g\geq g_0}(-1)^g \exp[-\pi(g+\frac{1}{2})^2]$$

$$\gamma_0(x,y) = \frac{1}{\sqrt{2L_xL_y}}(\frac{\pi}{K_0})^3 \exp\{\pi[(\frac{x}{L_x})^2 + (\frac{y}{L_y})^2]\}$$

$$l_0 = (x/L_x) - 1/2, g_0 = (y/L_y) - 1/2, K_0 = 1.85407$$

Maciel and Felsen found that for narrow waisted beams (meaning beams whose waists are much smaller than the aperture dimensions), there is no need to calculate the above integrals. They showed that in this case only shifted beams are important $(n, q = 0)$ and therefore the quadruple sum becomes a double sum:

$$\mathbf{F}(x,y,z) = \sum_m \sum_p \hat{\mathbf{z}} \times \mathbf{A}_{mp} B_{mp}(x,y,z)$$

$$B_{mp}(x,y,z) \sim \frac{\sqrt{2}L}{2\pi(z+jb)}\times \exp\{-jk[z + \frac{(x-mL)^2 + (y-pL)^2}{z+jb}]\}$$

where $b = L^2/\lambda$. The coefficients A_{mp} can be estimated as the samples of the aperture field:

$$\mathbf{A}_{mp} \sim L/\sqrt{2}\mathbf{f}(mL, pL)$$

So a number of shifted narrow waisted stigmatic GBs with equal waists with no angular rotation are launched from the aperture plane.

4.4 Beam Field Representations 2D and 3D

In order to find the beam field representation of the Gabor expansion for the 2D case substituting Eqn.(4.2) into Eqn.4.5 and using the Gaussian elementary function Eqn.(4.3)

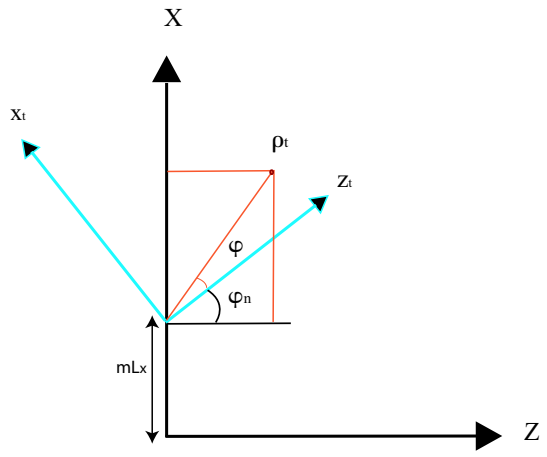

Figure 4.3: Shifted and rotated coordinate system for elementary beam fields

yields (C is constant than can be used to calibrate the field representation):

$$B_{mn}(x,z) = C\int_{-\infty}^{+\infty} \exp\{-\pi[(k_x - n\beta_x)/\beta_x]^2\} \exp\{j[k_x(x - mL_x) + z\sqrt{k_0^2 - k_x^2}]\}dk_x \tag{4.10}$$

In the far zone of the beam field propagators the steepest descent method can be used to evaluate the above integral [72]. The saddle point condition:

$$\frac{d\psi(k_x)}{dk_x} = 0 \tag{4.11}$$

where

$$\psi(k_x) = k_x \sin\theta + \sqrt{k_0^2 - k_x^2}\cos\theta + j\frac{\pi}{\rho_t}(\frac{k_x - n\beta_x}{\beta_x})^2 \tag{4.12}$$

and $\theta = \phi + \phi_n$, yields the explicit form:

$$(x - mL_x) - \frac{k_x}{\sqrt{k_0^2 - k_x^2}}z + j\pi\frac{L_x^2}{\lambda}(k_x - n\beta_x) = 0 \tag{4.13}$$

Alternatively [27] this integral can be found by converting it to polar coordinates:

$$k_x = k_0 \sin\alpha$$

According to [27] the following is obtained:

$$\alpha = \phi_n + \frac{x_t}{z_t + ja_n} + \text{higher order terms} \tag{4.14}$$
$$a_n = L_x^2 \cos\phi_n^2/\lambda$$

Where x_t, z_t and ϕ_n are shown in Fig.(4.3). Here it is shown that Eqn.(4.14) and Eqn.(4.13) are identical under paraxial approximation. First the coordinate system is transformed to the ray fixed coordinate system (x_t, z_t). After straightforward algebra, this transformation yields:

$$z_t \sin(\alpha - \phi_n) - \frac{jL_x^2}{\lambda}(\sin\alpha - \sin\phi_n).\cos\alpha - x_t\cos(\alpha - \phi_n) \tag{4.15}$$

If it is assumed that b is an unknown parameter proportional to the waist of a beam; in the paraxial regime of this beam the relation $x_t^2 \ll z_t^2 + b^2$ holds. Therefore a parameter $\epsilon = \frac{x_t}{z_t + jb}$ is defined whose smallness defines the paraxial approximation. Using a perturbation expansion

$$\alpha = \alpha_0 + \alpha_1\epsilon + \text{higher order terms} \tag{4.16}$$

and substituting in Eqn.(4.15) results in the following:

$$\begin{aligned} \alpha &= \phi_n + \frac{x_t}{z_t + jb} + \text{higher order terms} \\ b &= L_x^2\cos\phi_n^2/\lambda \end{aligned} \tag{4.17}$$

Therefore the equivalence of the two representations is obtained. The beam emanating from $(mL_x, 0)$ launched at an angle ϕ_n according to [27] can be obtained from what was derived above as a GB of the form:

$$B_{mn}(x,z) = C_1\sqrt{\frac{ja_n}{z_t + ja_n}}\exp[-jk_0(z_t + \frac{1}{2}\frac{x_t^2}{z_t + ja_n})] \tag{4.18}$$

where C_1 is a constant dependent on L_x.
For the 3D case according to [30], the saddle point conditions are two coupled equations containing k_x and k_y. Obtaining a very general form of solution in terms of beams emanating from a 2D lattice at arbitrary angles (θ_n, ϕ_n) with respect to the z axis is extremely difficult. Nevertheless a method is proposed in this work that extends the narrow waisted approximations derived by Felsen et. al. Here two cases are considered:

1. Beams having narrow waists in the y direction leading to $q = 0$ but no restriction on the beam waist in the x direction $n \neq 0$. This leads to astigmatic beams emanating from shifted positions m, p and launched at an angle ϕ_n in planes parallel to $x - z$ plane.

2. Beams having narrow waist in x direction leading to $n = 0$ but no restriction on the beam waist in y direction $q \neq 0$. This leads to astigmatic beams emanating from shifted positions m, p and launched at an angle θ_n with in planes parallel to $y - z$ plane.

In the 3D case the integral form of the beam representation (for Gaussian window functions) becomes [30]:

$$B_{mnpq} = \int_{-\infty}^{+\infty} \int_{-\infty}^{+\infty} g(k_x, k_y) \exp[j r_{mnpq} \psi_{mnpq}(k_x, k_y)] dk_x dk_y \tag{4.19}$$

$$g(k_x, k_y) = \frac{j\sqrt{2L_x L_y}}{(2\pi)^2 k_z}$$

$$k_z = \sqrt{k_0^2 - k_x^2 - k_y^2}$$

Where r is amplitude of the position vector and ψ is the complex phase given in [29, 30]. Therefore the saddle point conditions , $\frac{\partial \psi}{\partial k_x} = 0$ and $\frac{\partial \psi}{\partial k_y} = 0$ become:

$$(x - mL_x) - \frac{k_x z}{k_z} + \frac{jL_x^2}{2\pi}(k_x - n\beta_x) = 0 \tag{4.20}$$

$$(y - mL_y) - \frac{k_y z}{k_z} + \frac{jL_y^2}{2\pi}(k_y - q\beta_y) = 0 \tag{4.21}$$

Now if it is assumed that $q = 0$ so the beams are narrow waisted in the y direction then $k_z \simeq \sqrt{k_0^2 - k_x^2}$ and Eqn.(4.21) becomes identical to Eqn.(4.13). This suggests that the beam field has the following form:

$$B_{mnp} = C(L_x, L_y)\sqrt{\frac{ja_n}{z_t + ja_n}} \exp[-jk_0(z_t + \frac{1}{2}\frac{x_t^2}{z_t + ja_n})]$$

$$\times\sqrt{\frac{jL_y}{z_t + jL_y^2/\lambda}} \exp[\frac{1}{2}\frac{y^2}{z + jL_y^2/\lambda})] \tag{4.22}$$

This is an astigmatic GB which is narrow waisted in y direction. The same can be said for B_{mnp}. The fact that such an expansion is complete in reproducing the aperture field is obvious. Its properties and strengths in predicting the Fresnel zone and farfield of arbitrary aperture fields is part of our future work.

4.5 Properties of Gabor Expansion

The important properties of Gabor expansion are listed below. Only the 2D case is mentioned but all the properties apply equally well to the 3D case:

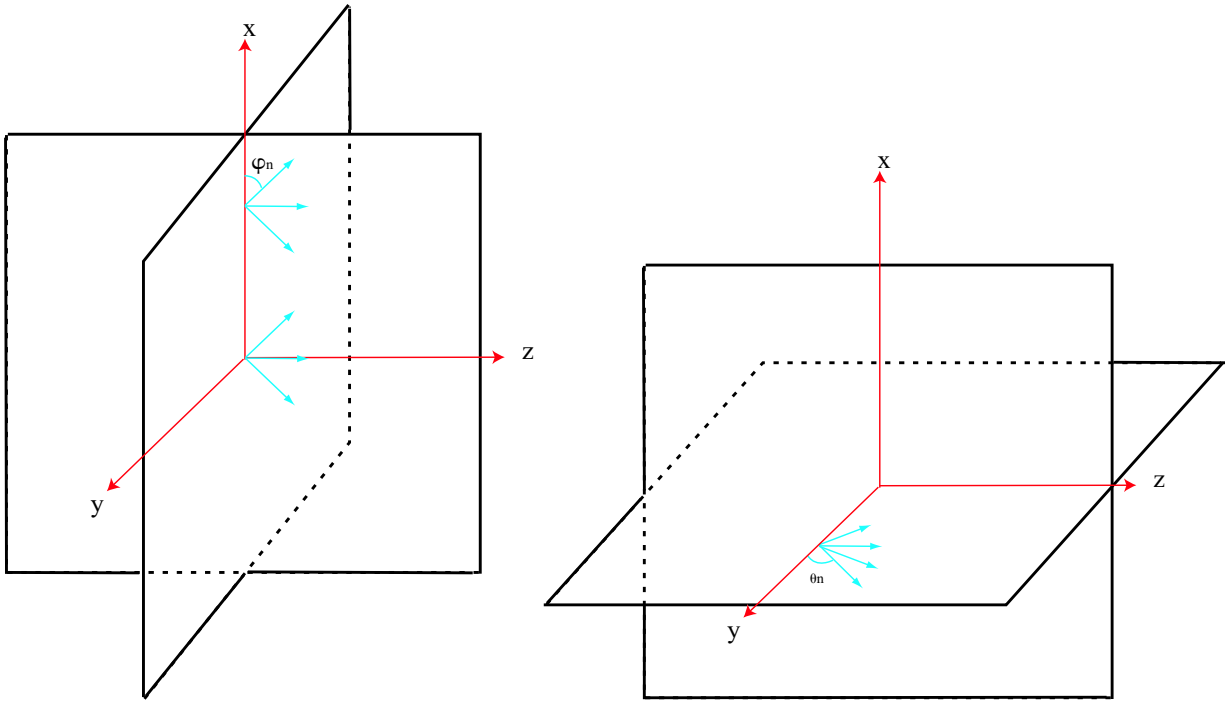

(a) x-z plane

(b) y-z plane

Figure 4.4: Rotated beams in $x-z$ and $y-z$ planes

1. The Gabor expansion is complete [27].

2. If the shift parameter L_x is large relative to the size of the aperture which also means that the resultant beams have large waists the amplitude of the expansion coefficients fall off rapidly with increasing m. This means that only a few shifted beams need to be included in the beam expansion. From each shifted position many rotated beams are launched (n is large). This is called the "matched" case. If L_x goes to infinity it can be shown that the summation becomes the usual plane wave expansion integral.

3. If the shift parameter L_x is small relative to the size of the aperture which also means that the resultant beams have narrow waists the amplitude of the expansion coefficients fall off rapidly with increasing n. This means that only a few rotated beams need to be included in the beam expansion. From each shifted position only a few rotated beams are launch (n is small). This is called the "narrow waist" case. In the limit as L_x goes to zero it can be shown that the summation becomes the Green function integral therefore the beams act like point sources.

4. The launch angle of the beams are given by $\sin\phi_n = n\beta_x/k = n\lambda/L_x$. Therefore if $n\beta_x/k > 1$ the beams become evanescent. In this work as GBT uses GBs only non-evanescent beams are considered.

4.6 Results and Numerical Simulation

4.6.1 Airy Disk

The problem of a circular aperture with constant amplitude and phase in front of a thin lens (intersection of two spheres with radius of $100mm$ and separation of $0.5mm$) and also two types of thick lenses are considered in this section. The aperture radius is $1.65mm$ and the lenses are assumed to be adjacent to the aperture. The wavelength is assumed to be $633nm$

The aperture field is expanded in terms of narrow waisted GBs (Fig.4.5). As the results show there is a very good agreement between the Airy function and our results in case of the thin lens. The focal point of the lens was found by maximizing the amplitude of the field (it was observed that this condition was coincident with the stationary phase condition). The focal point found is very close to the prediction of the lens designer's formula ($1/f = (n-1)2/R$), where f is the focal distance and R is the radius of each face). The aperture field, field of the aperture with no lens and field of the aperture placed

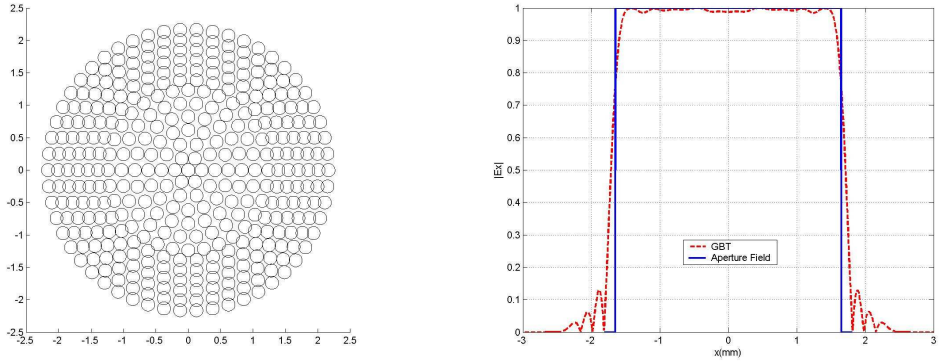

(a) Expansion into GBs

(b) Field at the aperture plane

Figure 4.5: The pulsed aperture decomposed into GB's and the field at the aperture plane

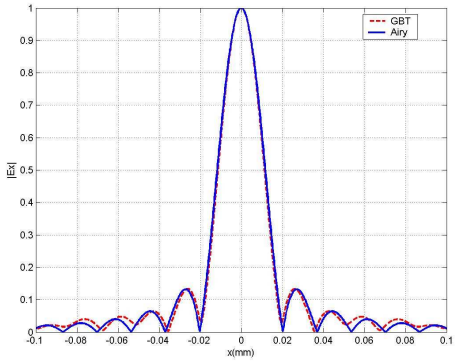

Figure 4.6: Comparison of the Airy function with GBT for a thin lens

in front of a thin lens are shown in Figs(4.6,4.7). It should be noted that after the coefficients of the aperture expansion are found (which takes less than $1min$ on a P4 PC for this particular case) for any arbitrary position of lens (any angle, any offset from optical axis and any distance from the aperture plane), the calculation of the field take less than a second for any point in space. Note that although more than 300 beams are launched, the time required to calculate the field is still very small (less than 1 min on a P4 3GHz machine). As it can be seen in Fig.(4.8), the method can equally well handle the case of a thick lens placed in front of the same aperture.

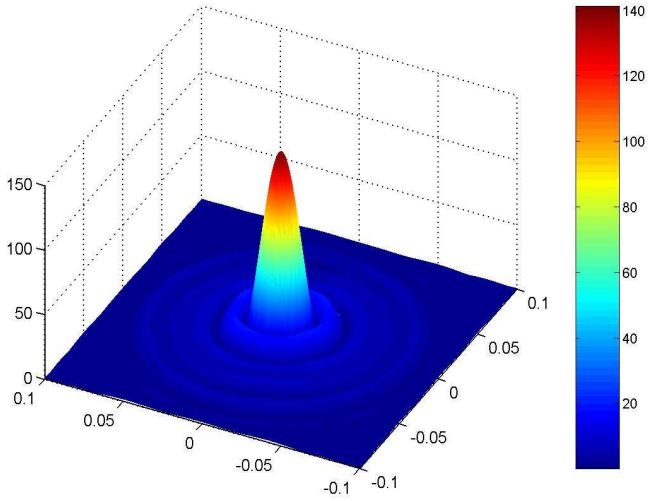

Figure 4.7: 3D plot of the field at the focal plane

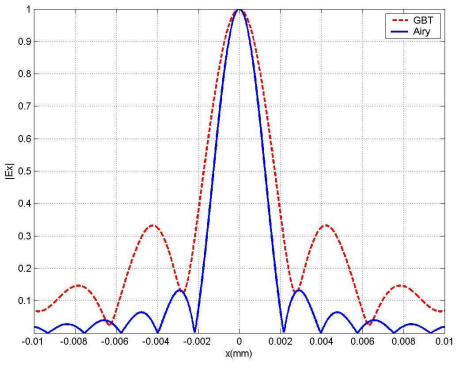

(a) Comparison of Airy function with GBT

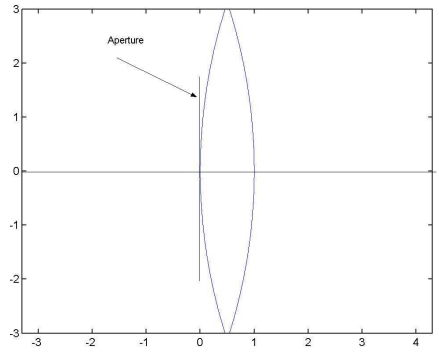

(b) Geometry of the thick lens

Figure 4.8: Thick lens

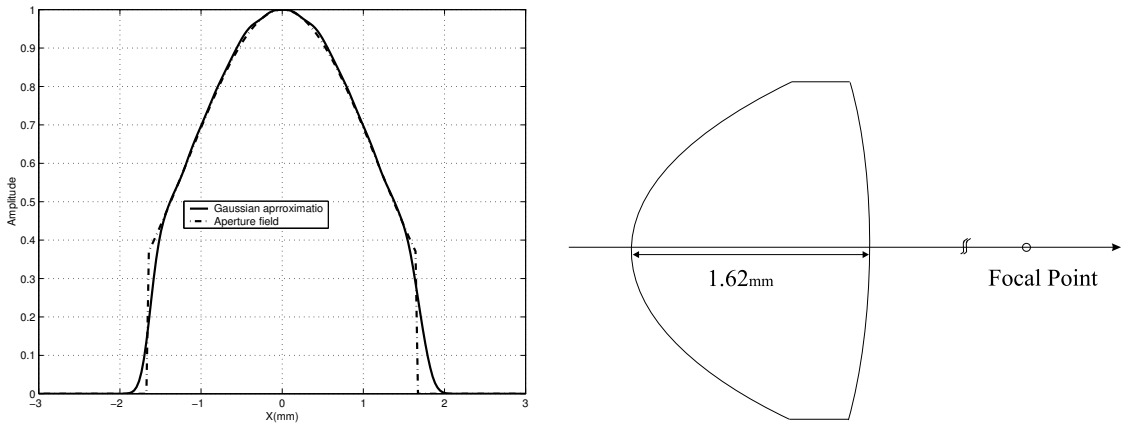

(a) Truncated Gaussian profile and it's Gabor approximation

(b) Geometry of the High Numerical Aperture Lens

Figure 4.9: High Numerical Aperture Lens

4.6.2 Thick High Numerical Aperture Lens

As a second example again the combination of GBT and Gabor expansion was used to find the propagation of a truncated Gaussian profile through a very high numerical aperture lens. As before due to the fact that the aperture is large in terms of wavelength (size of aperture and wavelength is the same as the above problem) the coefficients of the Gabor expansion can be easily obtained by sampling the aperture field. The geometry and the results are shown in Figs.(4.9,4.10,4.11,4.12).

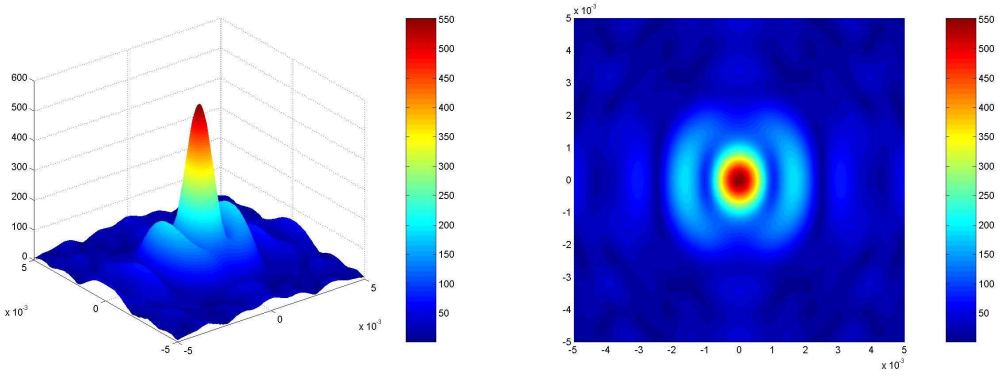

(a) (b)

Figure 4.10: $|E_x|$ and top $|E_x|$ at the focal point $z = 8.73mm$

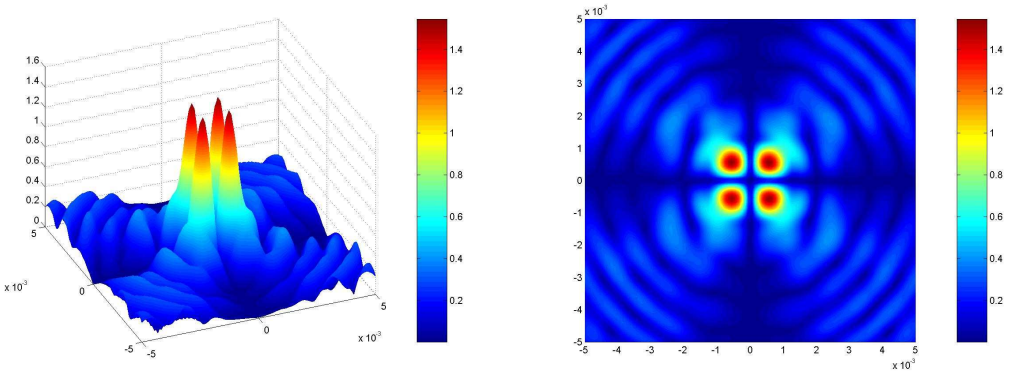

(a) (b)

Figure 4.11: $|E_z|$ and top $|E_z|$ at the focal point $z = 8.73mm$

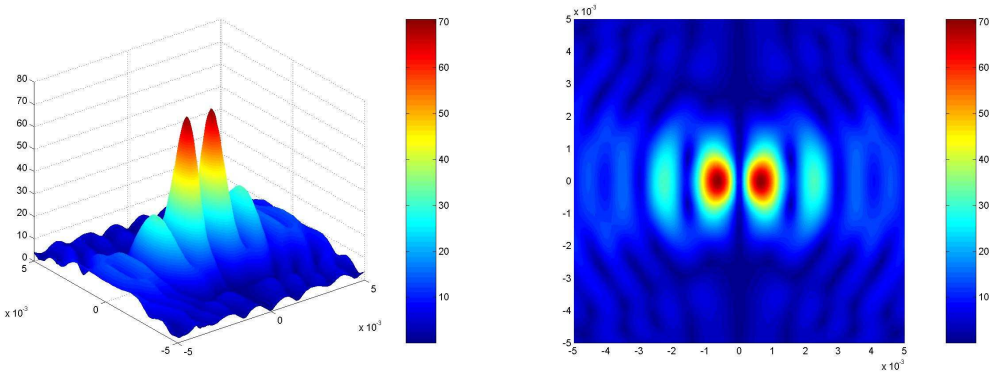

(a) (b)

Figure 4.12: $|E_y|$ and top $|E_y|$ at the focal point $z = 8.73mm$

Chapter 5

Hybridization with Finite Difference Time Domain Method

5.1 Objectives

The hybridization of GB expansion/tracing methods with Finite Difference Time Domain (FDTD) method forms the final stage of this research. This hybridization is essential because a typical photonic system may contain structures that cannot be analyzed using the combination of GB expansion and GB tracing methods discussed in the previous chapters. For example, the diffraction phenomena caused by very fine features of a structure, such as lenses with very small radii of curvature (in the order of wavelength) or diffraction by finite dielectric gratings with groove depths of the order of wavelength can not be handled by GBT and Gabor expansion alone. Special material such as left handed material or anisotropic material can not be handled accurately using GBT either. In these cases the scattering and diffraction effects are simulated by surrounding such structures with a virtual box in order to isolate them from the rest of the problem. The aperture launched GBs are then traced throughout the problem space ignoring the effect of the scatterer (the structure and its box). The fields over the planes (or the surface) of the virtual box are then found. Note that the fields must be found as functions of time and therefore beams reaching the same point on the surface from different paths will have different phases. The fields on these surfaces are then expanded using the Gabor expansion and the resulting set of GBs are launched inside the FDTD lattice. This approach has been used due to the fact that analytical form of a GB is utilized in the FDTD formulation and there is no need for time tracking. FDTD is then used to simulate the scattering (reflection or transmission) effect

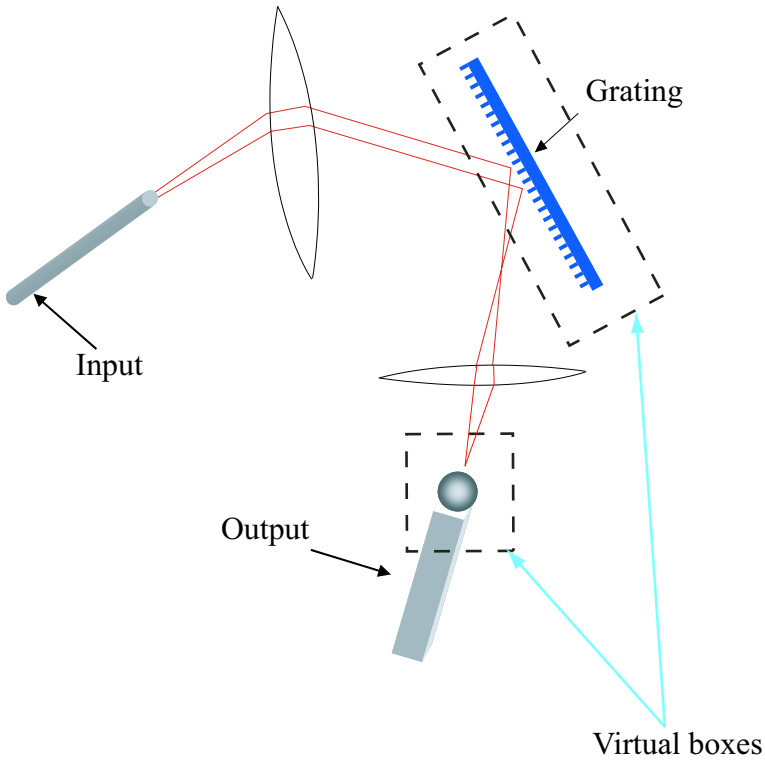

Figure 5.1: The structures that are analyzed by FDTD are surrounded by virtual boxes

of the box. These fields will then be added to the traced GBs. This hybrid scheme is a very powerful tool in the analysis and design of complex photonic structures Fig.(5.1). Using this method systems with sizes of hundreds of thousands of wavelengths can be designed and analyzed. The free space propagation and transmission through large structures are handled by the combination of Gabor expansion and GBT. The finer features are modelled by FDTD. Different combinations of the different components of the method can be used to analyze very complex structures.

As part of this research a number of commercially available software were used to evaluate their capabilities. To the best of the author's knowledge the most popular commercial FDTD software available are:

1. RSOFT's FULLWAVE: This is most popular commercial FDTD software designed specifically for optical structures. The latest version is available in the form of a simulation module that is added to the vendor's BPM software BeamProp. Although the vendor claims that the software can handle 3D structures with arbitrary incident fields, the performed tests proved that even a simple 2D tilted GB is not modelled correctly.

2. XFDTD: This software is a 3D simulator software that uses a so called quasi-2D method for solving 2D problems which is not very convenient. Furthermore the GB launching method is bi-directional, making it unsuitable for scattering problems.

3. EMPIRE: This software is also designed for microwave structures. The producers of the software claim that they are incorporating GB incident fields and also periodic boundary conditions for the software. The current version does not support any of these features.

4. CST: MAFIA and Microwave Studio: These programs are specifically designed for modelling of microwave structures. They do not have the capability of simulating arbitrary incident waveforms on the surface surrounding a typical structure. Therefore, they can not be used in conjunction with GB expansion/tracing methods.

It was concluded that virtually none of the available commercial software (at least those available to our group) can be effectively used as part of the hybrid method; therefore a version of this method had to be implemented.
This chapter and the next chapter of this thesis deal with 2D problems but as the only part which is 2D is the FDTD an implementation of a 3D FDTD is part of the future phase of this research. The basic requirements of the FDTD scheme needed for the hybrid method are as follows:

1. Possessing accurate truncation boundary conditions with a very low reflection coefficient (Perfectly match layer (PML) boundary condition was used).

2. Accurate modelling of the incident field (total field / scattered field TF/SF formulation was used).

3. Accurate modelling of GBs launched at arbitrary angles.

4. Ability to launch many GBs simultaneously.

5. A highly accurate near field to far field transformation method.

6. Accurate link with Gabor expansion.

5.2 Introduction to the FDTD

With the ever increasing speed and computational power of today's computers, problems that were once too expensive to be solved using numerical methods are becoming viable.

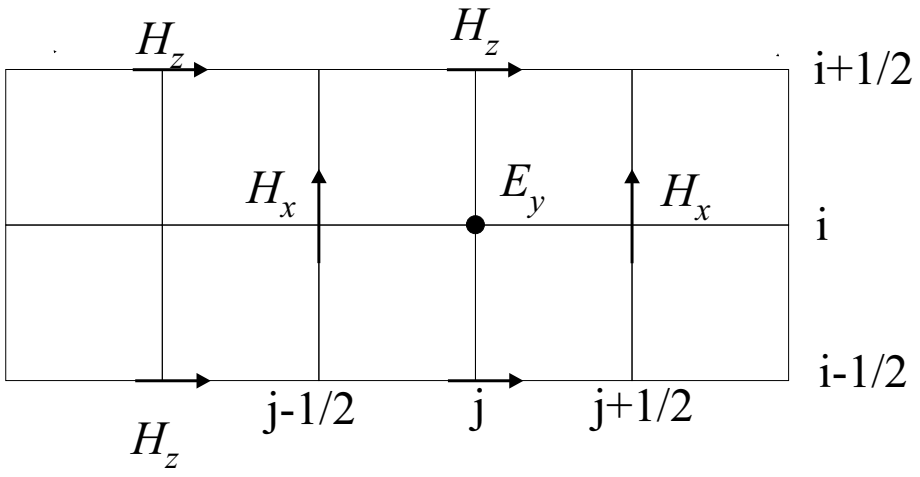

Figure 5.2: The Yee Mesh

The FDTD method was first used by Yee [32] for 2D electromagnetic problems and was then extended to 3D by Taflove and Brodwin [33].

This method is based on the time domain form of Maxwell's curl equations:

$$\vec{\nabla} \times \vec{\mathcal{E}} = -\mu \frac{\partial \mathcal{H}}{\partial t}$$
$$\vec{\nabla} \times \vec{\mathcal{H}} = \epsilon \frac{\partial \mathcal{E}}{\partial t} + \sigma \vec{\mathcal{E}} \tag{5.1}$$

These equations are discretized using a central difference scheme which attains a second order accuracy in both time and space. The divergence equations can be used for checking the validity of the predictions made by the curl equations. The FDTD method can be used to model the propagation of electromagnetic fields in a volume of space containing the structures of interest. The propagation procedure for the Cartesian coordinate system was originally developed by Yee in 1966 [32]. The problem space or the volume of interest is discretized into a number of *cells*. It can be shown that the mesh containing the values of the components of the electric field and the mesh containing the magnetic field components are staggered in space. Such a staggered lattice is called Yee's lattice Fig.(5.2). The coupled set of Maxwell's partial differential equations are then solved using the leap-frog method (time marching) [37]. The electric field and the magnetic field components are then updated at alternate half time steps (See section(5.4)). It is interesting to note that there is no need for any matrix inversion of any kind for this method. The field components are repeatedly updated as the method simulates the propagation of the electromagnetic wave in the volume of interest. The result is a set of complete field components in the

problem space. The advantages of the FDTD method are its simplicity and versatility. Because the computational scheme is both local and time-explicit, the complete interaction between the fields and the structures under consideration are found section by section and at any given time. The fact that the solution procedure is local, eliminates the need to find the simultaneous solution to the entire problem. Furthermore, the curl equations generate the internal boundary conditions (internal to the volume under consideration). The above mentioned features allow the natural implementation of FDTD on parallel processor computers, which can greatly enhance the speed of this method.

5.3 Formulation of 2D FDTD

Although FDTD is a major part of this research, the method itself is not a new contribution. Therefore the basics of this formulation is presented at a high level . Referring to Eqn.(5.1) the fields are normalized according to the following equations:

$$\vec{\mathcal{E}} = \sqrt{\mu_0}\,\mathbf{E}$$
$$\vec{\mathcal{H}} = \sqrt{\epsilon_0}\,\mathbf{H}$$

This normalization causes the magnitudes of $\mathbf{E}$ and $\mathbf{H}$ to be of the same order, and therefore, truncation and round off errors will be reduced [37]. If Δx and Δz are the size of the cells in x and z directions and Δt is the size of the temporal increment by writing a central difference scheme for both time and space the following is obtained (it is assumed that$\Delta x = \Delta z = \Delta$):

$$E_y^{n+1/2}(i,j) = E_y^{n-1/2}(i,j) + c\frac{\Delta t}{\Delta}[H_x^n(i,j+1/2) - H_x^n(i,j-1/2) - H_z^n(i+1/2,j) + H_z^n(i-1/2,j)] \tag{5.2}$$

$$H_x^{n+1/2}(i,j) = H_x^{n-1/2}(i,j) + c\frac{\Delta t}{\Delta}[E_y^n(i,j+1/2) - E_y^n(i,j-1/2)] \tag{5.3}$$

$$H_z^{n+1/2}(i,j) = H_z^{n-1/2}(i,j) + c\frac{\Delta t}{\Delta}[-E_y^n(i+1/2,j) + E_y^n(i-1/2,j)] \tag{5.4}$$

It is assumed that $i, j, n = i\Delta x, j\Delta z, n\Delta t$. The above formulation is valid for free space. Nevertheless material properties can be incorporated in these equations to allow modelling of many real physical cases. For example assuming that the medium under consideration is filled with a nonhomogeneous material with variable ϵ and σ the above equations have to be altered in the following form to incorporate the nonhomogeneity (only the update

equation for E_y is given):

$$E_y^{n+1/2}(i,j) = C_a(m)E_y^{n-1/2}(i,j) + C_b(m)[H_x^n(i,j+1/2) - H_x^n(i,j-1/2)]$$

where $m = MEDIA_{E_y(i,j)}$ and MEDIA(i,j) is an integer array defined for each set of field components (e.g. here E_y). This array enables the proper coefficients to be used at any point of the FDTD lattice. C_a and C_b are defined as follows:

$$C_a(m) = [1 - \frac{\sigma_{i,j}\Delta t}{2\epsilon_{i,j}}]/[1 + \frac{\sigma_{i,j}\Delta t}{2\epsilon_{i,j}}] \tag{5.5}$$

$$C_b(m) = [\frac{\Delta t}{\epsilon_{i,j}\Delta}]/[1 + \frac{\sigma_{i,j}\Delta t}{2\epsilon_{i,j}}] \tag{5.6}$$

In terms of the classes of material the capabilities of the implemented FDTD can be summarized as follows:

1. Perfect conductors.
2. Conductors with finite conductivities.
3. Normal dielectric material.
4. Dielectric with negative refractive index or left handed material [73]
5. Anisotropic material.
6. Inhomogeneous material with variable ϵ and μ.

5.4 Leap Frog Method (Time Marching)

The time marching procedure can be explained as follows: Assuming that the field components are known prior to some instant of time $t <= n$, the components of $\mathbf{H}$ at $t = n+1/2$ can be evaluated by updating its values at $t = n - 1/2$ by using $\frac{\partial \mathbf{H}}{\partial t}$ at $t = n$. Since $\frac{\partial \mathbf{H}}{\partial t}$ is related to $\vec{\nabla} \times \mathbf{E}$, its values at $t = n$ can be found from the values of $\mathbf{E}$ (in adjacent cells) at $t = n$, Eqn.(5.4). Knowing the value of $\mathbf{H}$ at $t = n + 1/2$ the components of $\mathbf{E}$ at $t = n + 1$ are readily found from Eqn.(5.4), Fig.(5.3). This procedure can continue until any desired time Fig(5.3).

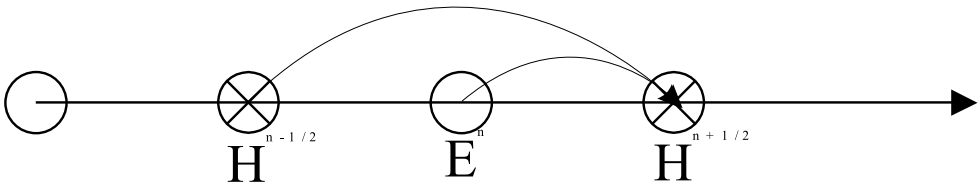

Figure 5.3: The Time Marching Procedure

5.5 Stability Criteria

It can be shown that a FDTD scheme will remain stable, in the sense that the field values will remain finite as the time marching procedure continues if the following criteria is satisfied:

$$v\Delta t \leq [\frac{1}{\Delta x^2} + \frac{1}{\Delta z^2}]^{-1/2} \tag{5.7}$$

where v is the maximum speed of light in the medium. This is called the Courant-Friedrichs-Lewy (CFL) condition. This criteria has a simple physical interpretation. When the CFL condition is satisfied, the FDTD grid (mesh) is causally connected, meaning that the speed of light limits the rate at which information is transformed across the mesh.

5.6 Numerical Dispersion

The satisfaction of the CFL condition guaranties that the fields will remain bounded. In free space or any non-dispersive media, plane waves travel at the same speed. It can be shown that this is not the case for an FDTD mesh. To demonstrate this phenomena, consider a one dimensional wave propagating in x direction . The wave equation and its discretized form in such media are give by:

$$\frac{1}{c^2}\frac{\partial^2 E}{\partial t^2} = \frac{\partial^2 E}{\partial x^2}$$

$$\frac{E^{n+1}(i) - 2E^n(i) + E^{n-1}(i)}{c\Delta t^2} = \frac{E^n(i+1) - 2E^n(i) + E^n(i-1)}{\Delta x^2} \tag{5.8}$$

Assume that a plane wave in such a media is given by

$$E^n(i) = e^{j(wn\Delta t - ki\Delta x)} \tag{5.9}$$

w is the angular frequency (rad/sec), and k is the wave number. In free space where $k = w/c$. If Eqn.(5.9) is substituted in Eqn.(5.8) the following is obtained :

$$\frac{1}{(c\Delta t)^2}\sin^2(\frac{w}{c}\frac{c\Delta t}{2}) = \frac{1}{\Delta x^2}\sin^2(\frac{k\Delta x}{2}) \tag{5.10}$$

It can be observed that if $w\Delta t \to 0$ and $k\Delta x \to 0$ the relationship $(w/c)^2 = k^2$ is obtained. Furthermore, if $c\Delta t = \Delta x$ the same relationship between k and w is obtained. In all other cases it is observed that waves at different frequencies travel at different speeds. Therefore, the FDTD mesh acts as a dispersive medium. Furthermore it can be shown that unfortunately, more stable schemes (according to the CFL condition) lead to more dispersive meshes.

5.6.1 Truncation Boundary Condition

In order to use the FDTD method to solve open or semi-open regions, theoretically the whole space needs to be discretized. This is obviously not possible. Therefore the FDTD mesh must be truncated by some method. This leads to the concept of truncating boundary conditions. In this work the perfectly match layer (PML) absorbing boundary condition is used. Applying such a boundary condition to a problem is a mechanism that ideally permits the electromagnetic fields to be absorbed by the walls where the PML is placed and therefore no reflection or distortion occur. There are many problems associated with absorbing boundary conditions and the subject has been an area of extensive research. For a detailed discussion of the PML refer to [33]

5.7 Modelling of Incident Field

In order to model an incident field on a wall of the virtual box, the following 2D case [33] Fig.(5.4) is used. The area around the structure under consideration is divided into two regions: total field region and scattered field region. According to field equivalence concepts, if a closed surface containing a scatterer is surrounded by the equivalent currents produced by the incident fields, $\mathbf{J}_s = \hat{n} \times \mathbf{H}_{inc}$ and $\mathbf{M}_s = -\hat{n} \times \mathbf{E}_{inc}$ and these currents radiate in the presence of the scatterer, they produce the scattered field outside the surface. Inside the surface the total field is produced [57]. Therefore if $\mathbf{E}_{inc}$ is known on the incident plane, inside the surface the total fields are given by:

$$\begin{aligned} \mathbf{E}_{tot} &= \mathbf{E}_{inc} + \mathbf{E}_{scat} \\ \mathbf{H}_{tot} &= \mathbf{H}_{inc} + \mathbf{H}_{scat} \end{aligned} \tag{5.11}$$

(The subscripts stand for total, incident and scattered respectively), and outside the surface $\mathbf{E}_{scat}$ and $\mathbf{H}_{scat}$ exist only. If the discretized form (2D) of the equation of $\mathbf{E}_z$ for a point inside the total field region is written, according to Fig.(5.4) the following is obtained (assuming $\Delta x = \Delta z = \Delta$):

$$E^{n+1}_{y,tot}(i,j) = E^{n}_{y,tot} + c\frac{\Delta t}{\Delta}[H^{n+1/2}_{x,tot}(i,j+1/2) - H^{n+1/2}_{x,scat}(i,j-1/2) - H^{n+1/2}_{z,tot}(i+1/2,j) + H^{n+1/2}_{z,tot}(i-1/2,j)] \tag{5.12}$$

but this result is wrong (or more precisely inconsistent) due to the fact that in order to find the value of E_y in the total field region the value of H_x in the scattered field region is used. Therefore the incident H_x is *added* to E_y :

$$E^{n+1}_{y,tot}(i,j) = E^{n}_{y,tot} + c\frac{\Delta t}{\Delta}[H^{n+1/2}_{x,tot}(i,j+1/2) - H^{n+1/2}_{x,scat}(i,j-1/2) - H^{n+1/2}_{x,inc}(i,j-1/2) - H^{n+1/2}_{z,tot}(i+1/2,j) + H^{n+1/2}_{z,tot}(i-1/2,j)] \tag{5.13}$$

The same concept has to be applied to the other field components. The above equation can be implemented in the following way: E_y is updated in the normal manner and then the incident H_x is *added* to it. One might assume that by having a very good absorbing boundary condition one does not need the TF/SF formulation. This is not true due to the fact that when we are simulating scattering problems the scattered field might be much smaller than the incident field. If the incident field is present at the point of observation, the scattered field may become similar to a noise added to that field. The TF/SF act as a numerical filter that filters the input signal from reaching the output. Although the literature on this formulation is quite rich [33, 74] the simple implementation used in this work is adequately accurate to serve our purposes. In Figs.(5.5 and 5.6) a plane wave propagating in the total field region of an FDTD lattice is shown. Note that in order to obtain such a plane wave, the TF/SF formulation needs to be applied to all four walls of the box. This is due to the fact that if TF/SF is applied to the left wall alone, then that wall would act as a uniformly (but phased) aperture that is radiating in free space and therefore it does not remain a plane wave. Taflov [33] has used a look up table scheme to accelerate this process. Another problem arises when the TF/SF region extends into the PML. Taflove et al. [74] have come up with a new formulation for TF/SF that allows such extension but this affects the simplicity of the method. Any other field can be propagated through an FDTD lattice using the TF/SF formulation. A GB is one excellent choice. Other choices may include guided modes of slab waveguides, phased raised cosine fields etc. The only problem is that both the electric field and magnetic field of the source in

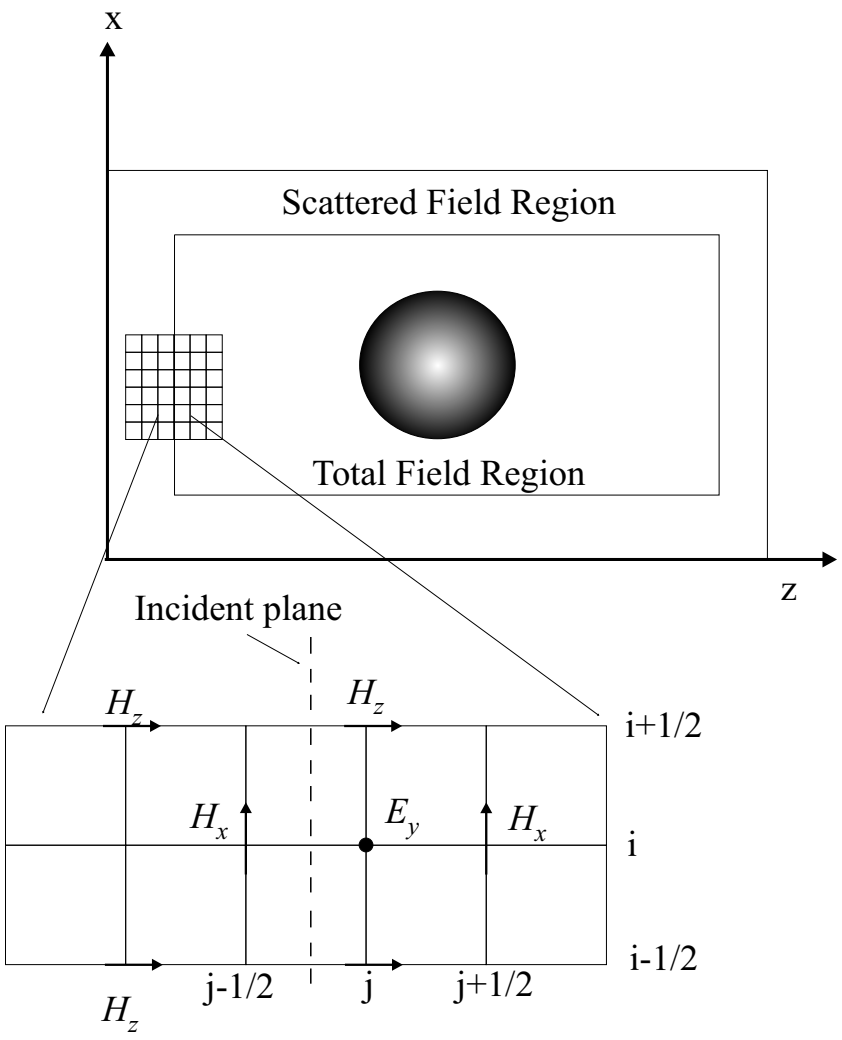

Figure 5.4: Modelling Scattered Field

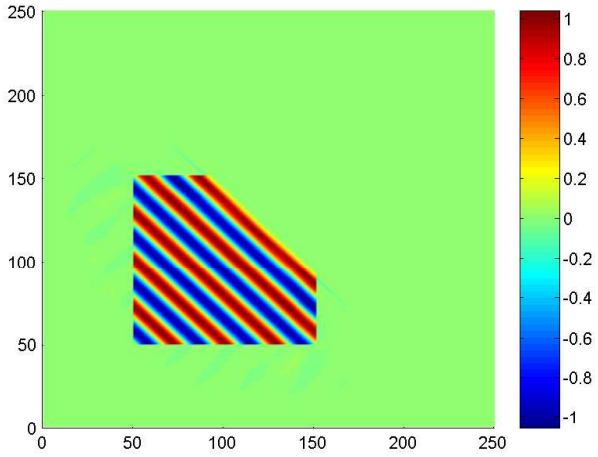

Figure 5.5: Plane Wave propagating at 45 degrees

a plane one cell before the TF/SF region need to be known. In case of a GB this field is known. In other cases a plane wave approximation can be used to find the magnetic field, i.e. it is assumed that the propagation from one cell to the adjacent cell is similar to plane wave and the magnetic field is obtained using simple plane wave formulas. Fig.(5.7) is a snap shot of a plane wave that is scattered by a rectangular piece of left handed material. This figure provides a qualitative understanding of how the TF/SF formulation yields only the scattered field in the SF region and the total field in the TF region.

5.8 Hybridization

In order to hybridize the GB Expansion/Tracing methods with FDTD, a virtual box must be drawn around the structure to be analyzed. GBs which have been traced through the system eventually impinge on this virtual box. Without loss of generality, it is assumed that the GBs impinge on only one of the surfaces of the virtual box. These beams are originally in time-harmonic form. Therefore the amplitude and phase of the the field are known on one of the boundaries of the TF/SF region. At this boundary, if the exact form of each GB is known then the problem is somewhat simplified; otherwise, using Gabor expansion, the field has to be expanded to a sum of GB emanating from different points of the boundary and travelling in different real directions. These spatially shifted and tilted GBs will then form the incident field to the 2D FDTD lattice. These beams must be propagated through the virtual box. Once the scattered field (which can be either the reflected field or the

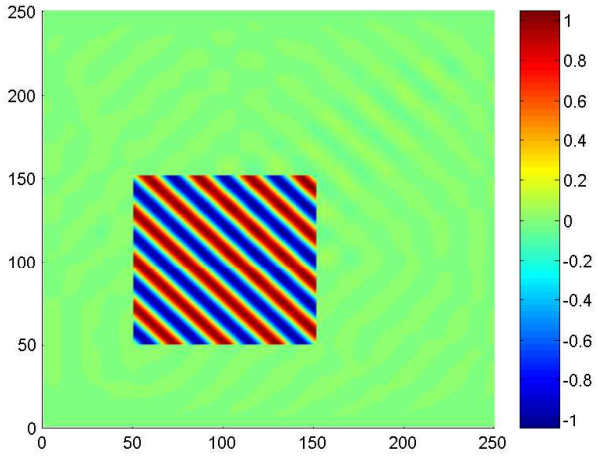

Figure 5.6: Plane Wave propagating at 45 degrees

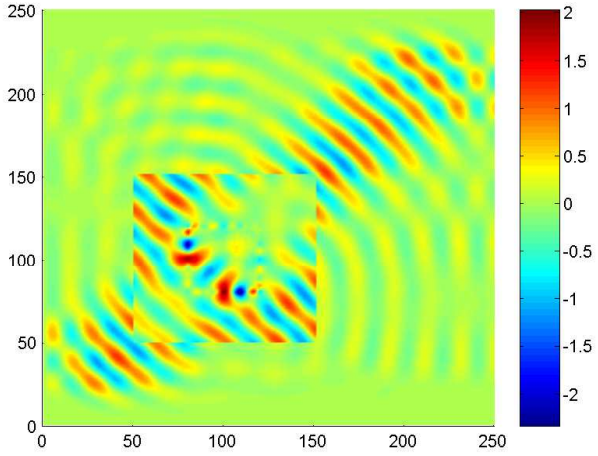

Figure 5.7: Plane Wave propagating at 45 degrees

transmitted field) is found, it has to be expanded in terms of GBs, again using the Gabor expansion. If the amplitude and/or phase variation of the field is too high relative to the wavelength over an extended aperture the field needs to be propagated a distance away (from the TF/SF region) using a near field to farfield and then expanded using Gabor expansion. The Gabor expanded GBs can then be propagated using GBT. It is clear that by using such a hybrid method, problems that are extremely large in terms of wavelength (hundreds of thousands or even larger) can be analyzed. The application of this method has been demonstrated for the 2D case but conceptually, the extension to 3D is trivial. We already have formulated the 3D GBT and 3D Gabor expansion; the only component missing is an accurate 3D FDTD. A number of applications of the method is demonstrated in the next chapter. Many of these problems can not be accurately solved by any single method. One of the other main merits of this method is that any of the components of the hybrid method can be made more accurate without affecting the other components. For example, if the existing FDTD is replaced with a highly optimized FDTD which runs on a parallel machine, the hybrid scheme can still be used without needing to change anything else. In terms of speed the only time consuming component of the method is obviously the FDTD. This time can always be shortened by reducing the size of the FDTD lattice and including a larger portion of the problem into the GBT/Gabor components.

5.9 GB Incidence

As mentioned above an FDTD method is needed that can accurately model the propagation of spatially shifted, tilted GB. In this work the TF/SF formulation has been used.

5.9.1 Field of Spatially Shifted Tilted GB at the Interface of the TF/SF Region

Referring to Fig.(5.8) and the analytic formulation of a 2D GB (Appendix C) the coordinate system of the shifted and tilted GB (x_t, z_t) to the problem's main coordinate system (x, z) as can be related as follows:

$$z_t = (x - h)\sin\theta + z\cos\theta$$
$$x_t = (x - h)\cos\theta - z\sin\theta$$

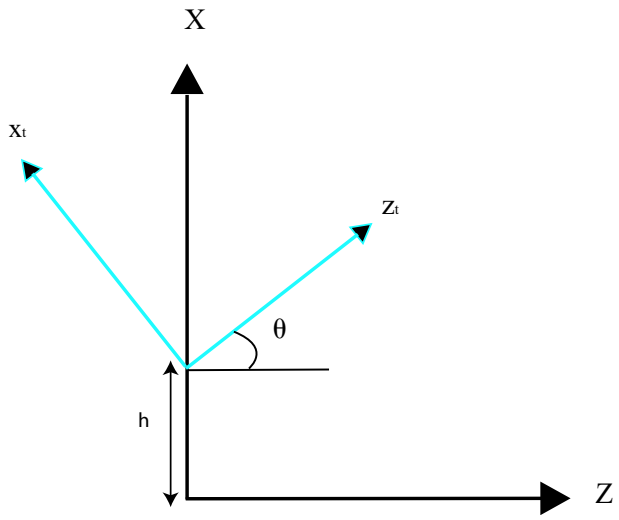

Figure 5.8: Coordinate system for a spatially shifted, tilted GB

$z = 0$ at the interface of the TF/SF region therefore:

$$z_t = (x - h)\sin\theta$$
$$x_t = (x - h)\cos\theta$$

If the above equations are substituted in the analytic formula for a 2D GB, the following is obtained:

$$\mathbf{E}(\mathbf{x}, \mathbf{0}) = E_{0y}\hat{y}\sqrt{\frac{jb}{(x-h)\sin\theta + jb}}\exp\{-jk(x-h)\sin\theta - \frac{jk}{2}\frac{[(x-h)\cos\theta]^2}{(x-h)\sin\theta + jb}\} \quad (5.14)$$

The above formula forms the incident electric field.

5.9.2 Magnetic Field of a GB

It was shown in [41] in a very simplified manner that the magnetic field of a GB is also GB and that the electric field, magnetic field and the direction of propagation form a right handed system and the ratio of $|E|/|H|$ is η the impedance of free space as long as the problem remains in the paraxial regime. It was shown that although the magnetic field may posses a component in the direction of propagation, the magnitude of this component is extremely small in the paraxial regime and it is therefore neglected.

5.9.3 GBs and the TF/SF Formulation

One of the main advantages of a GB when used in the TF/SF formulation is that the correction term can be added/subtracted on only one of the walls of the TF/SF region. This is due to the fact that if a launched GB is assumed to be a physical field emanating from a finite aperture, as long as the aperture is larger than the waist of the GB, the aperture radiated field will be a physical GB. This is of course due to the exponential nature of the field in planes perpendicular to the direction of propagation. As was mentioned above, this is not true for a plane wave. In order to implement the TF/SF formulation for a GB, E_y and H_x are updated normally and then $H_{x_{inc}}$ is added to the updated E_y and $E_{y_{inc}}$ is subtracted from the updated H_x, where $H_{x_{inc}}$ and $E_{y_{inc}}$ are represented by:

$$E_{y_{inc}} = \Im\{\exp(j\omega t)\sqrt{\frac{jb}{(x-h)\sin\theta + jb}}\exp\{-jk(x-h)\sin\theta - \frac{jk}{2}\frac{[(x-h)\cos\theta]^2}{(x-h)\sin\theta + jb}\}\}/j$$

$$H_{x_{inc}} = \Im\{\exp(j\omega t)\cos\theta\sqrt{\frac{jb}{(x-h)\sin\theta + jb}}\exp\{-jk(x-h)\sin\theta - \frac{jk}{2}\frac{[(x-h)\cos\theta]^2}{(x-h)\sin\theta + jb}\}\}/j$$

Here it is assumed that the driving source of the problem is $\sin(\omega t)$. Numerous numerical experiments were performed with beams launched at different angles. The performance of both the implemented PML and TF/SF formulation was tested at different angles. It was concluded that if the angle of incidence is less than 75 degrees both the PML and TF/SF formulation obtain very good results. In the worst case where the launch angle is 90 degrees the TF/SF formulation fails completely and therefore this angle must be avoided. In Figs.(5.9,5.10,5.11) snapshots of the propagated GBs at 18, 45 and 90 degrees in free space are shown. The waist of the beam is 2λ and 25 points per λ is used for the FDTD lattice. In Fig.5.12 a GB is launched at 45 degrees and the field in a plane perpendicular to the z axis is compared with the analytical formula of a GB at 4λ away from the source. The effect of the PML at the far right hand side of the plot should be noted. The field dies off perfectly after entering the PML which was set to 50 cells (2λ). In Fig.(5.13) a GB is launched at 60 degrees and the field in a plane perpendicular to the z axis is compared with the analytical formula of a GB at 3λ away from the source.

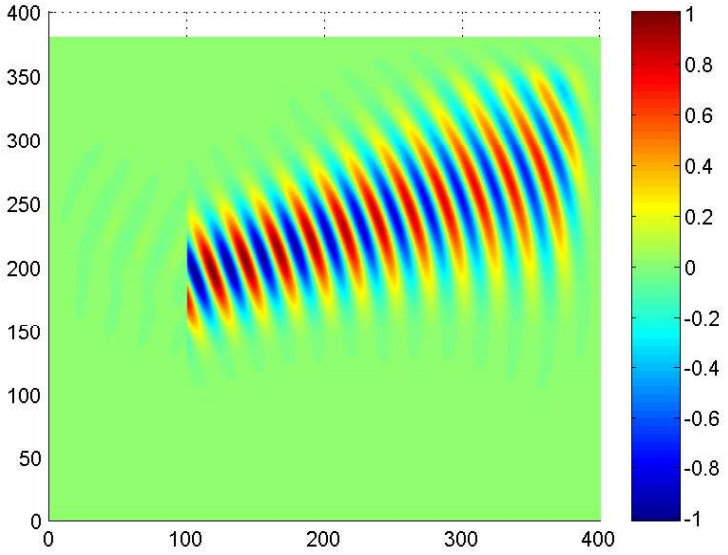

Figure 5.9: GB propagating at 18 degrees

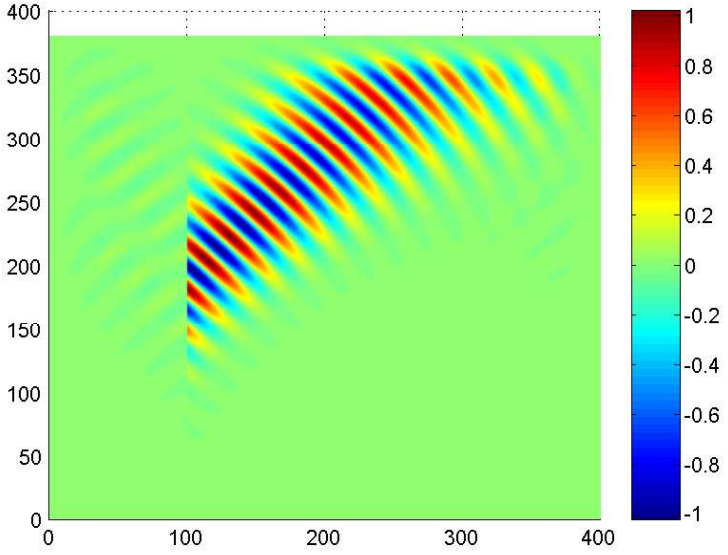

Figure 5.10: GB propagating at 45 degrees

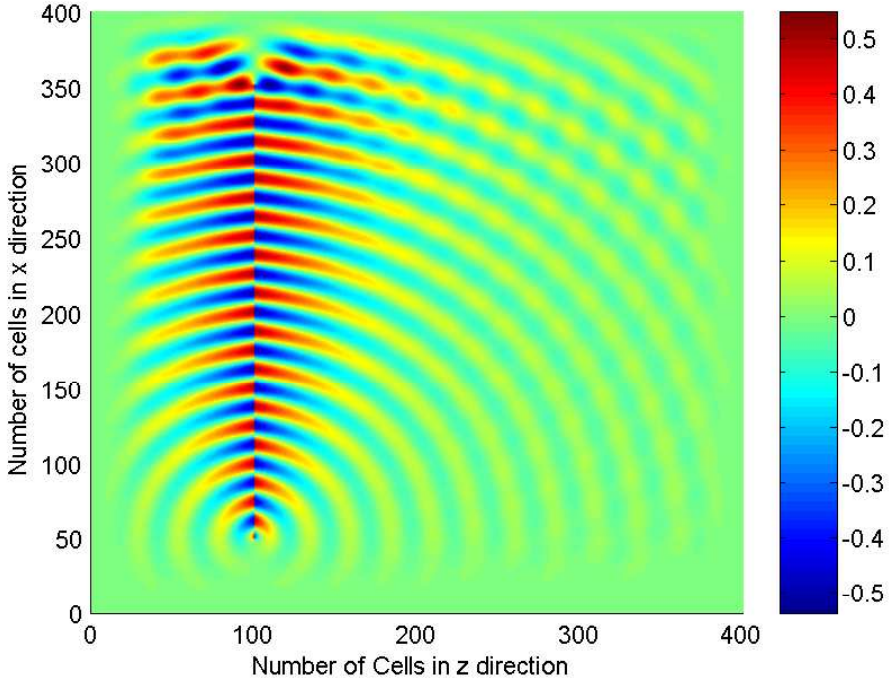

Figure 5.11: GB propagating at 90 degrees

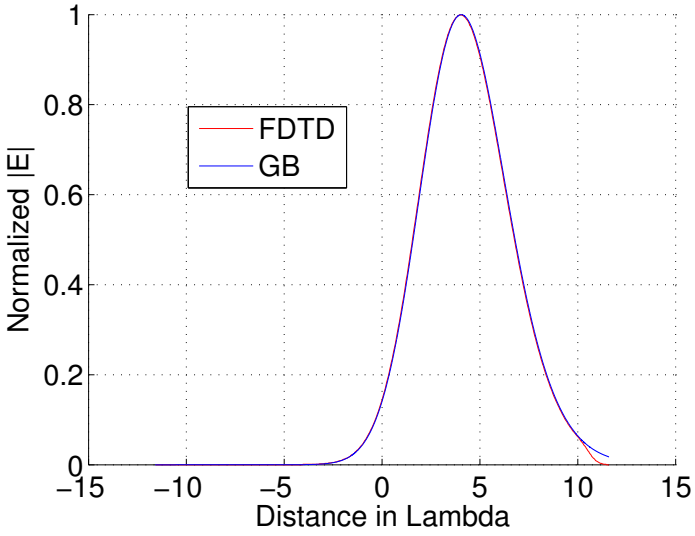

Figure 5.12: GB - FDTD comparison 45 degrees propagation

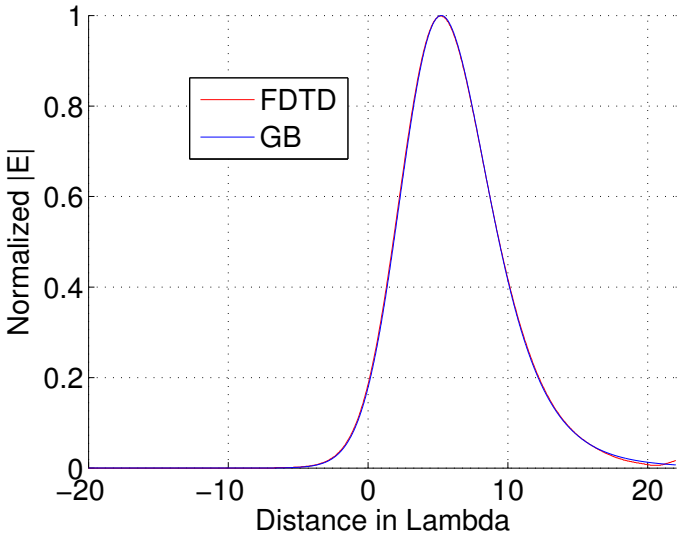

Figure 5.13: GB - FDTD comparison 60 degrees propagation

5.10 Combination of the FDTD Method with Gabor Expansion

In this section the hybridization of the FDTD method with the Gabor expansion is explained. This hybridization has two forms: The first at the input and the second at the output.

5.10.1 Combination of Gabor Expansion with FDTD at the Input

Here the incident field at the incident plane (which is formed by propagation of certain beams inside the photonic structure under consideration using GBT) is expanded using the Gabor expansion. Therefore at the input a number of spatially shifted and rotated GBs are obtained. These beams are launched inside the FDTD lattice all at once (Fig.(5.14)). At any time step a loop adds the contribution from each field and the routine finds the resultant $E_{y_{inc}}$ and $H_{x_{inc}}$. A test was performed where the matched case was used to propagate a phase cosine field inside the FDTD lattice. The length of the aperture is 4λ in the matched case and the L parameter of the Gabor expansion was chosen to be $L = 5.8\lambda$ so that each beam has a waist that is larger than the aperture itself. The reason a non-integer value for the L parameter was chosen is that if L is an integer then the

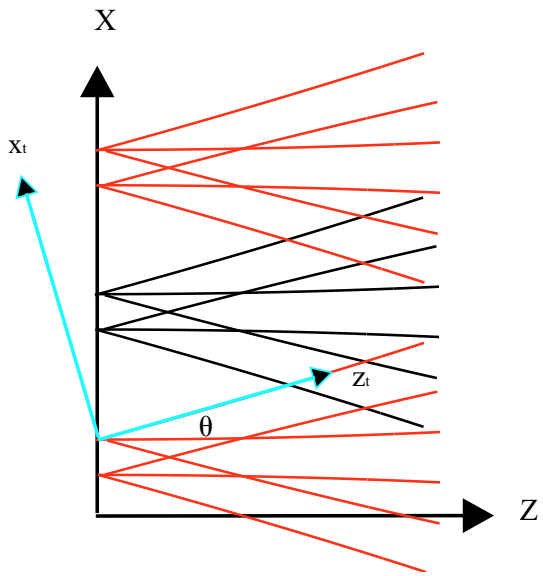

Figure 5.14: Gabor expanded fields launched inside a FDTD lattice

non-evanescent fields have launch angles equal to:

$$\arcsin(\frac{n\lambda}{L})$$

by changing n a non-evanescent beam will be produced that travels at 90 degrees which, as was mentioned above, is not desirable. The phased cosine distribution which is given by:

$$f(x) = \begin{cases} \cos(\frac{\pi x}{L_0})\exp(j\alpha x) & \text{if } -L_0/2 < x < L_0/2 \ ; \\ 0 & \text{otherwise.} \end{cases}$$

(where α determines the angle of the peak of the farfield) imposes a more severe test on the Gabor expansion due to the phasing of the field. α was chosen to be $0.1k$ where k is the wavenumber. 60 beams were launched into the FDTD lattice. The excellent agreement between the FDTD simulations and the rigorous solutions (Fig.(5.15,5.16))show that:

- The difference in wave velocities for beams launched at different angles (see [33]) is negligible.
- The errors caused by reflection from PML and the imperfection of the TF/SF formulation are negligible.
- As only non-evanescent beam fields are launched, the error caused by not including the evanescent beams are negligible even as close as 5λ to the source.

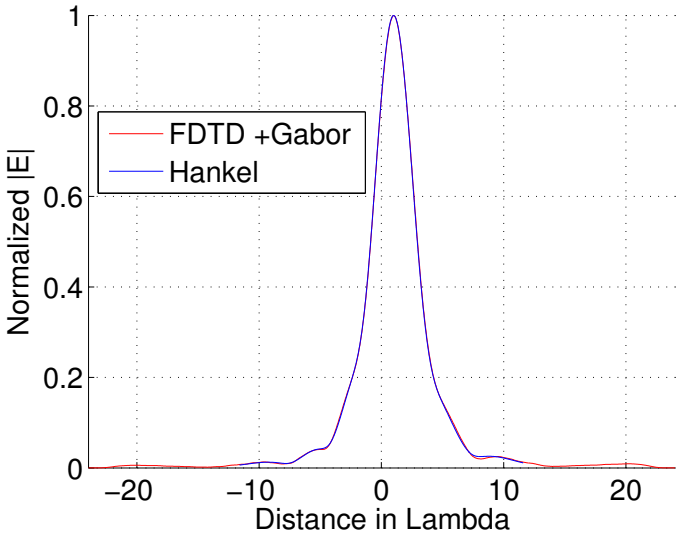

Figure 5.15: FDTD and Green function (Hankel) comparison Fresnel zone field

It was therefore concluded that the Gabor expansion can be successfully combined with the FDTD at the input.

5.10.2 Combination of Gabor Expansion and FDTD at the Output, Near Field to Far Field Transformation

Once the scattered field from the simulated structure is found (this can be in the form of a reflection or transmission), in order to further propagate the field inside the optical system, the field needs to be re-expanded in terms of GBs. As it is always desired to keep the FDTD lattice as small as possible, the field is observed as close as possible to the scatterer. The phase and amplitude of the field in phasor form at a plane near the scatterer is obtained from the time domain form of the field. Therefore the near scattered field in phasor form is obtained in this manner. The field in any region (near field, Fresnel zone and far field) can be found using a Hankel function approach. This method is explained in the next section. The knowledge of the phasor form of the total field in these regions is not sufficient in this method. As was mentioned earlier, the field at the output must be expressed in terms of a set of GBs. This is due to the fact that this output field must be further propagated inside the photonic system using GBT. If the field remains smooth with slowly varying phase over the output plane it can directly be expanded using Gabor expansion in the usual format. If the near field is rapidly fluctuating it might not be very

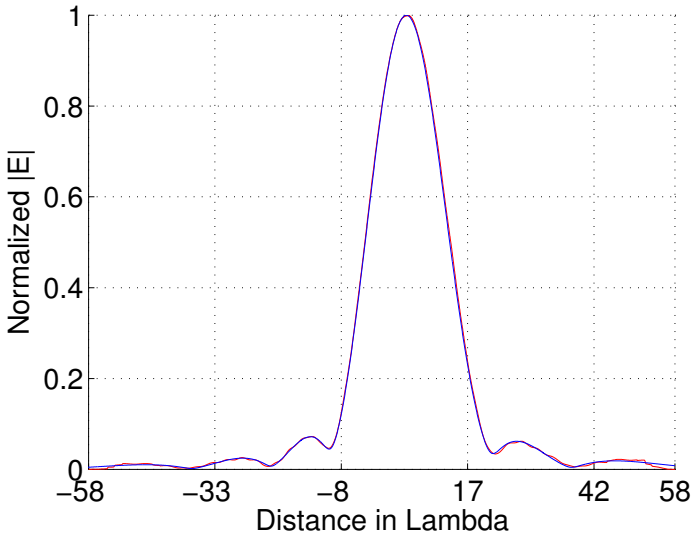

Figure 5.16: FDTD and Green function (Hankel) comparison far field

efficient to directly expand the fields into GBs. In these special cases which form the worst case scenario the field must be propagated using the Hankel function approach up to a distance where the field becomes well behaved. This field is then expanded into a set of GBs using a simple Gabor expansion.

Hankel Function Approach

At any plane parallel to the TF/SF region boundary (either inside the region or outside the region) the amplitude and phase of the field in phasor form can be obtained. Once these are known that plane can be considered as an aperture radiating in free space and the field on either side of it can be obtained using 2D Greens function (Hankel function) Egn.(5.15). It must be noted that this approach is rigorous and therefore the results obtained for the near, Fresnel zone and farfield regions are 100% accurate. For the near and Fresnel zone fields NAG library was used to calculate the Hankel function and the integral (Eqn.(5.15)). For farfield the large argument approximation of the Hankel function must be used.

$$\mathbf{E}(x,z) = \hat{y}\frac{jkz}{2}\int_{-\infty}^{\infty} f(x')H_0^{(2)}(kR)/R dx'$$
$$R = [(x'-x)^2 + z^2]^{1/2} \tag{5.15}$$

where k is the wavenumber and $H_0^{(2)}()$ is the 2D Greens function (Hankel function).

Chapter 6

Applications of the Hybrid Method

6.1 Introduction

In this chapter the hybrid method is used to analyze a number of passive photonic structures. Three different classes of problems have been considered:

- Scattering problems: In this class of problems a structure is placed inside the FDTD virtual box and is illuminated by a set of GBs which are produced by Gabor expansion of the incident field. The field scattered by the structure is then found close to the TF/SF region. This near field is then expanded using the Gabor expansion and the resultant GBs are then launched back into the photonic system. For example the effect of a thin lens placed many wavelengths away from the scattering structure can be found. Dielectric gratings were chosen for this class. The reason for this choice is twofold. The first is related to the very interesting properties of the gratings that make them applicable in many photonic systems (filters, couplers,etc). The second reason which is of primary importance to us, is that a dielectric grating imposes a very severe test on any numerical method used to analyze it. This is due to the fact that the size of a typical grating can be hundreds of wavelengths but it contains feature sizes (the elements of the grating) that are smaller than the wavelength. This large ratio between the overall size and the fine feature sizes make these structures difficult to analyze as any numerical method needs some type of discretization and the fine features set an upper bound for the size of the cells used in the numerical method's discretization scheme. In order to analyze and verify the result of our tests on a dielectric grating a systematic procedure was used. The grating was first illuminated by a single GB launched at different angles and the results were compared with the

general grating formula derived in section 6.2. The flat grating was then deformed by gradually shifting the elements of the grating forward up to its midpoint and then backwards (and vice versa)to form concave and convex structures. Surprisingly the far field was identical in both cases! Using a phased array of antenna it was proved that this was to be expected. This observation further confirmed the accuracy of this hybrid method. In order to put the hybrid method to full use, a general phased phased cosine aperture field was used. This field was then expanded to a set of GBs. The GBs were launched inside the FDTD lattice and the resultant scattered field was propagated for a distance of 100 lambda using the Green function formulation. The field at 100 wavelengths was then expanded using Gabor expansion and passed through a thin lens. This example (section 6.5) employs all the components of the hybrid method.

- Coupling problem: In many photonic structures once the beams have passed through various structures they are ultimately coupled into a waveguide. A simple grating coupler was used as an example to show the applicability of this method to this class of problems.

- Transmission Problems: In this class of problems, a structure is again placed in the FDTD lattice but instead of analyzing the scattered field, the transmitted field which is in the total field region is taken as the near field. A very simple transparency illuminated by a GB was considered and the properties of the structure was qualitatively observed.

In the next section it is shown that for a plane wave illumination the positions of the peaks of the far field of a dielectric grating are the same as those of a perfect electric conductor grating:

6.2 Grating Formula for a Dielectric Grating

In this section the general grating formula for a dielectric grating is derived. The geometry of the problem is shown in Fig.(6.1). Here the approach used by H. Haus [75] has been extended to include the dielectric case. It is assumed that the grating is illuminated by a plane wave given by:

$$\mathbf{E_i}(x,z) = E_{0i}\hat{y}\exp(-jk_{1x}x - jk_{1z}z)$$

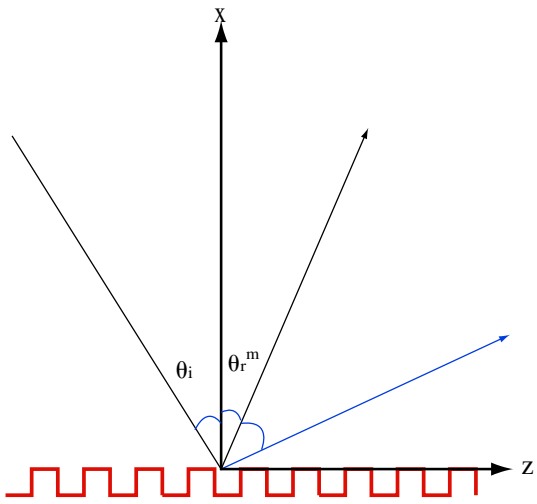

Figure 6.1: Geometry of the problem

The grating's geometry is defined by $x = f(z)$ where $f(z)$ is a periodic function with period Λ. The boundary condition at the surface of the grating is given by:

$$\forall(x,z);\ x = f(z)$$
$$\mathbf{E_i}(x,z) + \mathbf{E_r}(x,z) = \mathbf{E_t}(x,z)$$

or equivalently:

$$\forall(x,z);\ x = f(z)$$
$$E_{0i}\hat{y}\exp(-jk_{1x}x - jk_{1z}z) + \mathbf{E_r}(x,z) = \mathbf{E_t}(x,z)$$

From the above equations it is evident that:

$$\mathbf{E_t}(x,z) = h(x,z)\exp(-jk_{2z}z)$$
$$\mathbf{E_r}(x,z) = g(x,z)\exp(-jk_{1z}z)$$

where g and h are periodic with period Λ:

$$g(x,z+\Lambda) = g(x,z)$$
$$h(x,z+\Lambda) = h(x,z)$$

The proof is given for the reflected wave, the proof for the transmitted wave is identical and only the results are given. As g is periodic the reflected field can be expanded in terms of a Fourier series in z but this Fourier series is nothing but the plane wave expansion in

this case; i.e the continuous spectrum of plane waves becomes a discrete sum. Therefore the following is obtained:

$$\mathbf{E_r}(x,z) = \sum_m \Gamma_m \exp(-jk_{1z}z)\exp(-j\frac{2\pi m}{\Lambda}z)\exp(jk_m x)$$

As each plane wave must satisfy Helmholtz:

$$(k_{1z} + \frac{2\pi m}{\Lambda})^2 + k_m^2 = w^2\epsilon\mu$$

This means that for each m, k_m is found from the above equation. Furthermore as

$$k_{1z} = w\sqrt{\epsilon\mu}\sin\theta_i = \frac{2\pi}{\lambda}\sin\theta_i$$

therefore the following relation holds:

$$k_{1z} + \frac{2\pi m}{\Lambda} = w\sqrt{\epsilon\mu}\sin\theta_r^m$$

and therefore the Grating Equation for a general dielectric gratings is obtained:

$$\sin\theta_i + \frac{m\lambda}{\Lambda} = \sin\theta_r^m \tag{6.1}$$

Where λ is the wavelength. Note this result was obtained from phase matching considerations and is therefore identical to the equation for a metallic grating. With the exact same argument the following equation holds for the transmitted plane wave:

$$\sin\theta_i + \frac{m\lambda}{\Lambda} = n\sin\theta_t^m \tag{6.2}$$

where n is the refractive index of the dielectric.

6.3 Dielectric Grating

In this section a finite dielectric grating illuminated by a GB launched at different angles is considered. To the author's knowledge no analytical method that can predict the near field, Fresnel zone field and far field for this problem exists. Here the grating is illuminated with a single GB but obviously any field can be treated by the hybrid method. Five numerical tests were performed on a flat grating. In the first three the GBs were launched at 0,3,9 degrees. The waist of the beams are 25λ and the length of the grating is 150λ. The Λ of the grating is $3\lambda/2$. The depth of each tooth like element is $\lambda/4$. The fields are observed

at 15λ from the source in the scattered field region. The near field amplitude and phase and the far field in both cartesian and polar coordinate systems are shown in Figs.(6.2, 6.3, 6.5, 6.6). The angles of the peaks of the far fields matches the general grating extremely well. Fig.(6.4) is magnified version of the phase plots of the scattered field. It is provided for comparison with the phase plots of the fifth test.

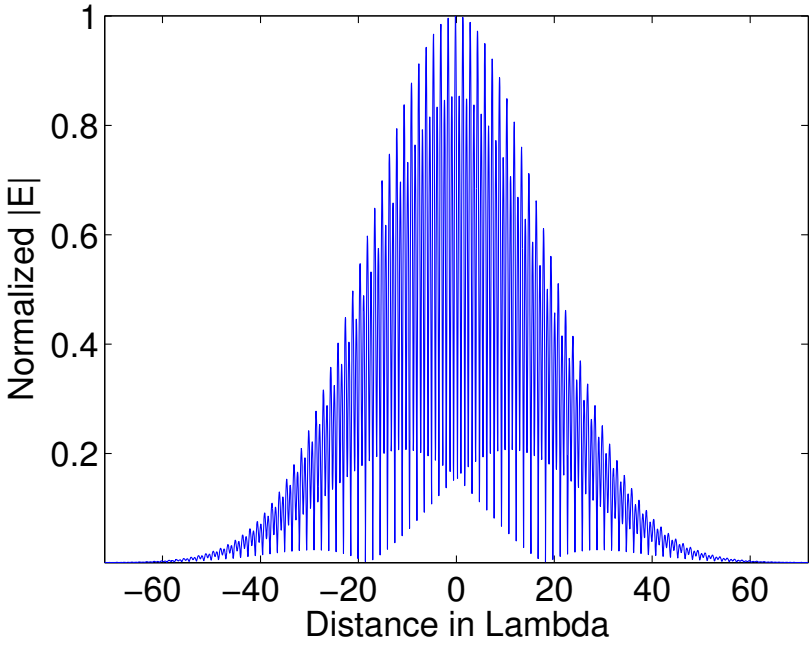

Figure 6.2: Near field, normal incidence

In all of the above cases according to the general grating formula 3 peaks exist in the farfield namely $m = -1, 0, 1$. In the next 2 tests the GB is launched at 18 degrees for two different grating periods namely 1.5λ and $.8\lambda$. The polar plot of the far field for $\Lambda = 1.5\lambda$ is shown in Fig.(6.7.d)(the near field and phase in this case is not shown). The near field, phase and polar plots for $\Lambda = .8\lambda$ are shown in Figs.(6.7.a,6.7.b,6.7.c). When the grating period is reduced to $\Lambda = .8\lambda$, according to the grating formula only 2 peaks exist. This is shown by comparing Figs.(6.7.c,6.7.d). For $\Lambda = .8\lambda$ the far field side lobe is accurately predicted to be 71.35 degrees. There is a very interesting observation in the phase of the near field in this case (Fig.(6.8)). Two clearly different regions can be distinguished in the phase plots. In the first region an increasing phase function reveals a beam propagating upwards. In the second region a decreasing phase function reveals a beam propagating downwards. The difference in the slope of the phase shows that the beams are travelling at different angles. Therefore the peaks observed in the amplitude of the near field will move

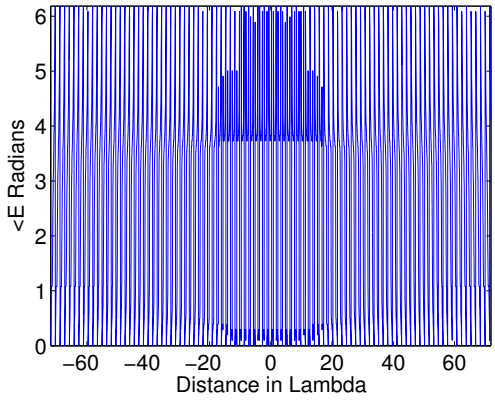

(a) Phase

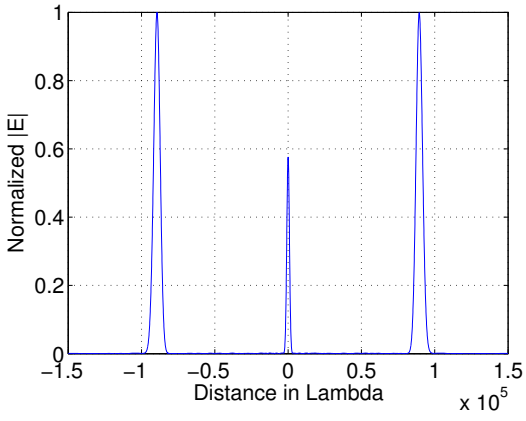

(b) Far Field

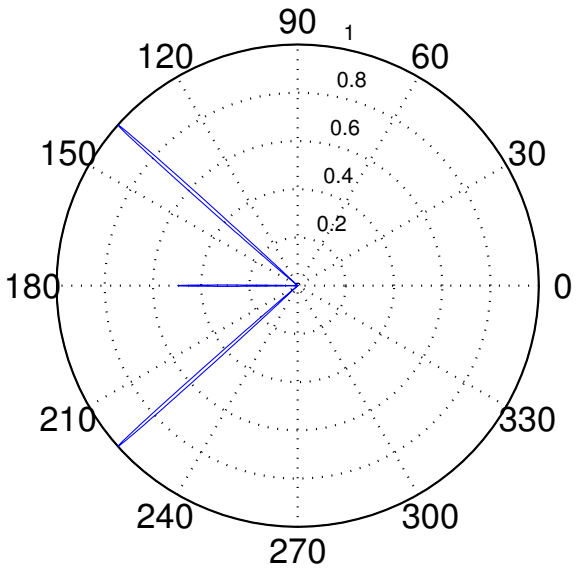

(c) Polar Plot

Figure 6.3: Normal Incidence

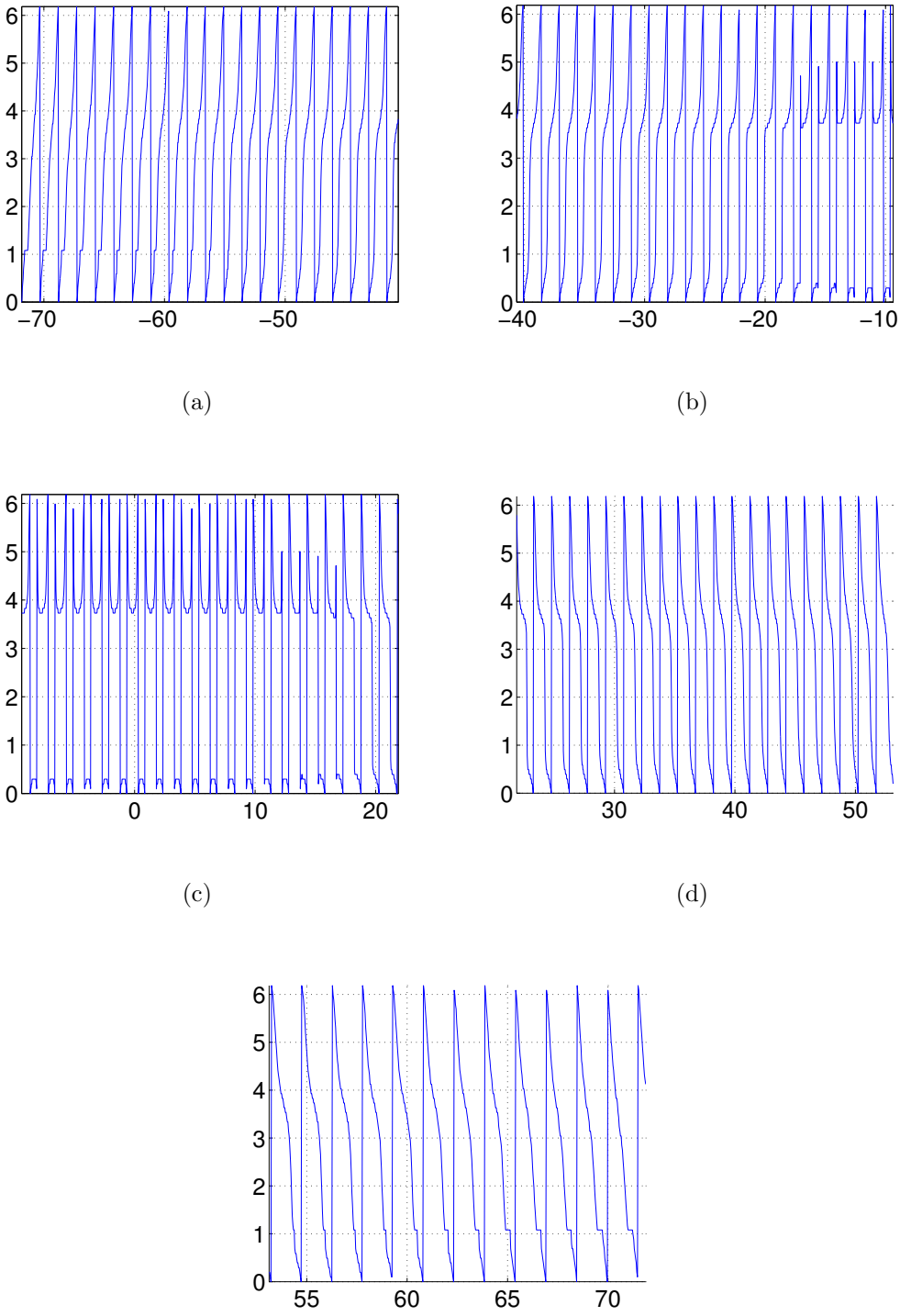

(a)

(b)

(c)

(d)

(e)

Figure 6.4: Magnified phase

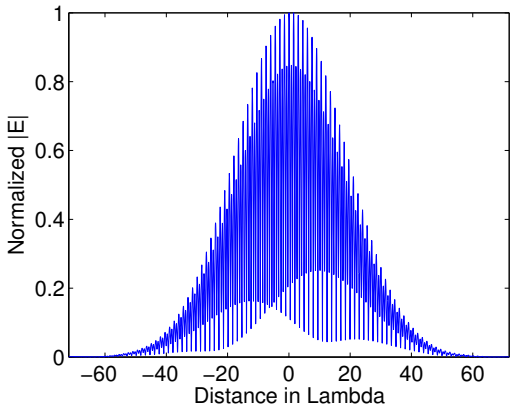

(a) Near Field

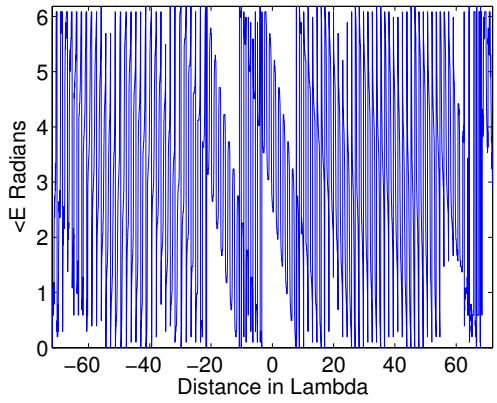

(b) Phase

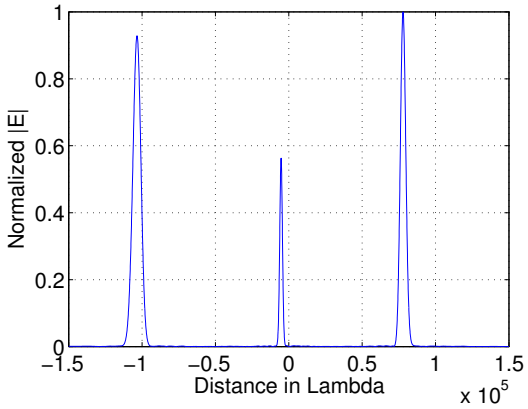

(c) Far Field

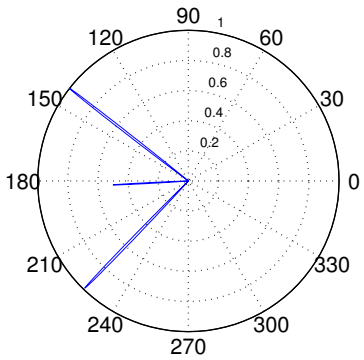

(d) Polar Plot

Figure 6.5: 3 Degrees Incidence

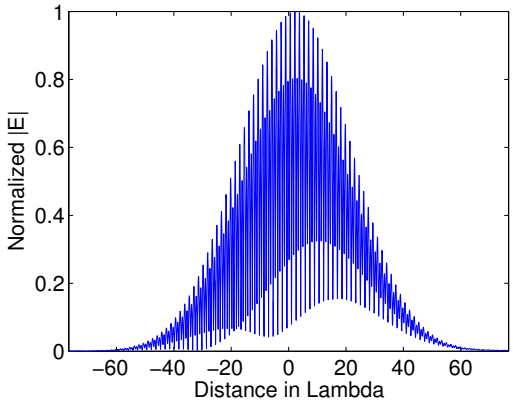

(a) Near Field

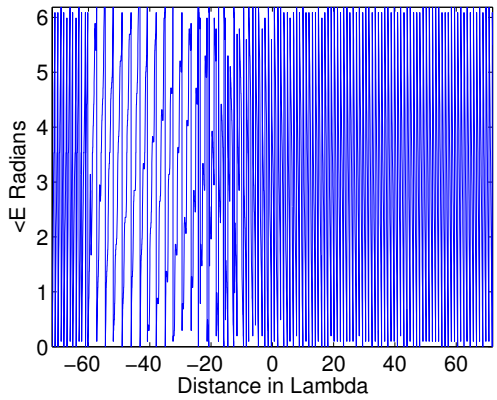

(b) Phase

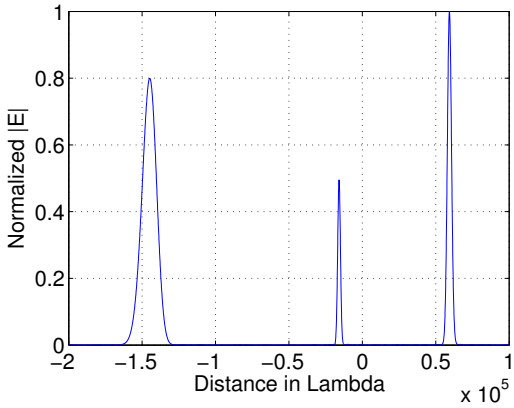

(c) Far Field

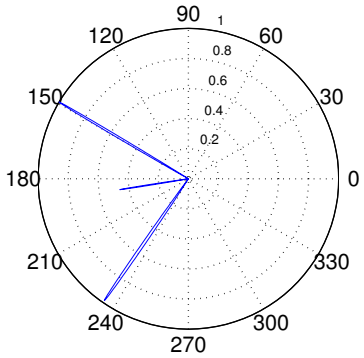

(d) Polar Plot

Figure 6.6: 9 Degrees Incidence

away from one another and eventually produce the two lobes in the farfield region. This can be compared with the normal incidence with $\Lambda = 1.5\lambda$, Fig.(6.4) where the fact that the equality of the slope of the phase in the left and right regions shows beams travelling at the same angle.

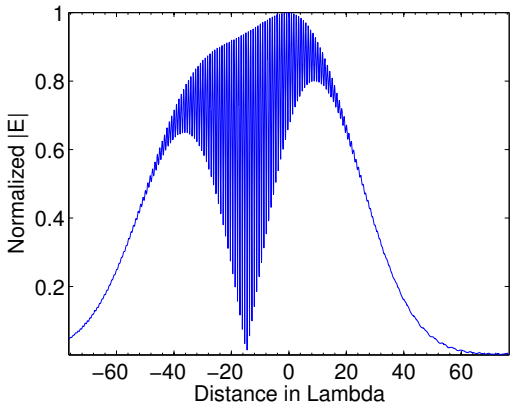

(a) Near Field $\Lambda = .8\lambda$

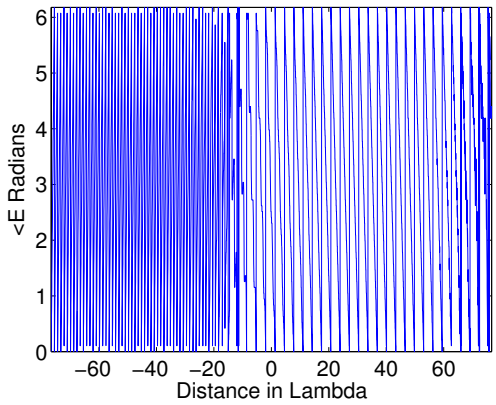

(b) Phase $\Lambda = .8\lambda$

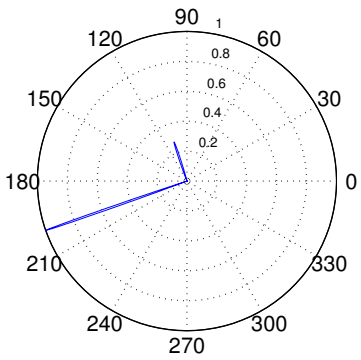

(c) Polar Plot $\Lambda = .8\lambda$

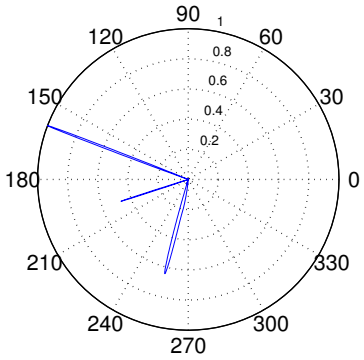

(d) Polar Plot $\Lambda = 1.5\lambda$

Figure 6.7: 18 Degrees Incidence

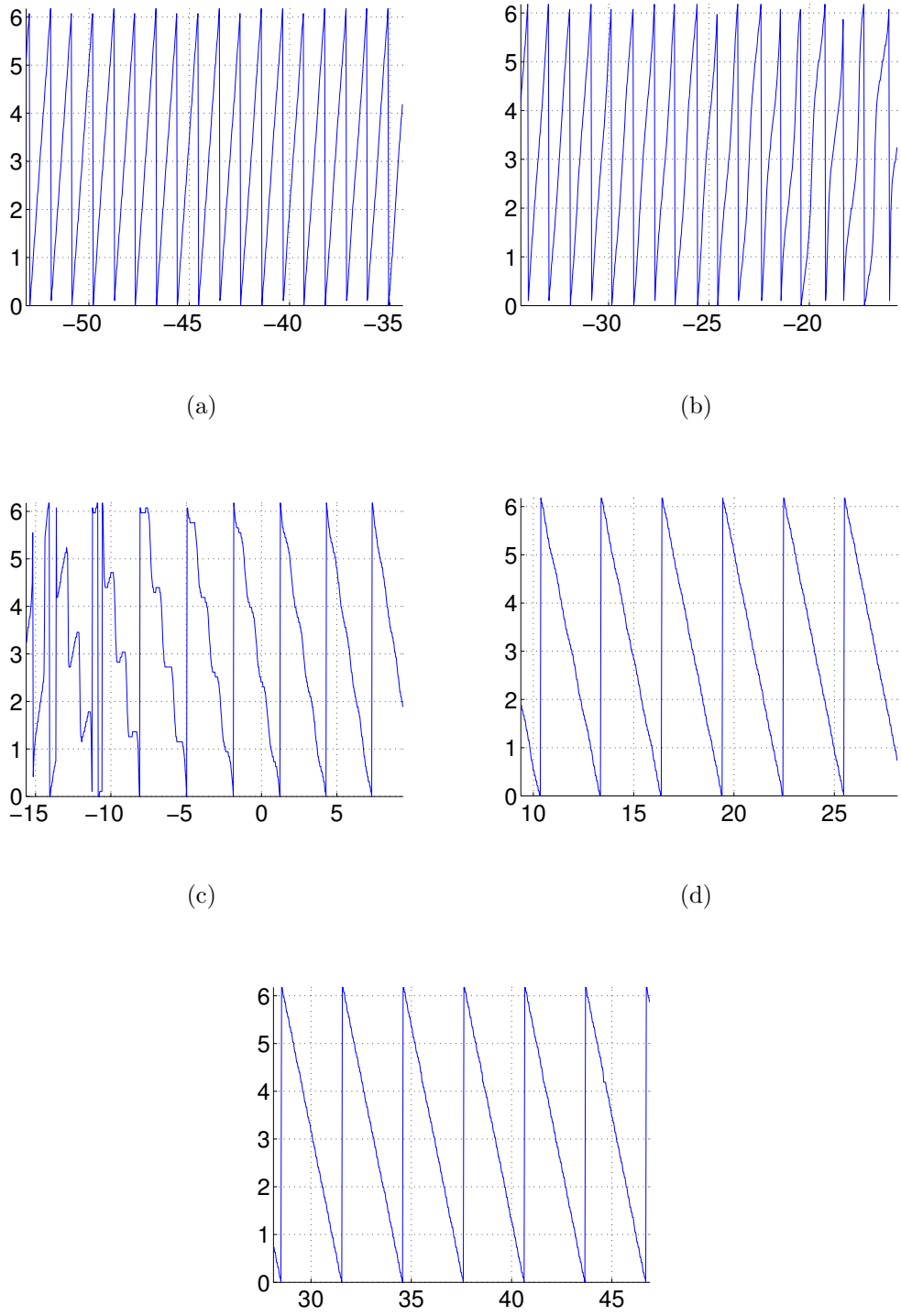

Figure 6.8: 18 Degrees incidence phase zoomed

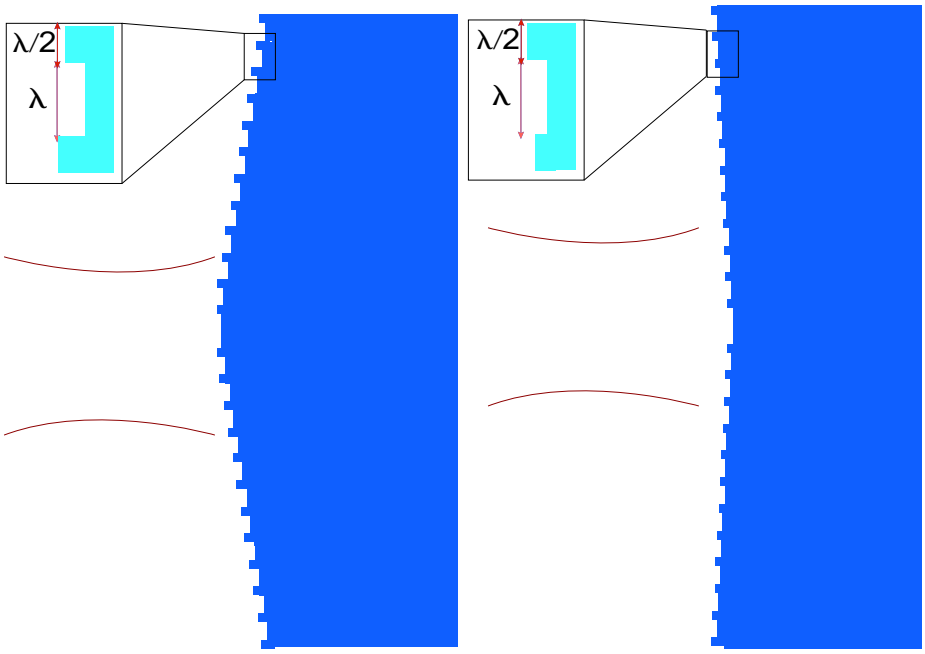

(a) Convex (b) Concave

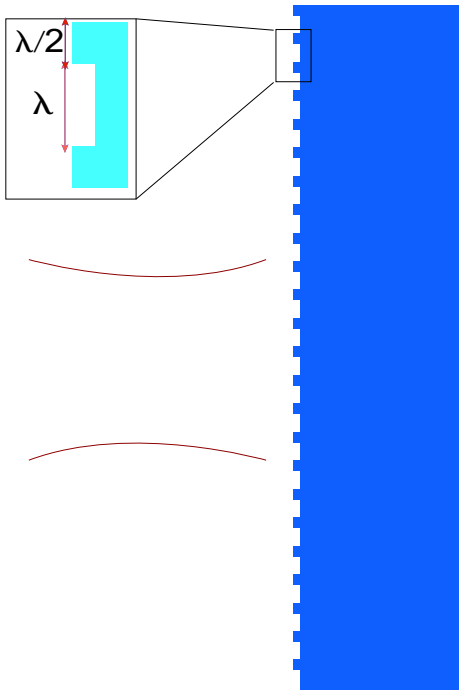

(c) Flat

Figure 6.9: Geometry of the problem

6.4 Concave and Convex Gratings

In this section the properties of concave and convex gratings were investigated. The concave and convex shapes were obtained by gradually shifting the elements of the grating forward and backward as was explained in the introduction. Very interesting results were obtained that further reveal the accuracy and versatility of the Hybrid method. Fig.(6.9) shows the different geometries simulated. The figures are not drawn in the actual proportion in order to depict the grating elements and their spacing. The actual gratings contain 100 elements. The length of the flat grating is therefore $100 * 3/2 * \lambda = 150\lambda$. The relative shift of the elements in the concave and convex grating is $\lambda/32$; therefore the mid point of the concave grating is $50 * \lambda/32 = 1.5625\lambda$ shifted relative to the endpoints. The same is true for the convex grating but the shift is in the other direction. The near field and far field of the scattered field which were created by a normally incident GB were calculated for each structure. The results are shown in Figs. 6.10, 6.11 and 6.12. The polar plots of the flat grating and the concave grating are also shown in Fig.(6.13). As it was shown in section 6.2 the grating formula for a dielectric grating is the same as a PEC grating. This can be easily seen from the polar plot and the grating formula. A strange phenomena was observed in that although the near and Fresnel zone fields of the concave and convex grating are very different, their far field match perfectly, see Fig.6.4. The reason for this cannot be the fact that the curvature of the curved gratings is small. If that was the case, the results should match the result of a flat grating; therefore, it was concluded that the phase distribution on the grating elements should be responsible for this phenomena. In order to show this, a phased array approach was used. A virtual grating was illuminated by a normal GB. At the centers of the elements of the grating the phase and amplitude of the GB was found. The pattern of the resultant phased array was thereby calculated. Therefore if x_i, z_i, $i = 1, 2, ..., 100$ are the coordinates of the centers of the elements of the imaginary grating the phased array is formed by

$$A_i \exp(j\phi_i) = \sqrt{\frac{jb}{z_i - z_0 + jb}} \exp\left(-jk(z_i - z_0) - \frac{jk}{2}\frac{x_i^2}{z_i - z_0 + jb}\right) \tag{6.3}$$

This phased array then radiates in free space and therefore the array factor is found simply by [76]:

$$AF = \sum_{i=1}^{100} A_i \exp(j\phi_i) \exp[-jk(x_i \sin\theta - z_i \cos\theta)] \tag{6.4}$$

The above procedure was implemented by a simple code and to our surprise the results were the same for the concave and convex case! The curvature was then changed by

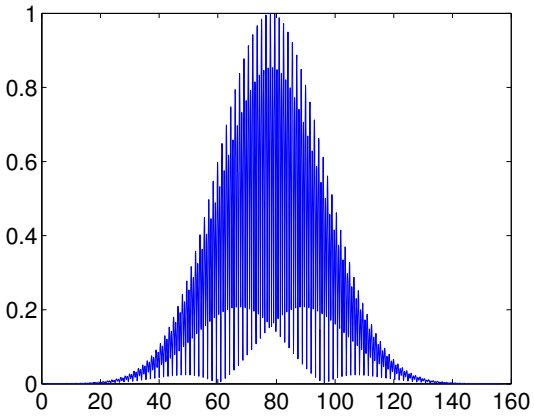

(a)

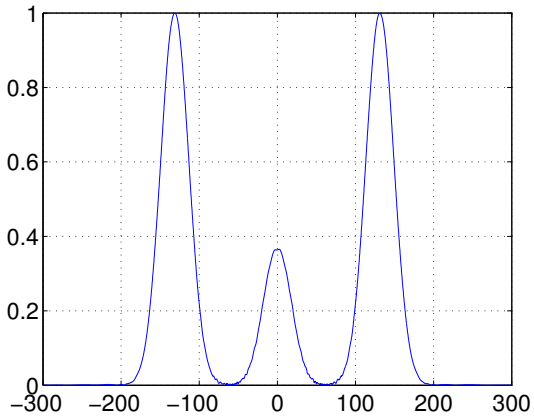

(b)

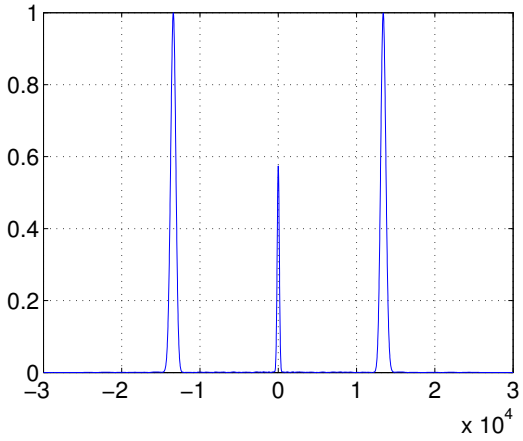

(c)

Figure 6.10: a. Near, b. Fresnel, c. Far field of the flat grating

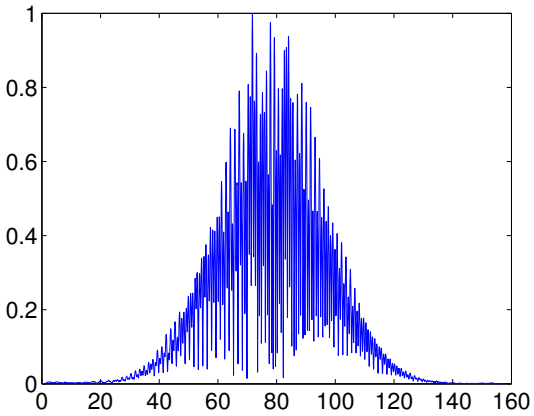

(a) Near Field

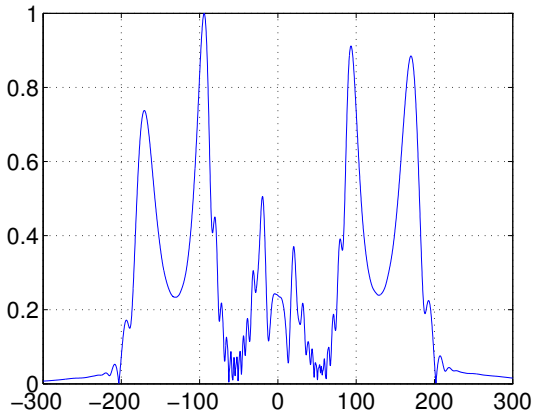

(b) Fresnel Zone Field

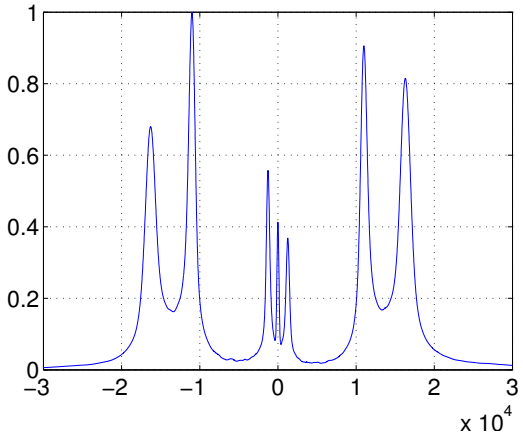

(c) Far Field

Figure 6.11: Concave Grating

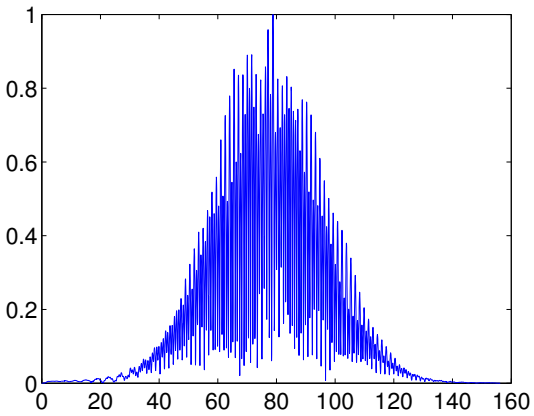

(a) Near Field

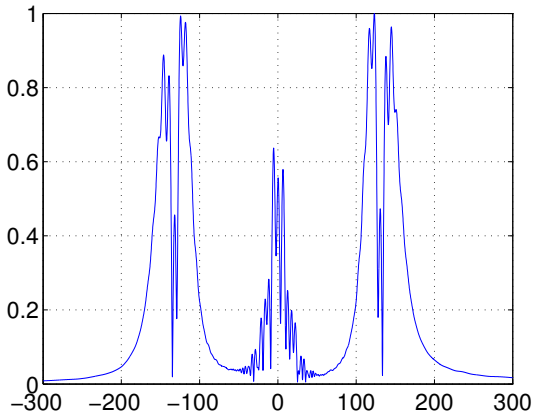

(b) Fresnel Zone Field

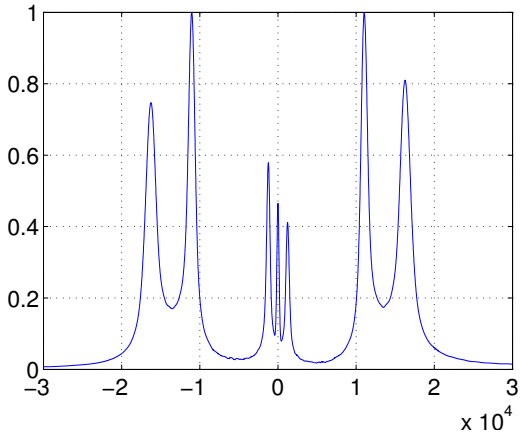

(c) Far Field

Figure 6.12: Convex Grating

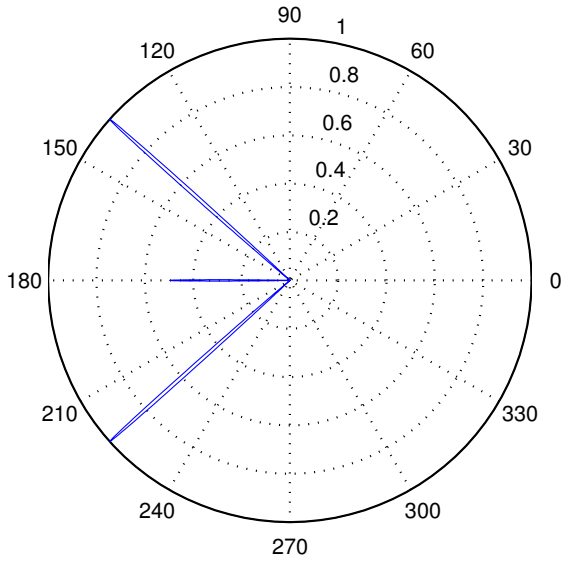

(a) Flat

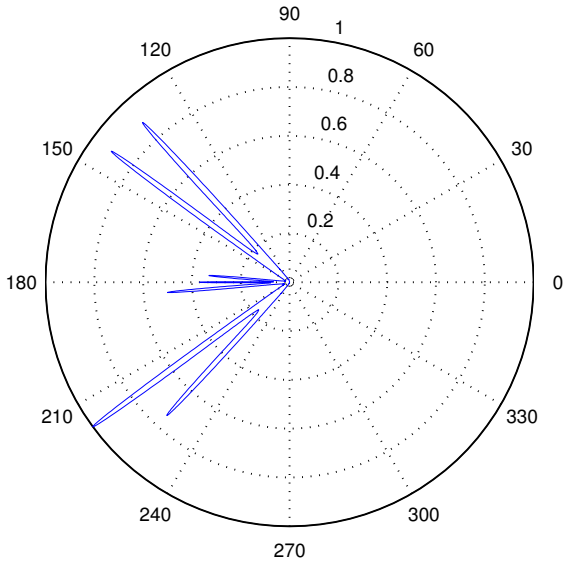

(b) Concave

Figure 6.13: Polar Plots of the Flat and Concave Gratings

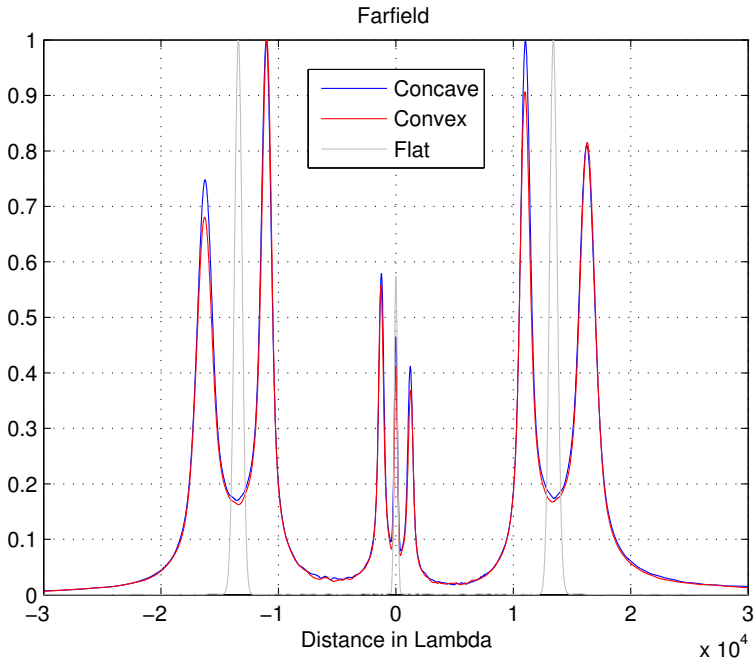

increasing the shift between consecutive elements. Even with a relative shift of $\lambda/2$ the result remained the same for the concave and convex case. It became clear that with s as the relative shift, the array factor has a term with $+s$ and another term with $-s$ therefore changing $+s$ to $-s$ (convex to concave) does not change the result. Another way of looking at the problem is that a translation of an array does not change its farfield as long as the phasing of the individual elements are not changed. By moving a tilted array in the field produced by a plane wave the phase difference between the elements remains the same. Therefore, the upper half of the concave array acts like the lower half of the convex array and vice versa. Another interesting observation is the qualitative similarity between the results obtained using the phased array approach and our method. The observation that the central lobe is missing from the phased array result is due to the fact that the phase array consists of 100 elements in *free space* therefore, there is no main structure to produce a normal reflection. In case of the grating the whole structure (not considering the grating elements) reflects the incident field; therefore, the central lobe exists. It is obvious that if somehow the symmetry of the problem is broken the results will not be the same. This can be achieved for example by tilting the incident beam.

(a) Concave (b) Convex

Figure 6.14: Position of the phased array elements

6.5 An Application comprised of all the components of the Hybrid method

All the different components of the hybrid method has been put to use in this example. The schematic of the problem is shown in Fig.(6.16). A dielectric grating is illuminated by a phased cosine aperture field. The phase variation in the aperture field causes a shift in the peak of the field as it propagates. This is similar to a spatial tilt of the phased cosine profile. The aperture field is first expanded into a number of GBs. The waists of the beams were chosen such that they cover the whole aperture. Due to the large size of the beam waists used for the Gabor expansion, a matched Gabor series is obtained. The coefficients of the Gabor series are shown in Fig.(6.18). The resultant beams are then launched inside the FDTD lattice. The field is then calculated in the SF region, in the near field of the scatterer (the grating). As was mentioned in the introduction of this chapter, a grating imposes a very severe test on the FDTD method. Although it is possible to expand this near field directly using a Gabor expansion, this approach is not very efficient. Numerous numerical experiments were performed and it was concluded that by propagating the field a distance of 100λ away from the grating using the Hankel function approach, the Gabor expansion becomes more efficient. The field is then expanded using the Gabor expansion. The resultant beams must be propagated through a thin lens. Multiple reflection/refraction of the beams inside the lens is used to find the output. As expected the farfield of the

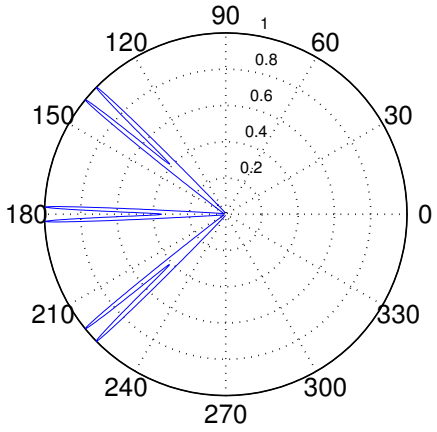

(a) Concave

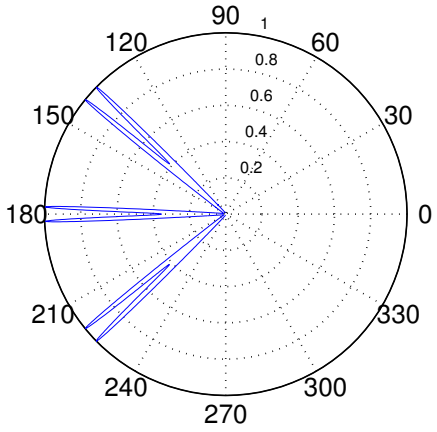

(b) Convex

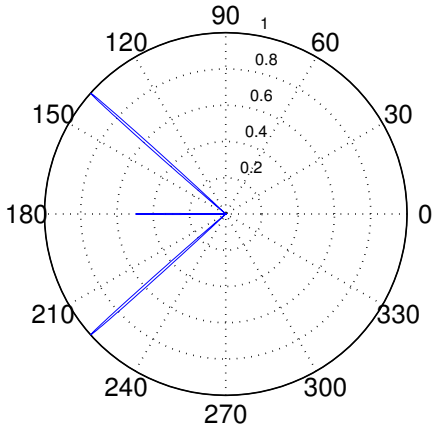

(c) Flat

Figure 6.15: Array factors of the phase arrays

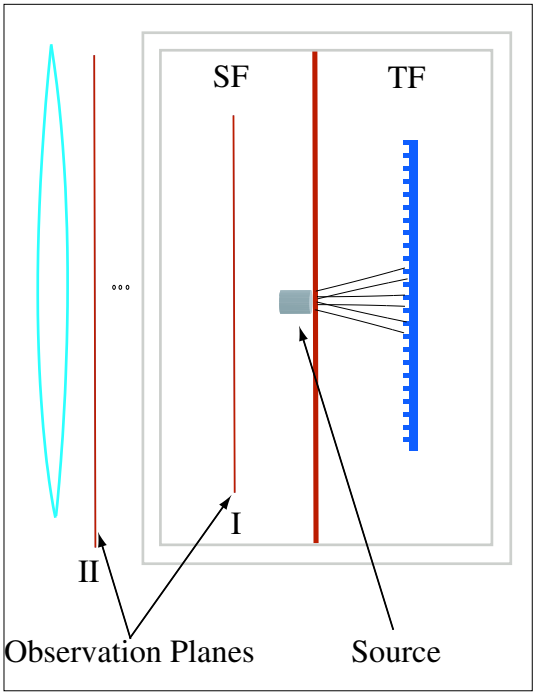

Figure 6.16: Schematic of the main problem

original field is brought to the focal plane of the lens. The side lobes around each peak in the far field are obviously due to the truncated aperture field.
In order to clarify the individual procedures the problem is broken down into different steps and each step is explained in detail in the following sections:

6.5.1 Step 1. Gabor Expansion of the Source

The driving source of the problem is a phased cosine function given by:

$$f(x) = \begin{cases} \cos(\frac{\pi x}{L_0}) \exp(j\alpha x) & \text{if } -L_0/2 < x < L_0/2 \ ; \\ 0 & \text{otherwise.} \end{cases}$$

The wavelength of operation was $\lambda = 1\mu m$. L_0 was chosen to be 50λ and $\alpha = -.1k$, k being the free space wavenumber. If such a source radiates in free space the far field pattern peaks at $\arcsin(-0.1) = -5.739°$. The source was expanded using Gabor expansion. The shift parameter of the Gabor expansion was chosen to be $L = 55.8$. Therefore the beam fields cover the whole aperture. According to the properties of the Gabor expansion as $L > L_0$ only a few shifted GBs need to be considered. The major contribution is due to the rotated beams. This can be seen in Fig.(6.18). Only A_{mn} where $m = -1, 0, 1$ have amplitudes

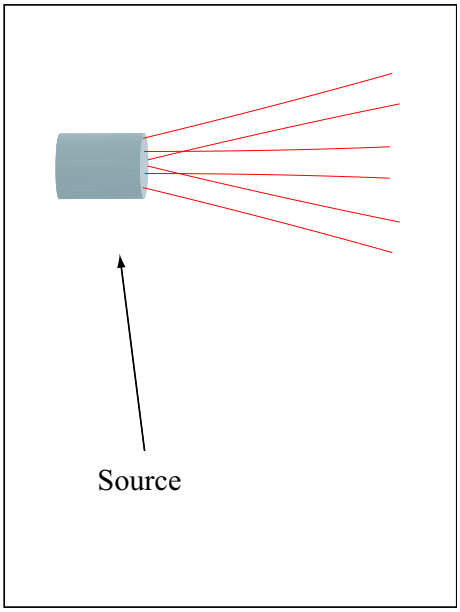

Figure 6.17: Source Expansion

larger than 0.1. To be on the safe side $|m| < 3$ and $|n| < 10$ (a total of $7 \times 21 = 147$ beams) were chosen. It can be seen in Fig(6.19) that the aperture field and the farfield (in absence of the scatterer) are accurately reproduced. According to the properties of Gabor expansion for $n > \lambda/L$ the fields become evanescent. In this case as $|n| < 10$ no evanescent beam is produced. The maximum angle of produced GBs is $\arcsin(10/55.8) = 10.32°$.

6.5.2 Step 2. FDTD Simulation

The coefficients of the 147 beams , A_{mn} are read by the FDTD routine. The analytic form of single frequency time domain GBs is then used by the code to produce the launched field at the boundary of the TF/SF region Fig.(6.20). The dielectric grating was placed in the TF region. The pitch of the grating was $\Lambda = 1.5\lambda$ and its dielectric constant was $\epsilon_r = 2.25$. A FDTD lattice of 5000×800 cells were chosen with 32 cells per λ. As it was mentioned in the introduction to this chapter, due to the large difference between the overall dimensions of the grating and the size of its elements, a large problem space is created. This is virtually the worst case scenario. The PML was chosen to be 100 cells or $(100/32)\lambda$ on each side. After 7200 time steps (around 10 hours on a P4 3GHz machine) steady state is reached. The observation plane was placed at 12λ away from the grating Fig.(6.20). The amplitude and phase of the steady state electric field is shown in Figs.(6.21,6.22) respectively. Using the Hankel function approach the farfield at $z = 10000\lambda$ was found and is shown in Fig.(6.23).

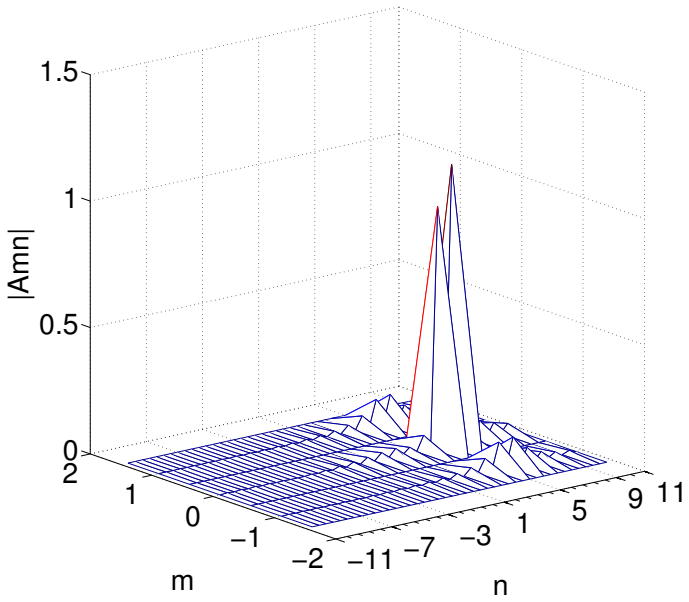

Figure 6.18: $|A_{mn}|$

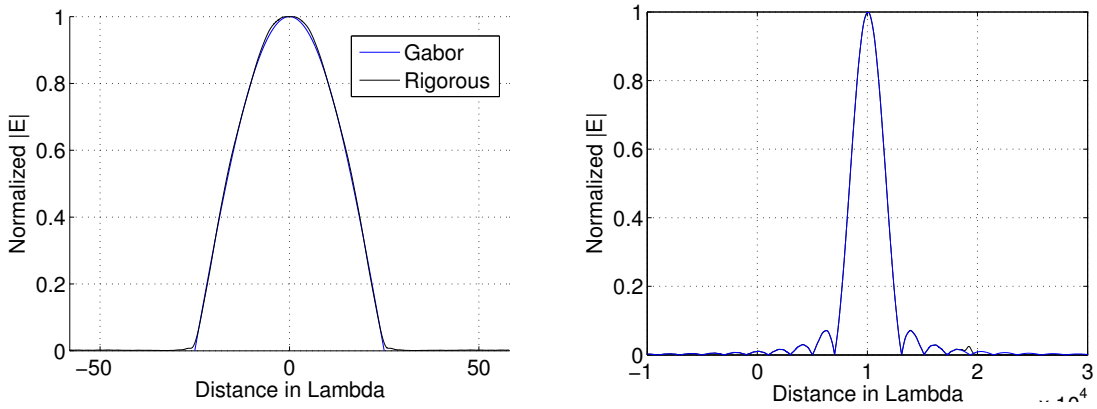

(a) Aperture Field

(b) Farfield

Figure 6.19: Aperture Field and Farfield of the Source in absence of the scatterer

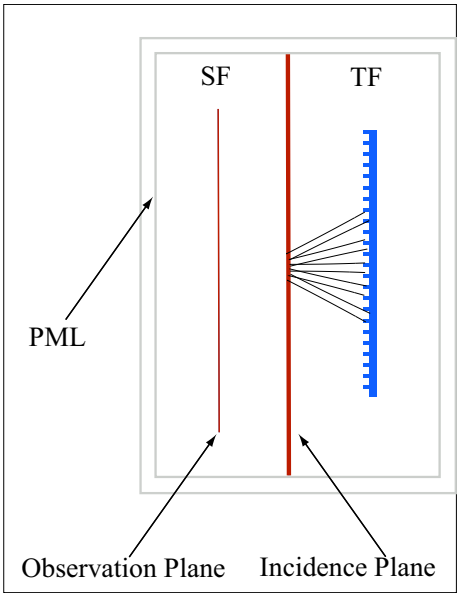

Figure 6.20: FDTD Schematic

The peaks of the farfield are located at $\theta_m = -50.053°, -5.73°, 34.51°$ which are the exact angles obtained from the general grating formula: $\theta_m = \arcsin(-.1+2/3m)$ for $m = -1, 0, 1$ (this m which represent the order of the grating lobes must not be confused with the m used in the Gabor expansion). The side lobes present in the farfield pattern are due to the truncation of the phased cosine function.

6.6 Step 3. Gabor Expansion of the Output Field

The near field shown in Fig.(6.21) could be directly expanded using the Gabor expansion Fig.(6.24), but because of the rapid changes in amplitude and phase a relatively large number of beams are required to represent the field. Therefore the near field is first propagated to the observation plane (II), which is 100λ away from observation plane (I) (Fig.(6.16)) using the Hankel function approach. The result is shown in Fig.(6.25). The field is smoothed out and a Gabor expansion becomes more efficient. The field at plane (II) was expanded using both narrow waisted beams: $L = 1.5\lambda$ and matched beams $L = 420.8\lambda$ Fig.(6.26). As it can be observed in Fig.(6.26), the matched expansion gives a much better approximation of the aperture field. A total of $701 * 3$ beams were created. Finding the coefficients of the expansion in this case takes around 2 minutes. The expansion of such a complicated field into GBs has not been reported in the literature.

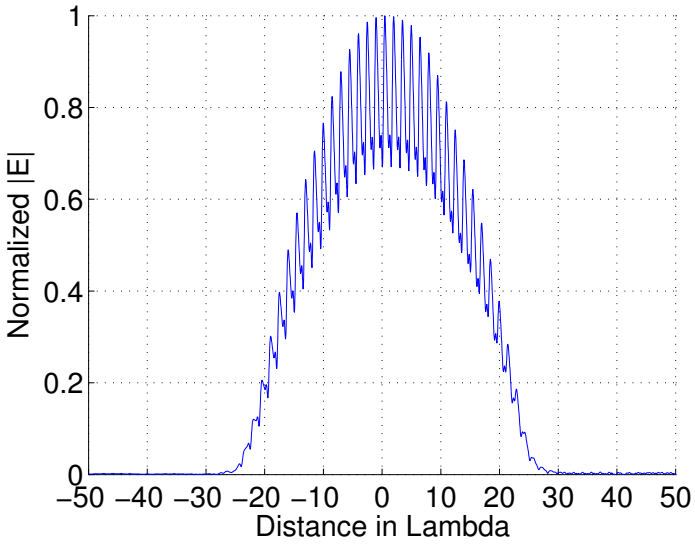

Figure 6.21: Near Field

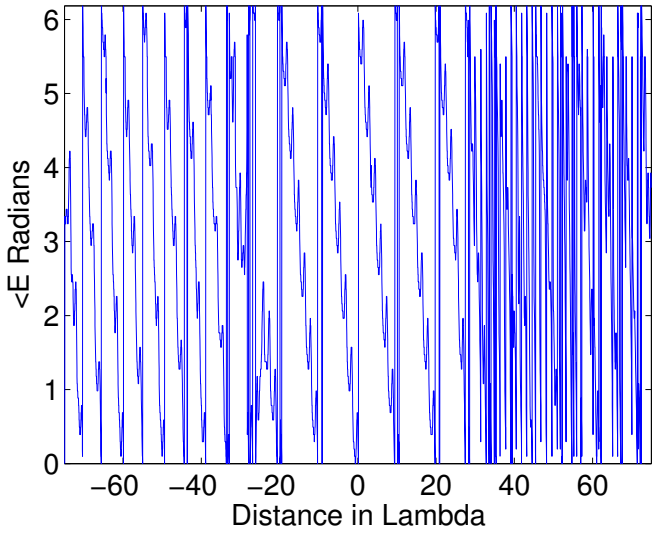

Figure 6.22: Phase of the Near Field

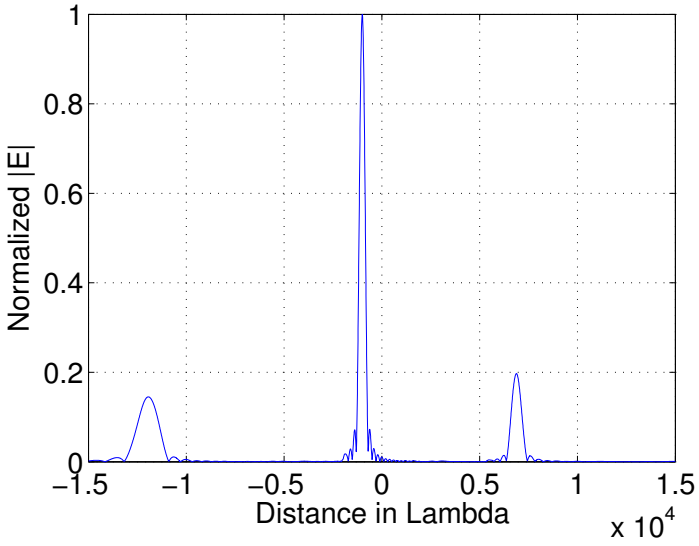

Figure 6.23: Far Field

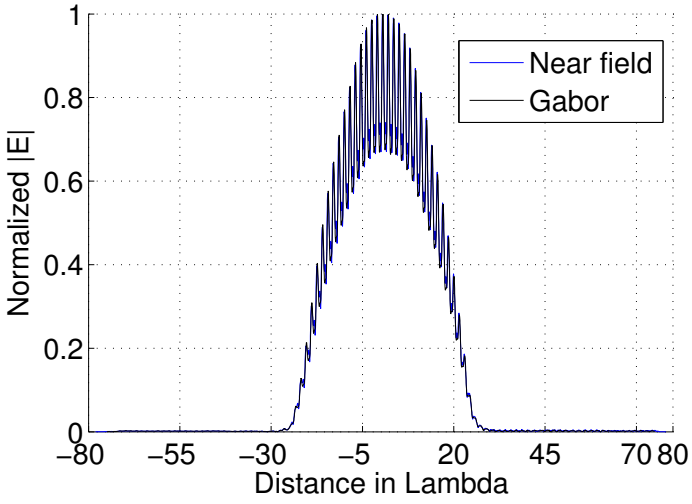

Figure 6.24: Gabor expansion of the near field

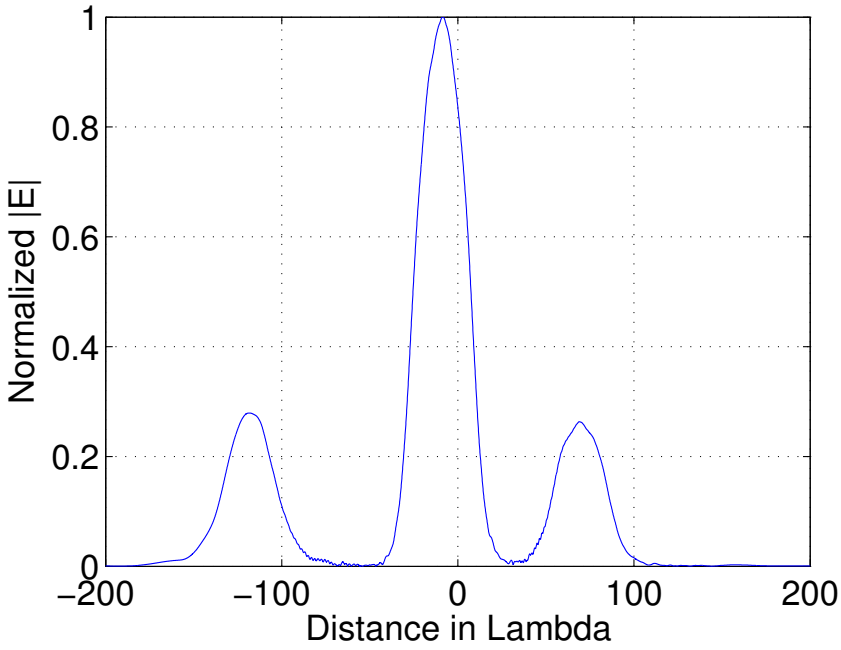

Figure 6.25: Field at 100λ

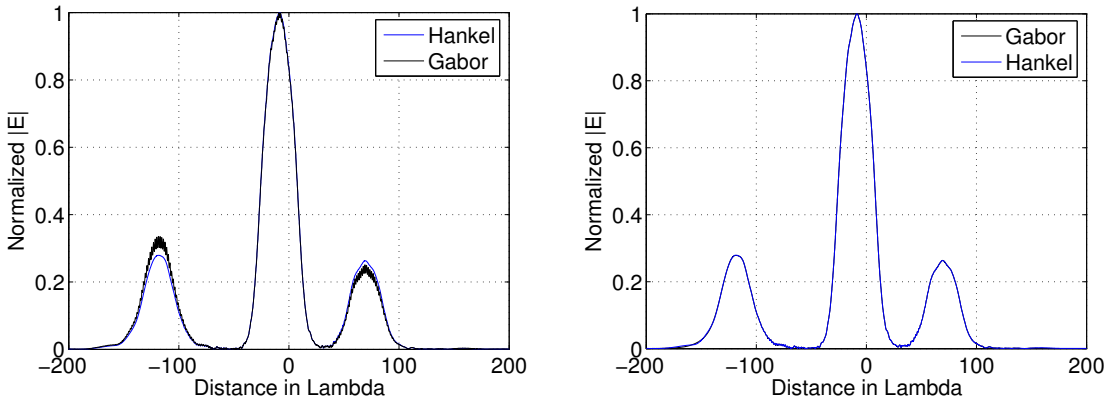

(a) Narrow Beams

(b) Matched Beams

Figure 6.26: Gabor expansion of the field at observation plane (II) using narrow waisted and matched beams

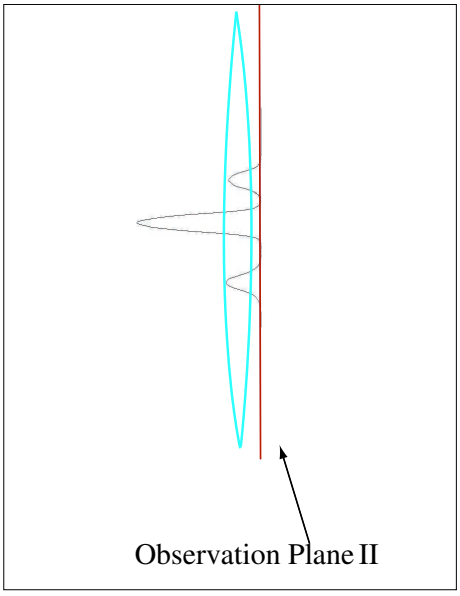

Figure 6.27: Schematic of the final step

6.7 Step 4. Propagation through a thin lens

In this step a thin lens is placed adjacent to observation plane (II) Fig.(6.27). The set of 2103 beams are propagated inside the thin lens using 2D GBT. This step takes less than a minute to complete. Multiple reflection inside the lens are used to find the field at the focal plane of the lens (Fig.6.28). The result is shown in Fig.(6.29). The horizontal axis is stretched to allow comparison with the rigorous Hankel function result.

All the features and components of the hybrid method is effectively utilized in this example. A problem of extremely large size compared to the wavelength is analyzed using this method. Therefore the full power of this method is revealed. Other applications of the hybrid method are demonstrated by the following examples.

6.8 Grating Coupling

In many photonic structures, light needs to be coupled to optical waveguides. This can happen either at the input (for example a laser entering an integrated photonic device) or at the output of a detector system. In many applications it is desirable to couple light to the midsection of a guide as opposed to its ends (butt coupling). In this example the problem of coupling of a GB into a slab waveguide is considered. The geometry of the problem is shown in Fig.(6.30). This example is used to demonstrate ability of the hybrid

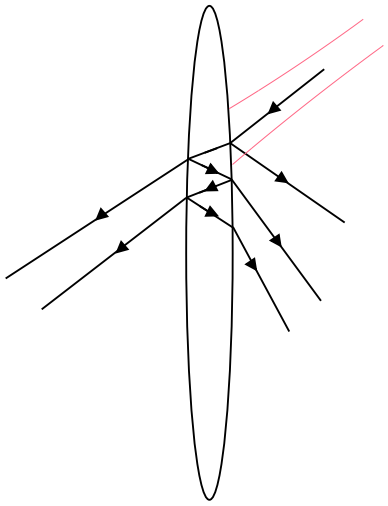

Figure 6.28: Multiple Reflections in the Lens

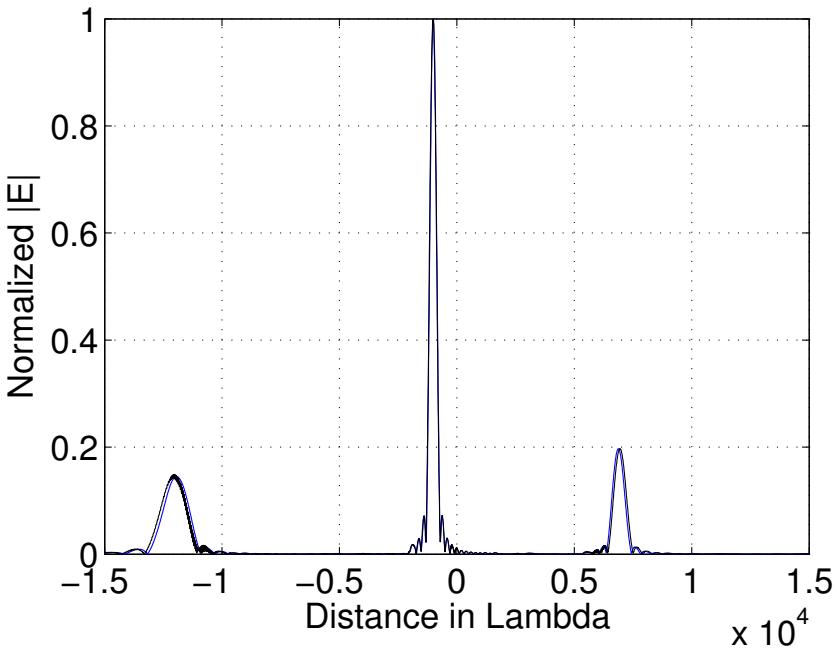

Figure 6.29: Field at the focal plane of the lens compared to the rigorous far field obtained using Hankel function.

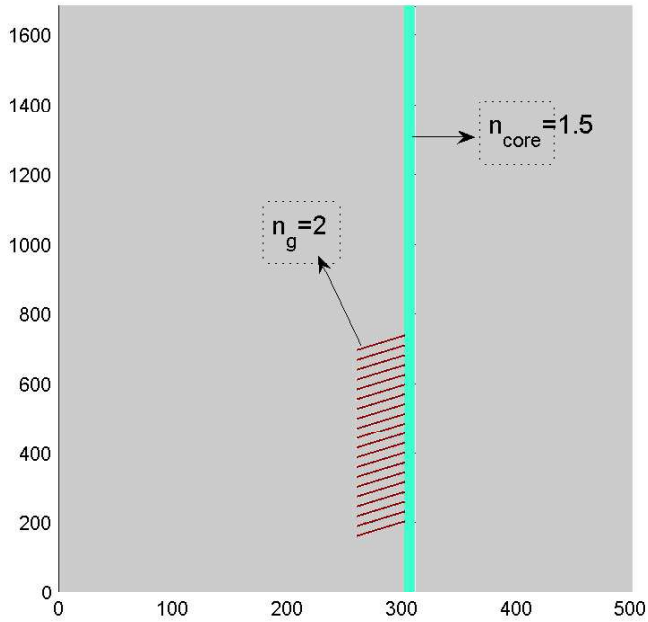

Figure 6.30: Geometry of GB Coupling

method in analyzing such structures and therefore, the actual coupling efficiency is not of primary interest. Due to the fact that relatively large sections of a weakly guiding slab are needed for the modes to become stable, FDTD is not very suitable for analyzing these waveguides. Therefore for this example a strongly guided waveguide is chosen with $n_{core} = 1.5$ and $n_{clad} = 1$. The refractive index of finite slanted grating was chosen to be $n_g = 2$. The angle of the slanted grating is 45 degrees and the entire grating is illuminated by the GB. The relatively large difference between the refractive index of the grating and slab causes the incident field to be strongly perturbed. This perturbed field is then coupled to the slab within a few wavelengths due the fact that the slab is strongly guiding. As it can be seen in Fig.(6.31) the field is strongly coupled to the waveguide and this coupling is unidirectional, although the incident field is perpendicular to the slab. Other methods of the grating coupling require the incident beam to be tilted at a very specific angle and the coupling efficiency is strongly dependent on this angle. A very good agreement between the simulated results and the fundamental mode (analytic solution) of the slab can be observed in Fig.(6.32). The fluctuation of the field far from the slab is due to the leakage from the coupling mechanism.

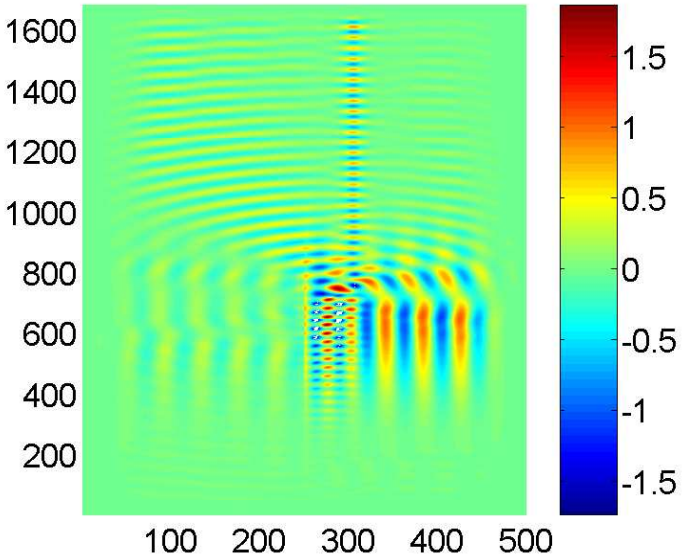

Figure 6.31: GB Coupling into a Slab Waveguide

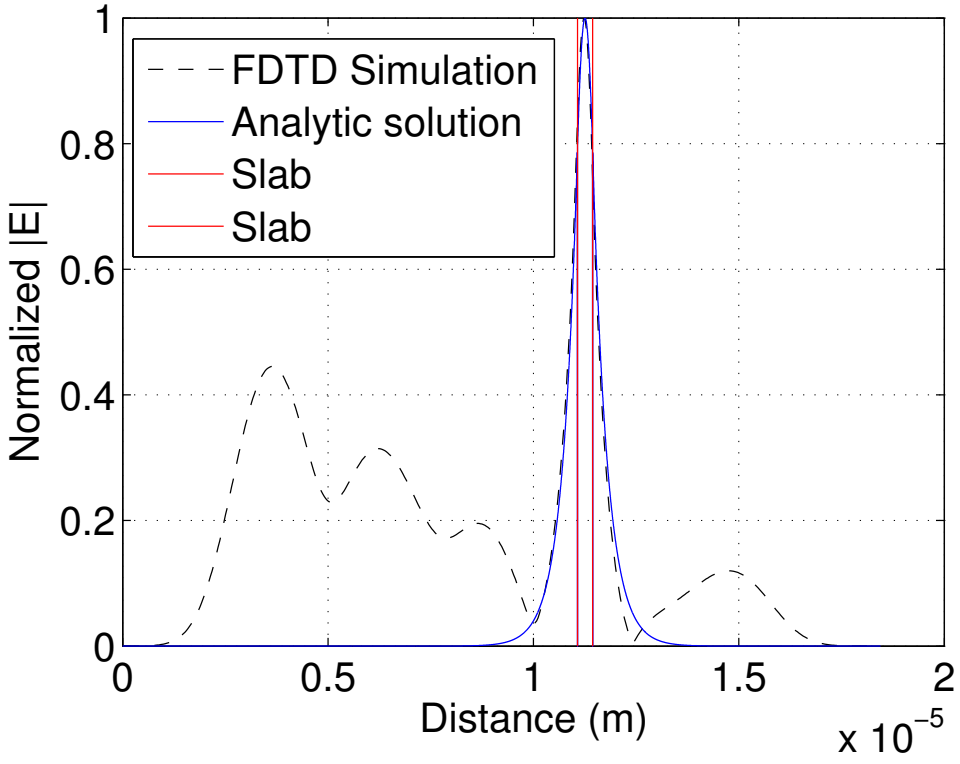

Figure 6.32: Comparison of the Fundamental Mode (FDTD-Analytic Solution)

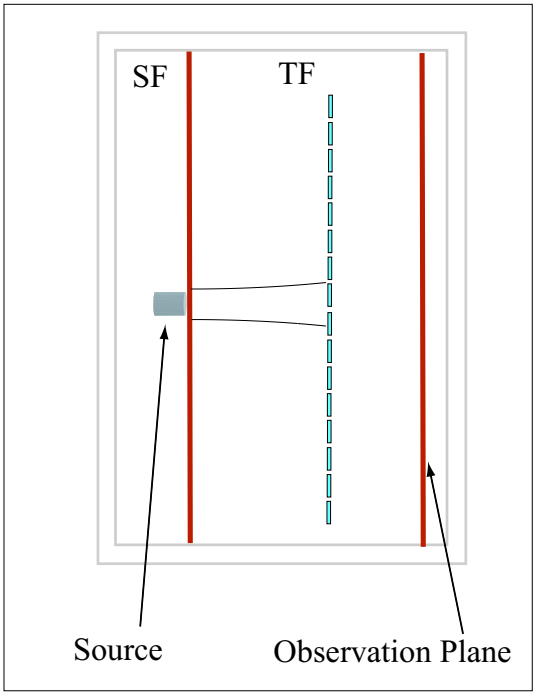

Figure 6.33: Schematic of the Transmission problem

6.9 A Transmission Problem

In this example, the very thin dielectric transparency is illuminated by a GB. The fact that the output field can be chosen in the TF region is demonstrated by this example. In many practical problems the transmittance of light through optical structures is of paramount importance. For example a laser beam passing through a Fresnel lens [76] or through a slab of LHM material. All these problems can be categorized as transmission problems. If these structures are placed inside an FDTD lattice the output field has to be calculated in the TF region as the collective effect of the incident and transmitted fields forms the output of the system. The applicability of the hybrid method to this class of problems is shown in this very simple example. The geometry of the problem is given in Fig.(6.33). The refractive index of the transparency was $n = 1.5$, its pitch $\Lambda = 1.5\lambda$ and the thickness was $\lambda/15$. Due to the very small thickness of the transparency the phase shift experienced by the beam does not differ significantly for the different points on the transparency. Therefore a very small fluctuation is seen in the transmitted field in the near field of the transparency. It must be noted that this field is calculated in the TF region. The amplitude of the beam is nevertheless reduced due to reflection from the surface. 100λ away from the transparency the original form of the beam is obtained.

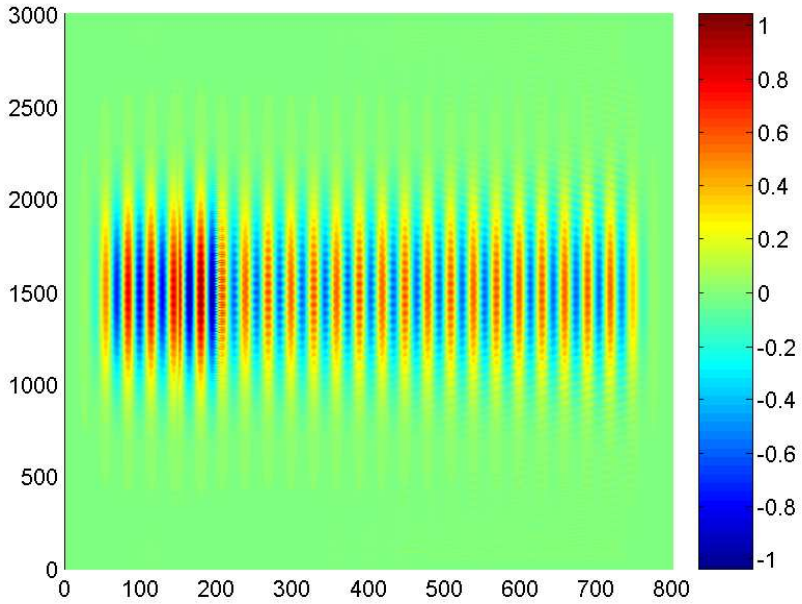

Figure 6.34: Top 3D Plot of the Transmission Problem

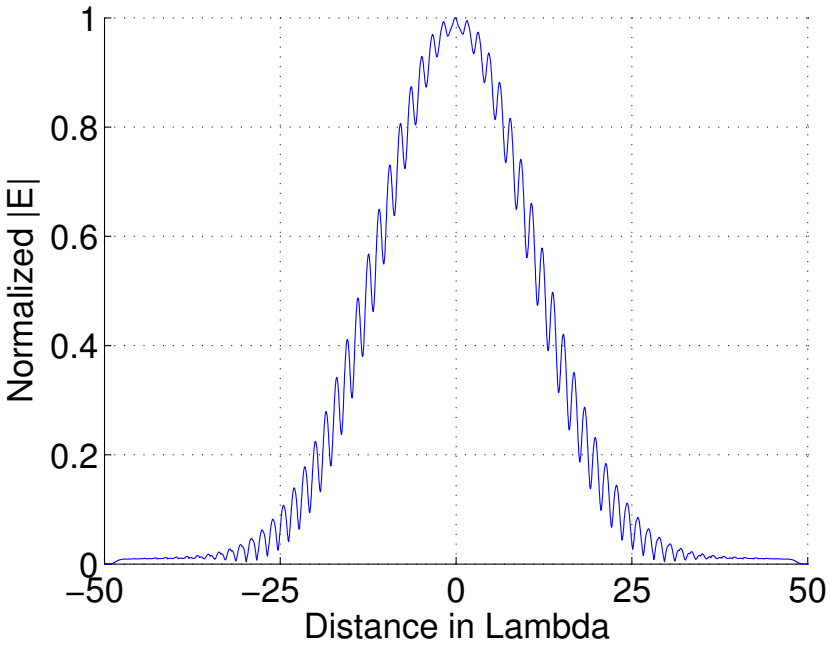

Figure 6.35: Near Field of the Transmitted Field

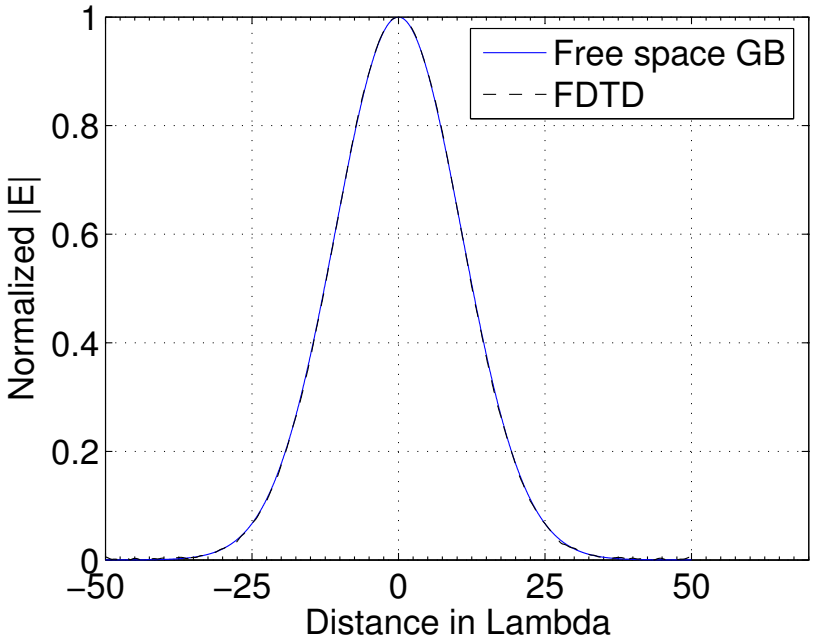

Figure 6.36: Comparison between FDTD results and free space GB propagation

6.10 Estimation of Error

Fig.(6.37) shows the sources of error created by the different components of the hybrid method: In Gabor expansion as a limited number of beams are used to represent the aperture plane, truncation errors are the main source of inaccuracy. The other source of error is representation of the aperture field using GBs (ignoring the higher order terms). In the FDTD region the main source of error is the error due to discretization. The finer the FDTD lattice the more accurate the results. The other source of error is the due to the finite size of the FDTD computational domain (reflections caused by PML). This problem can be overcome by increasing the size of this domain. Another problem is the imperfection of the TF/SF region formulation. Again by choosing a finer grid size the error due to this imperfection is reduced. The final source of error in the FDTD region is the fact that the results should reach steady state. The error caused by this can be estimated by curve fitting the field at some point on the observation plane by a pure sinusoidal function and finding the mean squared error. In utilizing the near field to farfield transformation the errors involved are those due to integration and calculation of Hankel functions.

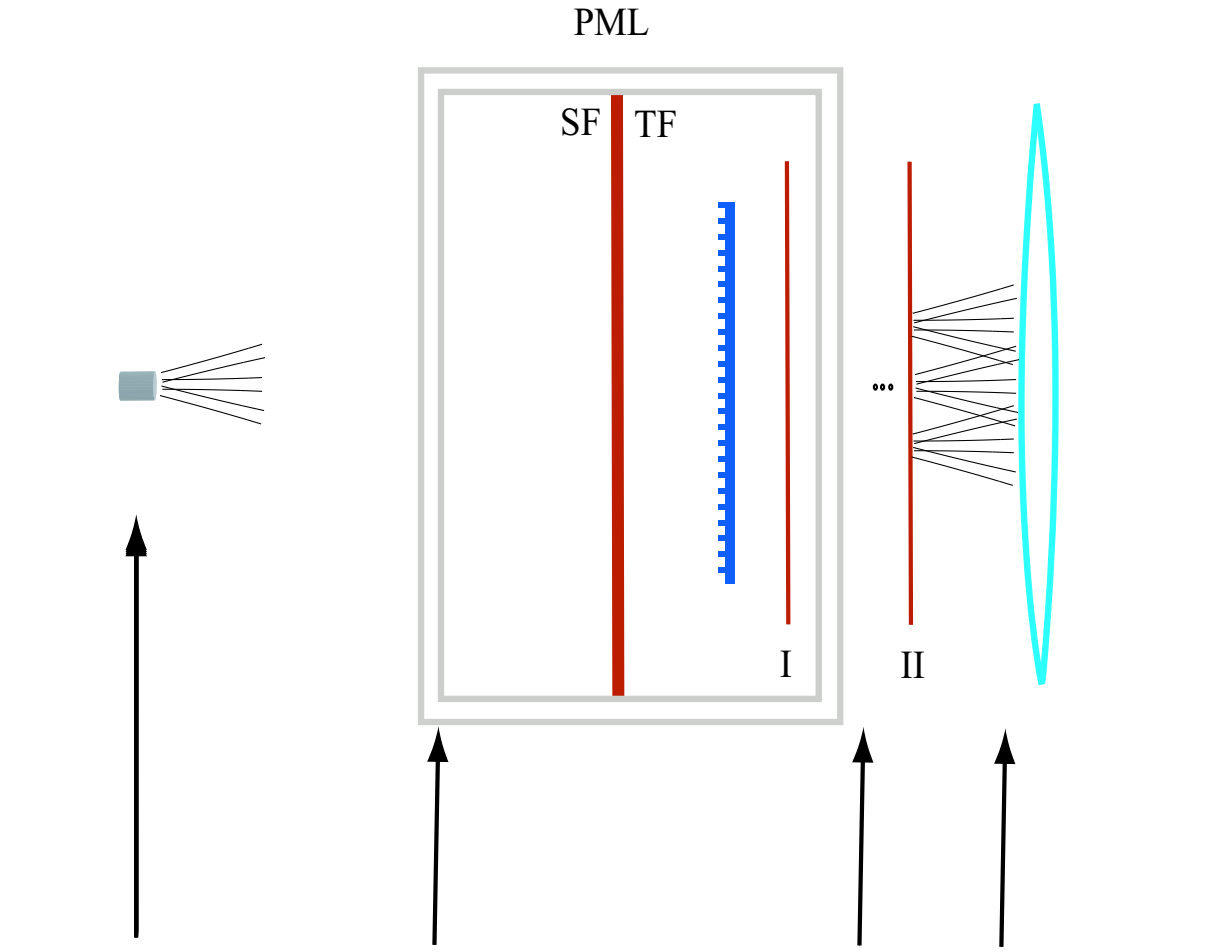

Figure 6.37: Different sources of Error

Chapter 7

Summary of Contributions and Future Work

7.1 Summary of Contributions

In this chapter the main contributions of our research and the major topics presented in this thesis are summarized. The main purpose of the research presented in this thesis has been to create a computationally efficient method for analysis and design of passive photonic structures. Our main focus has been on unbounded wave structures. As these structures are in general extremely large in terms of the optical wavelength of the driving sources a single ad hoc method can not be used to both accurately and efficiently analyze them. Therefore a hybrid method was used for this purpose.

The main contribution of this research has been the actual combination or "*hybridiztion*" of three methods:

1. The Gaussian Beam tracing method.
2. The Gabor expansion method.
3. The Finite Difference Time Domain method.

First a novel 3D Gaussian Beam Tracing method was developed based on phase matching techniques. This method which enables one to find the reflection and refraction of a Vectorial General Astigmatic Gaussian Beam from a general curved surface was formulated, implemented and verified. The fact that the hybrid method is computationally efficient is mainly due to the speed of the GBT. Free space propagation, reflection from

mirrors, reflection and refraction from lenses and prisms and many other similar problems can be accurately and efficiently handled by this method. Fields at the focal plane of lenses can be easily found and the problem of caustics does not exist in this method. The main limitation of GBT is that the surface under consideration much be relatively smooth. In general, diffraction phenomenon can not be modelled by this method. The use of many examples in this thesis has revealed the speed, accuracy and versatility of this method. A 2D version of this method has also been formulated in Appendix C.

If the source of electromagnetic wave in a specific problem is not of Gaussian form, it needs to be expanded in terms of a number of Gaussian beams. The Gabor expansion has been used in this research. This method which is based on a series expansion of an aperture field into elementary beam functions has been extensively investigated in the literature. In this method the field over a flat or curved surface is represented by a quadruple sum of Gaussian elementary function. Subsequently, using asymptotic techniques a beam field representation of the radiated field is obtained. A general 3D Gaussian beam representation of the radiated field is extremely difficult to formulate. In this work, a method for extending the 3D Gabor expansion to the case of astigmatic beam fields has been proposed where the resultant Gaussian beams are narrow waisted in one direction. Both the 2D and 3D Gabor expansion of a field on a flat surface has been implemented in this work. The class of problems considered in this work (for example the expansion of the Fresnel zone scattered field of a diffraction grating over an aperture size of 100λ) has not been reported in the literature. The GBT and the Gabor expansion have been combined in this research. The beam fields produced by the Gabor expansion are efficiently propagated using the GBT through optical structures. At any desired plane the Gaussian beams can be added up and then re-expanded in terms of a set of new Gaussian beams.

In some cases due to either the size of a structure or its physical properties the combination of GBT and Gabor expansion can not be used. In these cases the Finite Difference Time Domain method has been used in this work. As the space outside the FDTD lattice is analyzed by GBs, the FDTD method must have the capability of launching GBs at arbitrary angles. Due to the lack of suitable commercial software, a very robust 2D FDTD has been implemented as part of this research. The GBT has been combined with the FDTD. The time harmonic GBs used in GBT are first converted to their sinusoidal form and subsequently any number of shifted and rotated beams can be launched at the same time inside the FDTD lattice. To our knowledge no commercial software has this capability.

To demonstrate the power of the hybrid method, many practical examples have been presented. A systematic approach has been used to minimize any possible error. Many interesting results were obtained using the hybrid method that demonstrated its accuracy and generality for analysis and design of passive photonic structures. Although only a limited number of structures have been analyzed in this work, the problems that can be modelled using this method are virtually limitless.

7.2 Future Work

This research can be extended in many ways. Some of the proposed areas for future research are listed below:

1. Inclusion of the Goos-Hanchen shift for a 3D GAGB reflection from a curved surface.
2. GBT formulation for a pulsed GB.
3. Inclusion of edge diffraction from dielectrics and metals in the GBT.
4. Automation of the GBT.
5. General Gabor expansion for arbitrary beam waists at the aperture plane.
6. Implementation of a 3D FDTD.

Appendix A

Geometrical Optics Field

A.1 Astigmatic Rays in Homogenous Media

Using Maxwell's equations in time harmonic form:

$$\begin{aligned} \vec{\nabla} \times \mathbf{H}(\mathbf{r}) - jw\epsilon\mathbf{E}(\mathbf{r}) &= 0 \\ \vec{\nabla} \times \mathbf{E}(\mathbf{r}) + jw\mu\mathbf{H}(\mathbf{r}) &= 0 \\ \vec{\nabla}.\mathbf{B}(\mathbf{r}) &= 0 \\ \vec{\nabla}.\mathbf{D}(\mathbf{r}) &= 0 \end{aligned} \tag{A.1}$$

together with the constitutive relationships:

$$\begin{aligned} \mathbf{D} &= \epsilon\mathbf{E} \\ \mathbf{B} &= \mu\mathbf{H} \end{aligned}$$

leads to the Helmholtz equation:

$$\vec{\nabla}^2\mathbf{E} + k^2\mathbf{E} = 0 \tag{A.2}$$

where $k = \frac{w}{v}$ is the wave number of the medium and v is the velocity of light in the medium and is defined as $v = \frac{1}{\sqrt{\mu\epsilon}}$, and ϵ and μ are the permittivity and permeability of the medium and $\mathbf{r}$. According to Lunberg-Kline [38] asymptotic expansion of the electric and magnetic fields leads to:

$$\mathbf{E} = e^{-jk_0\Phi(\mathbf{r})} \sum_{m\geq 0} \frac{\mathbf{e}^{(m)}}{(jk_0)^{(m)}}, \qquad \mathbf{H} = e^{-jk_0\Phi(\mathbf{r})} \sum_{m\geq 0} \frac{\mathbf{h}^{(m)}}{(jk_0)^{(m)}} \tag{A.3}$$

where $\mathbf{e}^{(m)}$, $\mathbf{h}^{(m)}$ and ϕ are generally functions of position but not a function of $k_0 = w/c$. The leading term of this asymptotic expansion is referred to as the **Geometrical Optics field** (for very large k_0), and is represented by:

$$\begin{aligned} \mathbf{E_0}(\mathbf{r}) &= \mathbf{e}(\mathbf{r})e^{-jk_0\Phi(\mathbf{r})} \\ \mathbf{H_0}(\mathbf{r}) &= \mathbf{h}(\mathbf{r})e^{-jk_0\Phi(\mathbf{r})} \end{aligned} \tag{A.4}$$

Substituting Eqn.(A.4) in Maxwell's equations and the Helmholtz equation leads to differential equations relating $\mathbf{e}(\mathbf{r})$, $\mathbf{h}(\mathbf{r})$ and $\Phi(\mathbf{r})$ where $\Phi(\mathbf{r})$ is the **Phase**. For the geometrical optics field, the Eikenol and Transport equations are obtained respectively by:

$$|\vec{\nabla}\Phi|^2 = n^2 \tag{A.5}$$

$$(\nabla\Phi.\nabla)\mathbf{e} + \frac{1}{2}(\nabla^{\mathbf{2}}\Phi)\mathbf{e} = 0 \tag{A.6}$$

where $n = v/c$ is the refractive index of the medium and , $c = 3 \times 10^8$ is the speed of light in vacuum. The surfaces of constant phase are called **phase fronts** or **wave fronts** and the space curves normal to the wavefronts are called **rays**. Using Eqn.(A.5) the following important observations [38, 77, 78] can be made:

1. **Ray trajectories** In a homogenous medium the rays are straight lines; therefore if s is a variable measuring arc-length, then:

   $$\mathbf{r}(s) = \mathbf{A}s + \mathbf{B}$$

   where $\mathbf{A}$ and $\mathbf{B}$ are constant vectors.

2. **Phase continuation** The phase changes linearly:

   $$\Phi(s) = \Phi(s_0) + n(s - s_0)$$

   where s_0 denotes an arbitrary number.

3. **Amplitude continuation** The amplitude of the field changes according to:

   $$\mathbf{e}(s) = \mathbf{e}(0)\sqrt{\frac{R_1R_2}{(R_1+s)(R_2+s)}} \tag{A.7}$$

   where R_1 and R_2 are the radii of curvature of the phase front. See Fig.(A.1) and Fig.(A.2)

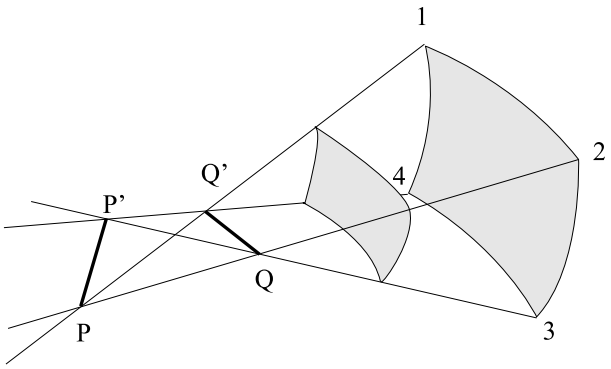

Figure A.1: Astigmatic Rays

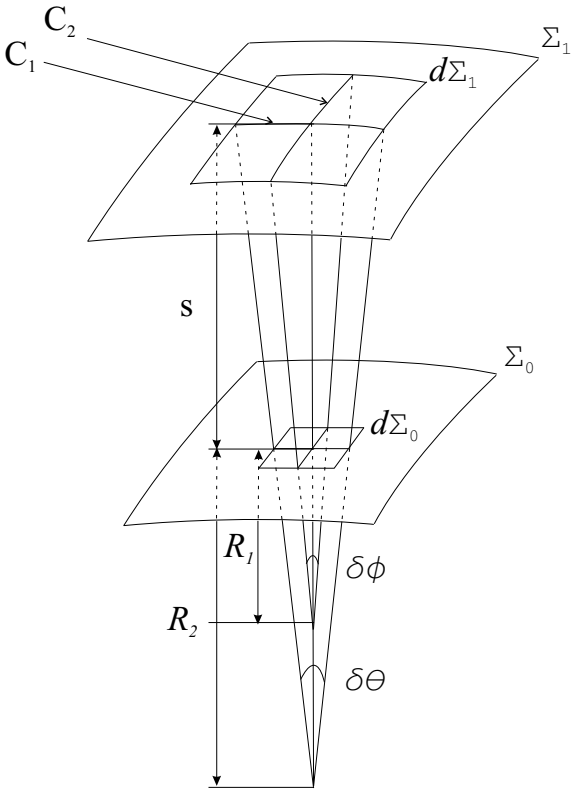

Figure A.2: Narrow ray Tube around a central ray.

This formula represents an Astigmatic Field as the phase front has two distinct radii of curvature. The plane wave, spherical wave and the cylindrical waves are special forms of this equation with ($R_1 = \infty$, $R_2 = \infty$), ($R_1 = R_2 \neq \infty$), ($R_1 = \infty$, $R_2 \neq \infty$) respectively. The points $s = -R_1$ and $s = -R_2$ are the two caustics of this field where in theory, an infinite number of rays pass through and therefore the geometric optics field predicts an infinite field. According to what was presented above, the geometric optics field can be represented as

$$\mathbf{E_0}(s) = \mathbf{e}(0)\sqrt{\frac{R_1 R_2}{(R_1+s)(R_2+s)}}e^{-jnk_0 s} \tag{A.8}$$

Appendix B

Phase Matching

Given the incident field (bundle of rays) and the equation of a general 3D surface, the only unknowns required to fully determine the reflected and transmitted rays are the curvature matrices of the reflected and transmitted rays. If the surface is approximated $\vec{r}(d_1, d_2)$ by a quadratic equation the following is obtained:

$$\vec{r}(\mathbf{d}) = \mathbf{d} - \frac{1}{2}(\mathbf{d}\bar{\mathbf{C}}\mathbf{d}^T)\hat{n} + O(d^3) \tag{B.1}$$

where $\mathbf{d} = d_1\hat{d}_1 + d_2\hat{d}_2$ and (d_1, d_2, n) is a local coordinate system describing the surface of incidence and $\hat{d}_1$ and $\hat{d}_2$ are unit vectors in the tangent plane to the surface at the point of incidence and $\bar{\mathbf{C}}$ is the curvature matrix of the surface. Now consider the phase of the incident field:

$$\phi(\mathbf{x}_i, z_i) = z_i + \frac{1}{2}\mathbf{x}_i.\bar{\mathbf{Q}}_i(z_i)\mathbf{x}_i^T$$

The phase needs to be found at all the points on the surface, therefore, $\mathbf{x}_i$ component and z_i components of $\vec{r}(\mathbf{d})$ are found. This yields

$$x_{1i} = \hat{x}_{1i}.\vec{r}(\mathbf{d}) = \hat{x}_{1i}.\hat{d}_1 + \hat{x}_{1i}.\hat{d}_2 - \frac{1}{2}(\mathbf{d}\bar{\mathbf{C}}\mathbf{d}^T)\hat{n}.\hat{x}_{1i} + O(d^3) \tag{B.2}$$

$$x_{2i} = \hat{x}_{2i}.\vec{r}(\mathbf{d}) = \hat{x}_{2i}.\hat{d}_1 + \hat{x}_{2i}.\hat{d}_2 - \frac{1}{2}(\mathbf{d}\bar{\mathbf{C}}\mathbf{d}^T)\hat{n}.\hat{x}_{2i} + O(d^3) \tag{B.3}$$

$$z_i = \hat{z}_i.\vec{r}(\mathbf{d}) = \hat{z}_i.\hat{d}1 + \hat{z}_i.\hat{d}_2 - \frac{1}{2}(\mathbf{d}\bar{\mathbf{C}}\mathbf{d}^T)\hat{n}.\hat{z}_i + O(d^3) \tag{B.4}$$

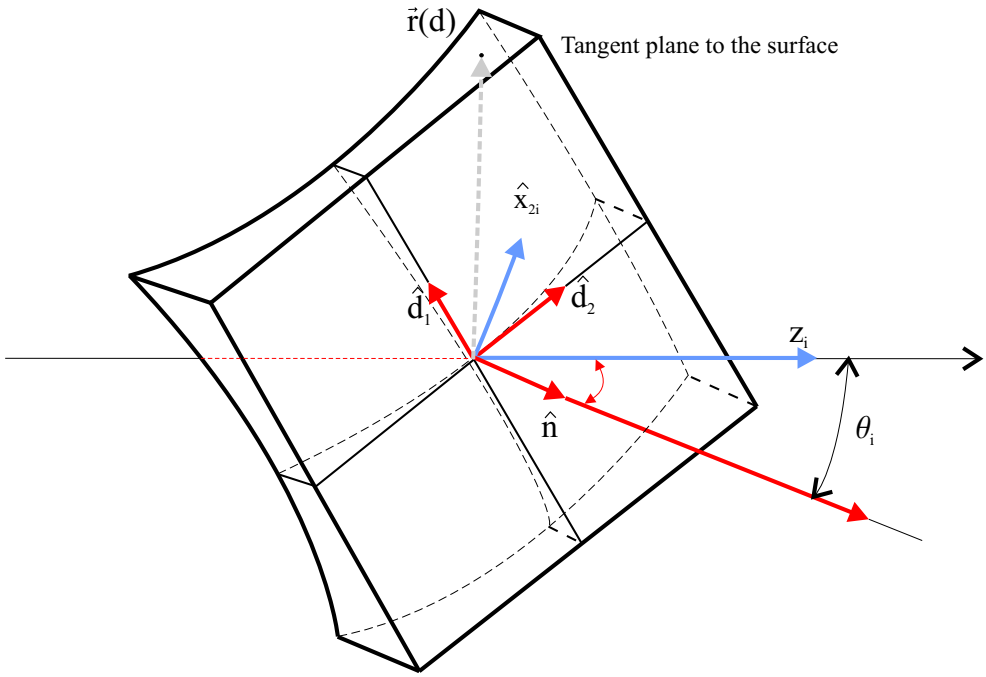

Figure B.1: Ray-fixed coordinate system.

In the first two equations ignore the terms in $O(d^2)$ are ignored [24]. This would greatly simplify the results. As mentioned earlier as long as $\hat{d}_1$, $\hat{d}_1, \hat{d}_2, \hat{x}_{1i}, \hat{x}_{2i}$ are vectors in the tangent plane of the surface and the tangent plane of the incident wavefront then the above equations hold. The results are further simplified by assuming that $\hat{d}_2 = \hat{x}_{2i}$. See Fig.(B.1). The fact that this can indeed be done is shown in Fig(B.2). This choice leads to the ray-fixed coordinate system for the incident field , and the above relationships would be greatly simplified:

$$\begin{aligned} \mathbf{x}_i &= \bar{\mathbf{K}}_i \mathbf{d} \\ z_i &= \hat{z}_i.\vec{r}(\mathbf{d}) = d_1 \hat{z}_i.\hat{d1} + d_2 \hat{z}_i.\hat{d2} - \frac{1}{2}(\mathbf{d}\bar{\mathbf{C}}\mathbf{d}^T)\hat{n}.\hat{z}_i \\ \bar{\mathbf{K}}_i &= \begin{bmatrix} \cos\theta_i & 0 \\ 0 & 1 \end{bmatrix} \end{aligned} \tag{B.5}$$

Although $\cos\theta_i$ has been used it is better to write $\hat{x}_{1i}.\hat{d}_1$ because the sign of this term might change depending on which side of the surface the pencil is incident upon. Therefore the phase at P_0 can be expressed as:

$$\phi_i = \hat{z}_i.\mathbf{d} + \frac{1}{2}.(\bar{\mathbf{K}}_i\mathbf{d})\bar{\mathbf{Q}}_i(z_i)(\bar{\mathbf{K}}_i\mathbf{d})^T \tag{B.6}$$

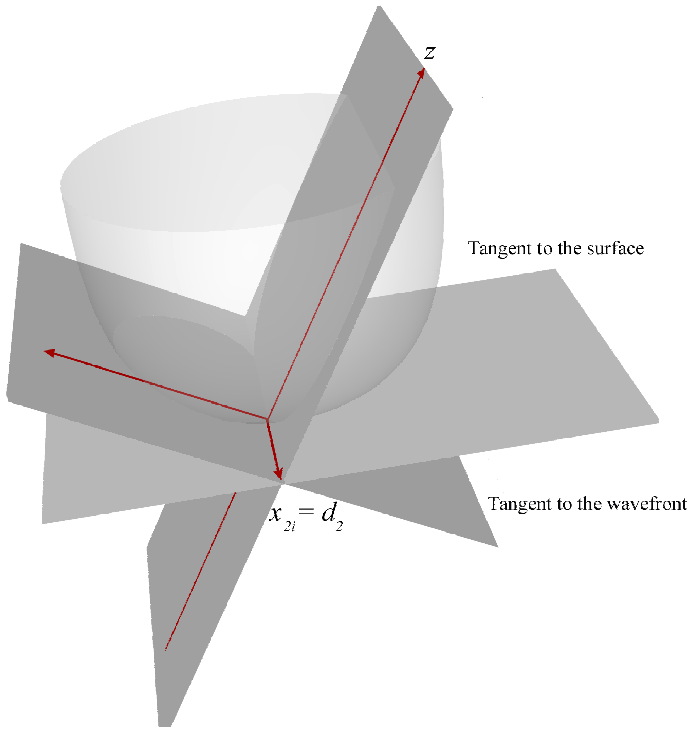

Figure B.2: 3D plot showing the point of incident ray and the surface .

The next approximation used is that although $\bar{\mathbf{Q}}_\mathbf{i}$ is a function of z_i for the points on the surface because the rays are paraxial it can be taken as $\mathbf{Q_i}(\bar{\mathbf{P}}_\mathbf{0})$ and denoted by simply $\bar{\mathbf{Q}}_\mathbf{i}$ for convenience, so that the phase can be expressed in the form:

$$\phi_i = \hat{z}_i.\mathbf{d} + \frac{1}{2}\mathbf{d}.\bar{\mathbf{\Gamma}}\mathbf{d}^T \tag{B.7}$$

$$\bar{\mathbf{\Gamma}}_i = \bar{\mathbf{K}}_i^T\bar{\mathbf{Q}}_\mathbf{i}\bar{\mathbf{K}}_i + \bar{\mathbf{C}}\cos\theta_i \tag{B.8}$$

Exactly the same thing can be said for the reflected and transmitted pencils.

$$\bar{\mathbf{\Gamma}}_r = \bar{\mathbf{K}}_r^T\bar{\mathbf{Q}}_\mathbf{r}\bar{\mathbf{K}}_r - \bar{\mathbf{C}}\cos\theta_r \tag{B.9}$$

$$\bar{\mathbf{\Gamma}}_t = \bar{\mathbf{K}}_t^T\bar{\mathbf{Q}}_\mathbf{t}\bar{\mathbf{K}}_t + \bar{\mathbf{C}}\cos\theta_t \tag{B.10}$$

$$\bar{\mathbf{K}}_r = \begin{bmatrix} -\cos\theta_r & 0 \\ 0 & 1 \end{bmatrix} \tag{B.11}$$

$$\bar{\mathbf{K}}_t = \begin{bmatrix} \cos\theta_t & 0 \\ 0 & 1 \end{bmatrix} \tag{B.12}$$

Now the phase of the incident, reflected and transmitted pencils are matched on the surface. The phase has a linear term and a quadratic term which should be matched separately.

The linear term confirms Snell's law and the quadratic terms gives us the equations from which the curvature matrix of the reflected and transmitted pencils can be found;

$$k_1\bar{\mathbf{\Gamma}}_i = k_1\bar{\mathbf{\Gamma}}_r = k_2\bar{\mathbf{\Gamma}}_t \tag{B.13}$$

Which yields

$$\bar{\mathbf{Q}}_r = (\bar{\mathbf{K}}_r)^{-1}[\bar{\mathbf{K}}_i^T\bar{\mathbf{Q}}_\mathbf{i}\bar{\mathbf{K}}_i + \bar{\mathbf{C}}(\cos\theta_i + \cos\theta_r)](\bar{\mathbf{K}}_r)^{-1} \tag{B.14}$$

$$\bar{\mathbf{Q}}_t = \frac{n_1}{n_2}(\bar{\mathbf{K}}_t)^{-1}[\bar{\mathbf{K}}_i^T\bar{\mathbf{Q}}_\mathbf{i}\bar{\mathbf{K}}_i + \bar{\mathbf{C}}(\cos\theta_i - \frac{n_2}{n_2}\cos\theta_t)](\bar{\mathbf{K}}_t)^{-1} \tag{B.15}$$

These equations have been simplified and explicit equations for Q_r and Q_t exist [40],[77]. Once the elements of the curvature matrices are found, the principal radii of curvature from can easily be obtained:

$$\frac{1}{R_{1,2}} = \frac{1}{2}Q_{11} + Q_{22} \pm \sqrt{[(Q_{11} - Q_{22})^2 + 4Q_{12}^2]}$$

Appendix C

2D GB Tracing

In this appendix it is shown how the above phase matching can be used for tracing 2D GBs. Although the tracing of a 2D beam is simpler and less general than the 3D case we need it for the hybrid method. It must be noted that the 2D case can not be simply derived from the 3D case and it needs separate treatment.

C.1 2D GBs

The 2D GB propagating in the z direction in a medium with refractive index n is given by:

$$\mathbf{E}(\mathbf{x},\mathbf{z}) = E_{0y}\hat{y}\sqrt{\frac{jb}{z+jb}}\exp\left(-jkz - \frac{jk}{2}\frac{x^2}{z+jb}\right) \tag{C.1}$$

where $b = n\pi w_0^2/\lambda$ is the Rayleigh range w_0 is the minimum waist and λ is the wavelength and $k = 2\pi/\lambda$. If this function is written in the form:

$$\mathbf{E}(\mathbf{x},\mathbf{z}) = \mathbf{E}(0)\psi\exp(-jkz) \tag{C.2}$$

it can easily be verified that ψ is a solution of the paraxial Helmholtz equation:

$$\frac{\partial^2\psi}{\partial x^2} - 2jk\frac{\partial\psi}{\partial z} = 0$$

Therefore, Eqn.(C.2) is valid in the paraxial regime meaning that such function would satisfy the wave equation only when it remains relatively well focused. If the denominator of $x^2/(z+jb)$ is multiplied by its conjugate, Eqn.(C.2) can be written in the following standard form:

$$\mathbf{E}(x,z) = \mathbf{E_0}\sqrt{\frac{jb}{z+jb}}e^{-jkz}e^{-j\frac{1}{2}k\frac{x^2}{R(z)}}e^{-\frac{x^2}{w^2(z)}} \tag{C.3}$$

where:

$$w(z) = w_0\sqrt{1+(\frac{z}{b})^2}$$
$$R(z) = z[1+(\frac{b}{z})^2] \tag{C.4}$$

Clearly the *spot size* w_0, the *Rayleigh range* b (sometimes referred to as z_r), the direction of propagation, the position of minimum waist and the complex amplitude E_0 completely specify a GB.

C.2 Reflection and Transmission from a General Curved Surface

Consider a 2D GB that is incident upon a general curved surface, Fig.(C.1). It can be shown that if at the point of incidence the waist of the beam is smaller than both the radius of curvature of the surface and also than the radius of curvature of phase front $R(z)$ then the reflected and transmitted beams would remain GBs. The goal is to find the reflected and transmitted beams from the interface once the incident beam is known. For this problem two different coordinate systems are considered:
1. Main Coordinate system (x, z) is a fixed coordinate system in which the equation of the interface is known.
2. (x_l, z_l) refers to the ray fixed coordinate system [40] for $l = i, r, t$ for incident, reflected and transmitted respectively.
The point of incidence with the surface $z = f(x)$ is 0. The normal vector to the surface at the point of incidence is given by

$$\hat{n} = \vec{\nabla}(f(x) - z)$$

The reflection and transmission directions are determined from Snell's laws:

$$\hat{z_i}.\hat{n} = \hat{z_r}.\hat{n} \quad \text{or} \quad \theta_i = \theta_r \quad \text{(Law of reflection)} \tag{C.5}$$
$$n_1(\hat{z_i} \times \hat{n}) = n_2(\hat{z_t} \times \hat{n}) \quad \text{or} \quad n_1 \sin\theta_i = n_2 \sin\theta_t \quad \text{(Law of refraction)} \tag{C.6}$$

where n_1 and n_2 are the refractive indices of the two medium shown in Fig.(C.1). The case of reflection from a perfect conductor can also be easily handled by only considering the reflected beam. The angle of incidence, reflection and transmission are denoted by θ_i, θ_r and θ_t. Once these directions are known the ray fixed coordinate system of the incident, reflected and transmitted beams can be found from (see for example [41]):

$$\begin{aligned}\hat{x_i} &= \frac{\hat{z_i} \times (\hat{n} \times \hat{z_i})}{|\hat{z_i} \times (\hat{n} \times \hat{z_i})|} \\ \hat{x_r} &= -\frac{\hat{z_r} \times (\hat{n} \times \hat{z_r})}{|\hat{z_r} \times (\hat{n} \times \hat{z_r})|} \\ \hat{x_t} &= \frac{\hat{z_t} \times (\hat{n} \times \hat{z_t})}{|\hat{z_t} \times (\hat{n} \times \hat{z_t})|}\end{aligned} \tag{C.7}$$

Now that the direction of propagation of the reflected and refracted beams are obtained the other parameters can easily be found.

C.3 Phase Matching and Determination of the Amplitude of the Reflected and Refracted Beams

Phase matching is used to find the spot size and origin of the reflected and transmitted GB's. It is assumed that the reflected and refracted beams remain GB's so there exists three different GB's:

$$\begin{aligned}\mathbf{E_i}(\mathbf{x},\mathbf{z}) &= E_{0i}\hat{y}\sqrt{\frac{jb_i}{z_i+jb_i}}\exp\left(-jk_1z_i - \frac{jk_1}{2}\frac{x_i^2}{z_i+jb_i}\right) \\ \mathbf{E_r}(\mathbf{x},\mathbf{z}) &= E_{0r}\hat{y}\sqrt{\frac{jb_r}{z_r+jb_r}}\exp\left(-jk_1z_r - \frac{jk_1}{2}\frac{x_r^2}{z_r+jb_r}\right) \\ \mathbf{E_t}(\mathbf{x},\mathbf{z}) &= E_{0t}\hat{y}\sqrt{\frac{jb_t}{z_t+jb_t}}\exp\left(-jk_2z_t - \frac{jk_2}{2}\frac{x_t^2}{z_t+jb_t}\right)\end{aligned} \tag{C.8}$$

The procedure for the reflected beam is explained only, the details of obtaining the parameters of the transmitted beam is identical so only give the results are given. In Fig.(C.1) If $\vec{r}(t)$ is a vector whose tip traces the surface of incidence in the (x, z) plane, if it is assumed

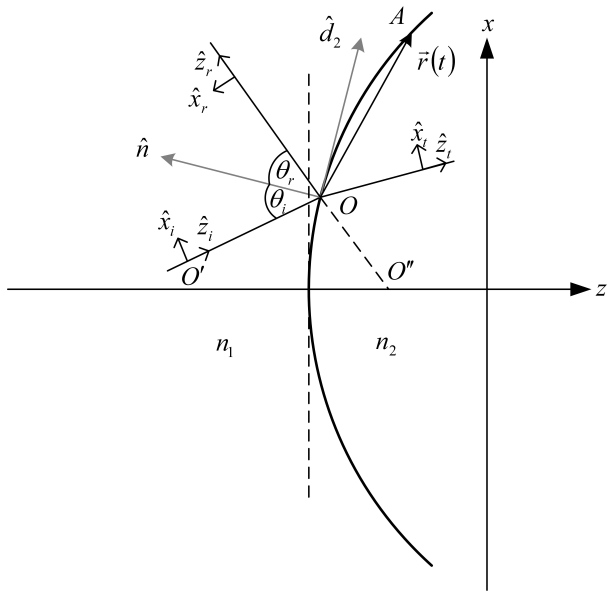

Figure C.1: The geometry of GB reflection and transmission

that the beam waist (spot size) at point of incidence is much smaller (about half) than the radius of curvature of the surface, a quadratic approximation for the surface can be used:

$$\vec{r}(t) = t\hat{d}_2 + n\hat{n} = t\hat{d}_2 - \frac{1}{2R}t^2\hat{n} \tag{C.9}$$

where R is the radius of curvature of the surface and n and t are the coordinate of the point. The next step is to express the coordinates of the surface (tip of $\vec{r}(t)$) in the (x_i, z_i) and (x_r, z_r) systems. This is done so for points that are close to the point of incidence the phase of the incident and reflected beams can be correctly matched. If $\vec{OO}'$ and $\vec{OO}''$ are the vectors connecting the origins of the incident and reflected beams to the point of intersection, it is easily shown that:

$$\begin{aligned}
\vec{r}'(t) &= \vec{OO}' + (t\cos\theta_i + n\sin\theta_i)\hat{x}_i + (t\sin\theta_i - n\cos\theta_i)\hat{z}_i \\
\vec{r}''(t) &= \vec{OO}'' + (-t\cos\theta_r + n\sin\theta_r)\hat{x}_r + (t\sin\theta_r + n\cos\theta_r)\hat{z}_r
\end{aligned} \tag{C.10}$$

Where $\vec{r}'(t)$ and $\vec{r}''(t)$ are expressed in the incident and reflected beam coordinate systems. Note that $\vec{OO}'$ and $\vec{OO}''$ are in the direction of $\hat{z}_i$ and $\hat{z}_r$ respectively and therefore create a constant phase term which shall be dealt with later. Matching the phase of the incident and transmitted waves the following relations are obtained:

$$t\sin\theta_i + \frac{1}{2R}\cos\theta_i + \frac{1}{2Q_i}t^2\cos^2\theta_i = t\sin\theta_r - \frac{t^2}{2R}\cos\theta_r + \frac{t^2}{2Q_r}\cos^2\theta_r \tag{C.11}$$

where Q_i and Q_r are the so called *complex curvature* of the wavefronts of the incident and reflected beams and are given by

$$\begin{aligned} Q_i &= z_i + jb_i \\ Q_r &= z_r + jb_r \end{aligned} \tag{C.12}$$

The second approximation that used is that Q_i and Q_r remain constant and equal to there values at the point of incidence. This approximation implies that the *waist of the incident and reflected beams must be much smaller than the radius of curvature of the wavefronts.* Eqn.C.11 must hold for all values of t. The first order terms yield the law of reflection ($\theta_i = \theta_r$) and the second order terms yield:

$$\frac{1}{Q_i} = \frac{1}{Q_r} + \frac{2}{R\cos\theta_i} \tag{C.13}$$

where $Q_i = \rho_i + jb_i$ and $Q_r = \rho_r + jb_r$; ρ_i and ρ_r are the distances from the origin of the incident and reflected beams from the surface, Fig.(C.2). Following the exact same procedure for the transmitted beam it can be shown that the following equation for obtaining the curvature matrix of the refracted beam is obtained:

$$\frac{1}{Q_i} = \frac{n_1}{n_2}(\frac{\cos\theta_i}{\cos\theta_t})^2\frac{1}{Q_t} + \frac{n_1\cos\theta_i - n_2\cos\theta_t}{n_2\cos\theta_t^2 R} \tag{C.14}$$

From the above equation the spot size and the position of minimum waist (origin of the coordinate system of the beam) are obtained.
To determine the amplitude, Fresnel coefficients are used, $\gamma(\theta_i)$, at the point of incidence. This is obviously justified as long as the beam waist remains small over the region of interest. Therefore the amplitude of the reflected beam is given by:

$$E_{0r} = \gamma(\theta_i)E_{0r}\sqrt{\frac{b_i(\rho_r + jb_r)}{b_r(\rho_i + jb_i)}} \tag{C.15}$$

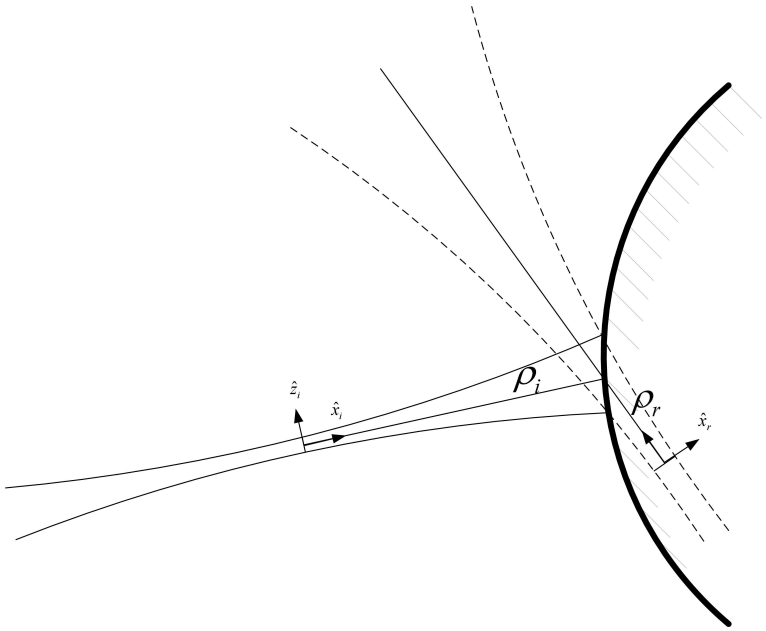

Figure C.2: The geometry of GB reflection and transmission

Bibliography

[1] Allan W. Snyder and John D. Love, *Optical Waveguide Theory*. Chapman and Hall, London, New York, 1983.

[2] C. L. Xu and W. P. Huang. *Pier 11 Progress in Electromagnetics Research*, chapter 1, pp. 1–49. EMW Publishing, Cambridge, USA, 1995.

[3] Weiping Huang, Chenglin Xu, Sai-Tak Chu, and Sujeet K. Chaudhuri, "A finite difference vector beam propagation method: Analysis and assessment," *Journal of Lightwave Technology*, vol. 10, no. 3, pp. 295–305, 1992.

[4] Sai-Tak Chu and Sujeet K. Chaudhuri, "A finite difference time-domain method for the design and analysis of guided-wave optical structures," *Journal of Lightwave Technology*, vol. 7, no. 12, pp. 2033–2038, 1989.

[5] Sai-Tak Chu and Sujeet K. Chaudhuri, "Combining modal analysis and the finite-difference time-domain method in the study of dielectric waveguide problems," *IEEE Transactions on Microwave Theory and Technique*, vol. 38, no. 11, pp. 1755–1760, 1990.

[6] W. P. Huang, S. T. Chu, and S. K. Chaudhuri, "A scalar finite difference time-domain approach to guided-wave optics," *IEEE Photonics Technology Letters*, vol. 3, no. 6, pp. 524–526, 1991.

[7] Herwig Kogelnik, "On the propagation of gaussian beams of light through lenslike media including those with a loss or gain variation," *Applied Optics*, vol. 4, no. 12, pp. 1562–1569, 1965.

[8] H. Kogelnik and T. Li, "Laser beams and resonators," *Applied Optics*, vol. 5, no. 10, pp. 2407–2416, 1966.

[9] Bahaa E. A. Saleh and Malvin C. Teich, *Fundamentals of Photonics*. John Wiley and Sons, Inc., New York, 1991.

[10] Anthony A. Tovar and Lee W. Casperson, "Generalized beam matrices," *J. Opt. Soc. m. A*, vol. 14, no. 4, pp. 882–893, 1997.

[11] Georges A. Deschamps, "Gaussian beam as a bundle of complex rays," *Proceeding of the IEEE*, vol. 60, no. 9, pp. 1022–1035, 1971.

[12] J. Arnaud, "Representation of gaussian beams by complex rays," *Applied Optics*, vol. 24, no. 4, pp. 538–543, 1985.

[13] Satinath Choudhary and Leopold Felsen, "Analysis of gaussian beam propagation and diffraction by inhomogenous wave tracking," *Proceedings of IEEE.*, vol. 62, no. 11, pp. 1530–1540, 1974.

[14] H. L. Berton J. W. RA and Leopold B. Felsen, "Reflection and transmission of beams at a dielectric interface.," *SIAM Journal of Applied Mathematics.*, vol. 24, no. 3, pp. 396–413, 1973.

[15] Y. Z. Ruan and L. B. Felsen, "Reflection and refraction of beams at a curved interface," *The Journal of the Optical Society of America. A*, vol. 3, no. 4, pp. 566–568, 1986.

[16] Sang-Yung Shin and L. B. Felsen, "Multiply reflected gaussian beams in a circular cross section," *IEEE Transctions on Microwave Theory and Techniques*, vol. 26, no. 11, pp. 845–851, 1978.

[17] John J. Maciel and Leopold B. Felsen, "Gaussian beam analysis of propagation from and extented aperture distribution through dielectric layers, part i-plane layer," *IEEE Transactions on Antennas and Propagation*, vol. 38, no. 10, pp. 1607–1617, 1990.

[18] John J. Maciel and Leopold B. Felsen, "Gaussian beam analysis of propagation from and extented aperture distribution through dielectric layers, part i-circular cylindrical layer," *IEEE Transactions on Antennas and Propagation*, vol. 38, no. 10, pp. 1618–1624, 1990.

[19] Hsi-Tseng Chou and Prabhakar H. Pathak, "Uniform asymptotic solution for electromagnetic reflection and diffration of and arbitrary gaussian beam by a smooth surface with an edge," *Radio Science*, vol. 32, no. 4, pp. 1319–1336, 1997.

[20] Hsi-Tseng Chou, Prabhakar H. Pathak, and Robert J. Burkholder, "Novel gaussian beam method for rapid analysis of reflector antenna," *IEEE Transactions on Antennas and Propagation*, vol. 49, no. 6, pp. 880–893, 2001.

[21] Jin Seung Kim and Sang Soo Lee, "Scattering of laser beams and the optical potential well for a homogenous sphere," *Journal of the optical society of America*, vol. 73, no. 3, pp. 303–312, 1983.

[22] James a. Lock, "Scattering of diagonally incident focused gaussian beam by an infinitely long homogeneous circular cylinder," *Journal of the optical society of America A*, vol. 14, no. 3, pp. 640–652, 1997.

[23] G. A. Massey and A. E. Siegman, "Reflection and refraction of gaussian beams at tilted ellipsoidal surfaces," *Applied Optics*, vol. 8, no. 5, pp. 975–978, 1969.

[24] Georges A. Deschamps, "Ray techniques in electromagnetics.," *Proceeding of the IEEE*, vol. 60, no. 9, pp. 1022–1035, 1972.

[25] J.A Arnaud and H. Kogelnik, "Gaussian light beams with general astigmatism," *Applied Optics*, vol. 8, no. 8, pp. 1687–1693, 1969.

[26] D. Gabor, "Theory of communication," *Journal of the Institute of Electrical Engineering*, vol. 93, no. 3, pp. 429–457, 1946.

[27] P.D. Einziger, S. Raz, and M. Shapira, "Gabor representation and aperture theory," *Journal of Applied Optics*, vol. 3, no. 4, pp. 508–522, 1986.

[28] J. J. Maciel and L. B. Felsen, "Systematic study of fields due to extended apertures by gaussian beam discretization," *IEEE Transactions on Antenna and Propagation*, vol. 37, no. 7, pp. 884–892, 1989.

[29] J. J. Maciel and L. B. Felsen, "Discretized gabor-based beam algorithm for time-harmonic radiaiton from two-dimensional truncated planar aperture distributions-i: Formulation and solution," *IEEE Transactions on Antenna and Propagation*, vol. 50, no. 12, pp. 1751–1759, 2002.

[30] J. J. Maciel and L. B. Felsen, "Discretized gabor-based beam algorithm for time-harmonic radiaiton from two-dimensional truncated planar aperture distributions-ii: Asymptotics and numerical tests," *IEEE Transactions on Antenna and Propagation*, vol. 50, no. 12, pp. 1760–1768, 2002.

[31] Zho Haijing and Ruan Yingzheng, "A new method of aperture analysis based on gaussian beam expansion," *Journal of System Engineering and Electronics*, vol. 8, no. 2, pp. 7–18, 1997.

[32] K. S. Yee, "Numerical solution of initial boundary value problems involving maxwell's equaions in isotropic media," *IEEE Transactions on Antenna and Propagation*, vol. 14, pp. 302–307, 1966.

[33] Allen Taflov and Susan Hagness, *Computational Electrodynamics*. Artech House, 2000.

[34] Sujeet K. Chaudhuri Ying Wang, Safieddin Safavi-Naeini, "A hybrid technique base on combining ray tracing and fdtd methods for site-specific modeling of indoor radio wave propagation," *IEEE Transactions on Antenna and Propagation*, vol. 48, no. 5, pp. 743–754, 2000.

[35] Ying Wang. *Site-Specific Modeling of Indoor Radio Wave Propagation*. PhD thesis, University of Waterloo, Waterloo, Ontario, Canada N2L-3G1, 2000.

[36] W. P. Huang, S. T. Chu, and S. K. Chaudhuri, "A semivectorial finite difference time-domain method," *IEEE Photonics Technology Letters*, vol. 3, no. 9, pp. 803–806, 1991.

[37] Sai Tac Chu. *Modelling of Guided-Wave Optical Structures by the Finite Difference Time Domain Method*. PhD thesis, University of Waterloo, Waterloo, Ontario, Canada N2L-3G1, 1990.

[38] Max Born and Emil Wolf, *Principles of optics*. Pergamon Press, Oxford, 1980.

[39] J. J. Stoker, *Differential Geometry*. Wiley-Interscience, New York, 1969.

[40] Graeme L. James, *Geometrical Theory of Diffraction for Electromagnetic Waves*. Peter Peregrinus Ltd., Oxford, 1980.

[41] Arash Rohani. A fast hybrid method based on a gaussian beam tracing scheme for photonic structures. Master's thesis, University of Waterloo, 2002.

[42] A. Rohan, A.A. Shishegar, and S.S. Naeini, "A fast gaussian beam tracing method for reflection and refraction of general vectorial astigmatic gaussian beams from general curved surfaces," *Optics Communications*, vol. 232, no. 1.

[43] Galdi V., Kosmas P., Rappaport C.M., Felsen L.B., and Castanon D.A., "Short-pulse three-dimensional scattering from moderately rough surfaces: a comparison between narrow-waisted gaussian beam algorithms and fdtd," *IEEE Transactionson Antennas and Propagation*, vol. 54, no. 1, pp. 157–67, 2006.

[44] Galdi V. and Felsen L.B., "Two-dimensional pulsed propagation from extended planar aperture field distributions through a planar dielectric layer via quasi-ray gaussian beams," *IEEE Transactions on Antennas and Propagation*, vol. 51, no. 7, pp. 1549–58, 2003.

[45] Galdi V., Pavlovich J., Karl W.C., Castanon D.A., and Felsen L.B., "Moderately rough dielectric interface profile reconstruction via short-pulse quasi-ray gaussian beams," *IEEE Transactions on Antennas and Propagation*, vol. 51, no. 3, pp. 672–7, 2003.

[46] Galdi V., Felsen L.B., and Castanon D.A., "Quasi-ray gaussian beam algorithm for short-pulse two-dimensional scattering by moderately rough dielectric interfaces," *IEEE Transactions on Antennas and Propagation*, vol. 51, no. 2, pp. 171–83, 2003.

[47] Galdi V. and Felsen L.B., "Gabor-based quasi-ray gaussian beam analysis of 2-d pulsed propagation from extended aperture field distributions through planar dielectric layers," *Journees Internationales de Nice sur les Antennes*, vol. 2, no. 2, pp. 221–24, 2002.

[48] Galdi V., Felsen L.B., and Castanon D. A., "3-d short pulse scattering by moderately rough dielectric interfaces via quasi-ray gaussian beams," *IEEE Antennas and Propagation Society International Symposium.*

[49] Heyman E. and Felsen L.B., "Gaussian beam and pulsed-beam dynamics: Complex-source and complex-spectrum formulations within and beyond paraxial asymptotics," *Journal of the Optical Society of America A*, vol. 18, no. 7, pp. 1588–611, 2001.

[50] Galdi V., Felsen L.B., and D.A. Castanon, "Narrow-waisted gaussian beam discretization for pulsed radiation from 2d large apertures," *IEEE Antennas and Propagation Society International Symposium*, vol. 2.

[51] Galdi V., Felsen L.B., and D.A. Castanon, "Narrow-waisted gaussian beam discretization for short-pulse radiation from one-dimensional large apertures," *IEEE Transactions on Antennas and Propagation*, vol. 49, no. 9, pp. 1322–32, 2001.

[52] Blanca C.M. and C. Saloma, "Efficient analysis of temporal broadening of a pulsed focused gaussian beam in scattering media," *Applied Optics*, vol. 38, no. 25, pp. 5433–7, 1999.

[53] Porras M.A., "Ultrashort pulsed gaussian light beams," *Physical Review E*, vol. 58, no. 1, pp. 1086–93, 1998.

[54] Hwang H.E., "Far-field diffraction characteristics of a time dependent gaussian-shaped pulsed beam from a rectangular mask with a circular aperture array," *Optical and Quantum Electronics*, vol. 35, no. 15, pp. 1335–50, 2003.

[55] Zhongyang Wang, Zhengquan Zhang, Zhizhan Xu, and Qiang Lin, "Space-time profiles of an ultrashort pulsed gaussian beam," *IEEE Journal of Quantum Electronics*, vol. 33, no. 4, pp. 566–573, 1997.

[56] Richard W. Ziolkowski and Justin B. Judkins, "Propagation characteristics of ultrawide-bandwidth pulsed gaussian beams," *Journal of the Optical Society of America*, vol. 9, no. 11, pp. 2021–203–, 1992.

[57] Akira Ishimaru, *Electromagnetic Wave Propagation, Radiation and Scattering*. Prentice Hall. Inc, Toronto, 1991.

[58] K. Artman, "Berechnung der seitenversetzung des total reflectierten strahles," *Ann. Physik*, vol. 2.

[59] R. H. Renard, "Total reflection: a new evaluation of the goos-hanchen shift," *Journal of the Optical Society of America*, vol. 54.

[60] H. M. Lai and W. K. Tang, "Goos-hanchen effect around and off the critical angle," *Journal of the Optical Society of America A*, vol. 3, no. 4, pp. 550–557, 1986.

[61] Simon M.C. and Perez L.I., "Goos-hanchen effect of an ordinary refracted beam," *Joutnal of Modern Optics*, vol. 52, no. 4, pp. 515–28, 2005.

[62] Y.M.M. Antar and W.M. Boerner, "Gaussian beam interaction with a planar dielectric iterface," *Canadian Journal of Physics*, vol. 52, pp. 962–972, 1974.

[63] B.R. Horowitz and T. Tamir, "Lateral displacement of light beam at a dielectric interface.," *Journal of the Optical Society of America*, vol. 61, pp. 586–594, 1971.

[64] Bretenaker F., Le Floch A., and Dutriaux L., "Direct measurement of the optical goos-hanchen effect in lasers," *Physical Review Letters*, vol. 68, no. 7, pp. 931–3, 1992.

[65] A. Rohani, "A fast hybrid method for analysis and design of photonic structures," technical report, Agilent Thechnologies, April 2005.

[66] S. Safavi-Naeini and Y. L. Chow. *Pier 11 Progress in Electromagnetics Research*, chapter 5, pp. 199–253. Cambridge, USA, 1995.

[67] Constantine A. Balanis, *Advanced Engineering Electromagnetics*. Wiley, Toronto, New York, 1989.

[68] A. J. E. M. Janssen, "Gabor representation of generalized functions," *J. Math. Anal. Appl.*, vol. 83, pp. 337–394, 1981.

[69] M. J. Bastiaans, "Gabor's expansion of a signal into gaussian elementary signals," *Proceedings of the IEEE*, vol. 68, pp. 538–539, 1980.

[70] M. J. Bastiaans, "Expansion of an optical signal into a discrete set of gaussian beams," *Optik*, vol. 57, pp. 95–101, 1980.

[71] M. J. Bastiaans, "A sampling theorem for the complex spectogram and gabor's expansion of a signal into gaussian elementary signals," *Optical Engineering*, vol. 20, p. 594, 1981.

[72] Felsen L. B., *Radiation and scattering of waves*. IEEE Press Series on Electromagnetic Waves, 1994.

[73] Hamid Salehi, *Electromagnetic Left Handed Media Physics and Device Applications*. 2006.

[74] Allen Taflov, *Advanced in Computational Electrodynamics*. Artech House, 1998.

[75] Hermann A. Haus. *Waves and Fields in Optoelectronics*, pp. 113–116. Prentice-Hall, New Jersey, 1984.

[76] R. S. Elliott, *Antenna Theory and Design*. Prentice Hall, London, New York, 1981.

[77] Robert G. Kouyoumjian, "Asymptotic high frequency methods," *Proceedings of IEEE*, vol. 53, pp. 864–876, 1965.

[78] Kline and Kay, *Electromagnetic Theory and Geometrical optics*. Interscience Publishers, London, New York, 1980.